Applied Magnetic Resonance (2020) 51:773–850
https://doi.org/10.1007/s00723-020-01240-y

Applied
Magnetic Resonance

REVIEW

Soft Dynamic Confinement of Membrane Proteins by Dehydrated Trehalose Matrices: High-Field EPR and Fast-Laser Studies

Klaus Möbius, et al. ***[full author details at the end of the article]***

Received: 24 July 2020 / Revised: 24 July 2020 / Published online: 30 August 2020

Abstract

In memory of the 85th birthday of Yakov S. Lebedev (Moscow), who died in 1996, we start this Review on soft-glass matrix effects in donor–acceptor complexes with an appreciation of his pioneering work on high-field EPR spectroscopy on tribochemically generated donor–acceptor complexes. The mechanochemical activation of polycrystalline mixtures of porphyrins (and other donors) and quinone acceptors was found to produce large concentrations of triplet donor molecules and donor–acceptor radical pairs with unusual stability. The Review is continued with reporting on W-band high-field EPR and fast-laser studies on disaccharide matrix effects on structure and dynamics of donor–acceptor protein complexes related to photosynthesis, including the non-oxygenic bacterial reaction center (RC) and the oxygenic RCs Photosystem I (PS I) and Photosystem II (PS II, preliminary results). Some organisms can survive complete dehydration and high temperatures by adopting an anhydrobiotic state in which the intracellular medium contains large amounts of disaccharides, in particular trehalose and sucrose. Trehalose is most effective in protecting biostructures, both in vivo and in vitro. To clarify the molecular mechanisms of disaccharide bioprotection, structure and dynamics of sucrose and trehalose matrices at different controlled hydration levels were probed by perdeuterated nitroxide spin labels and native cofactor intermediates in their charge-separated states. Trehalose forms a homogeneous amorphous phase in which the hosted molecules are uniformly distributed. Notably, their rotational mobility at room temperature is dramatically impaired by the trehalose H-bonding network confinement to an extent that in normal protein–matrix systems is only observed at low temperatures around 150 K. From the experimental results, formation of an extended H-bonding network of trehalose with protein molecules is inferred, involving both bulk and local water molecules. The H-bond network extends homogeneously over the whole matrix integrating and immobilizing the hosted protein. Taken together, these observations suggest that in photosystems, such as bacterial RCs and PS I complexes, of different size and complexity regarding subunit composition and oligomeric organization, the molecular configuration of the cofactors involved in the primary processes of charge separation is not significantly distorted by incorporation into trehalose glass, even under extensive dehydration. By means of pulsed W-band high-field multiresonance

EPR spectroscopies, such as ELDOR-detected NMR and ENDOR, in conjunction with using isotope labeled water (D_2O and $H_2{}^{17}O$), the biologically important issue of sensing and quantification of local water in proteins is addressed. The bacterial RC embedded into the trehalose glass matrix is used as model system. The two native radical cofactor ions of the primary electron donor and acceptor as well as an artificial nitroxide spin label site-specifically attached to the protein surface are studied in the experiments. The three paramagnetic reporter groups probe distinctly different local environments. They sense water molecules via their magnetic hyperfine and quadrupole interactions with either deuterons or ^{17}O nuclei. It is shown that by using oxygen-17 labeled water, quantitative conclusions can be drawn differentiating between local and bulk water. It is concluded that dry trehalose operates as anhydrobiotic protein stabilizer by means of selective changes in the first solvation shell of the protein upon trehalose–matrix dehydration with subsequent changes in the hydrogen-bonding network. Such changes usually have an impact on the global function of a biological system. Finally, preliminary results of optical and W-band EPR experiments on the extremolytes ectoine and its derivative hydroxyectoine are reported; these compounds appear to share several stress-protecting properties with trehalose in terms of stabilizing protein matrices. For instance, they display remarkable stabilizing capabilities towards sensitive proteins and enzymes with respect to freeze-thawing, heat-treatment, and freeze-drying procedures. Moreover, hydroxyectoine is a good glass-forming compound and exhibits a remarkable bioprotective effect against desiccation and heat denaturation of functional protein complexes.

1 Prologue

When Prof. Kev M. Salikhov, Editor-in-Chief of *Applied Magnetic Resonance,* asked us to contribute to a Special Issue devoted to the memory of Professor Yakov Sergeevich Lebedev (1935–1996) we did not falter for a moment in accepting the invitation. We felt honored to be among those who will again pay tribute to this unforgotten eminent scientist and great human being on the occasion of his 85th birthday. We are sure that many papers collected in this Special Issue will be of interest to a wide audience of junior and senior scientists from physical chemistry, material sciences and structural biology, especially those, of course, who still have personal memories of Yakov Lebedev.

He had focused his work on many different aspects of magnetic resonance spectroscopy in physical chemistry, molecular biology and material science. In particular, he did pioneering work on high-field/high-frequency EPR spectroscopy, a field where Yakov Lebedev has left so many distinctive footprints over the years—despite his much too early death in 1996.

To the frequently asked question "Who started high-field EPR?" one can fairly answer that, as with many major developments in science, high-field/high-frequency EPR spectroscopy has several fathers who took the decisive actions in a similar period of time. Thorough historical overviews on such developments are provided, for instance, by Refs. [1–3]. Historically, it was Yakov Lebedev in Moscow in the early 1970s who was the first to start a dedicated research program on high-field/

high-frequency EPR in physical chemistry. In his group, Oleg Grinberg and Alexander Dubinskii were primarily involved in the instrument development [2]. About a decade later, the Möbius group at Free University Berlin started with their 95 GHz EPR and ENDOR projects—and extended them in subsequent years to 360 GHz EPR and ENDOR, ready for applications also to biological samples [3].

Several of the present authors knew Yakov Lebedev personally since a long time (K. M., W. L. and A.Yu. S.), even dating back to the mid-1970s, highly respecting him as a great and open-minded scientist and one of the leading electron magnetic resonance spectroscopists. Over the years, he became a stimulating cooperation partner of us—and a noble friend, who is good for the heart and for the mind. What started during the troubled times of the Cold War with its division of Europe and the world, continued in the better times of a beginning political openness after overcoming the Iron-Curtain in 1990.

1.1 Yakov Lebedev, as a Colleague and Friend

Yakov S. Lebedev started his scientific research in 1957 in the N. N. Semenov Institute of Chemical Physics of the Academy of Sciences of USSR [now Russian Academy of Sciences (RAS)] under the direction of Academician Vladislav V. Voevodsky (1917–1967). The scientific research of Yakov Lebedev was mainly concerned with two fields: elementary chemical processes in solid-state materials and new methods of EPR spectroscopy. In 1966, Yakov Lebedev became head of the Laboratory of Chemical Radiospectroscopy. For many years, he was in charge of the Scientific-Methodological Center of the Academy of Sciences for the matters of EPR spectroscopy. He was promoted to head of the Kinetics and Catalysis Department of the N. N. Semenov Institute of Chemical Physics and professor of the Chemical Physics Chair of the Moscow Physical–Technical Institute, and served as member of the Editorial Boards of the scientific journals "Strukturnaya Khimiya", "Fizicheskaya Khimiya" and "Applied Magnetic Resonance".

In 1957, the Siberian Branch of the Academy of Sciences of USSR had been established in Novosibirsk under the leadership of mathematician and physicist Mikhail A. Lavrentiev (1900–1980). He played a most important role in the foundation of Siberia's *Academic Town*, Akademgorodok, which soon became a municipal district of Novosibirsk. V. V. Voevodsky was chosen to build up a potent research group on elementary processes in physical-chemistry. He accepted and moved from the N.N. Semenov Institute of Chemical Physics in Moscow to the Institute of Kinetics and Combustion in Akademgorodok—accompanied by his highly capable and motivated research associates Yu. N. Molin and Yu. D. Tsvetkov. Together with the theoretical physical chemist Kev M. Salikhov (born in 1936), they established a new "scientific school of chemical magnetic spectroscopy". They included the experimental physicist and engineer Anatoly G. Semenov in the group, an excellent instrument builder who thereafter led the technical development and production of a number of specialized EPR and NMR spectrometers for various fundamental and applied tasks; they satisfied the needs for many years in numerous Soviet laboratories. At the peak of Soviet research,

Akademgorodok was home to 65,000 scientists and their families, it was a privileged zone of the academic elite. A total of about 200,000 people lived here. After the collapse of the Soviet Union, Akademgorodok also began to decline, as many scientists left the institutes for Western Europe or the USA. By 1999, the population fell to about 50,000.

While Yu. N. Molin and Yu. D. Tsvetkov had moved to Akademgorodok, another highly gifted disciple of V. V. Voevodsky, Yakov S. Lebedev (1935–1996), stayed in Moscow and started a dedicated research program on pioneering high-field/high-frequency EPR in physical chemistry. This included the mandatory development of suitable instrumentation for microwave sources and detectors as well as sweepable cryomagnets. The ultimate success of his program was a great step forward in view of the on-going research activities of advanced EPR spectroscopy around the world, and was recognized accordingly. In fact, high-field/high-frequency EPR—together with pulsed EPR—became essential ingredients of the success story to put EPR into the position of catching up with NMR in modern magnetic-resonance spectroscopy. In 1988, Yakov Lebedev was awarded the USSR State Prize in Science and Technology for developing new methods of chemical radiospectroscopy. In 1994, Yakov Lebedev was awarded the International Zavoisky Prize for his research on developing high-field EPR spectroscopy.

High-field/high-frequency EPR has blossomed during the past decades, especially after the original pioneering work of Yakov Lebedev and his group at the N. N. Semenov Institute of Chemical Physics in Moscow. Although Lebedev's scientific work suffered heavily under the economic constraints of Soviet Union's Fundamental-Research policy and, even more so, under the restricted travel opportunities to attend scientific conferences in the West to exchange ideas, he and his group did ground-breaking work during the 1970s, 1980s and 1990s which today is still considered to be the gold standard by the research community practicing EPR at high magnetic fields and microwave frequencies [2]. The more it is tragic that after the end of the political restrictions, in 1996, at the peak of his scientific career, he succumbed to cancer. Perhaps, one consolation is that several of his former students carry on his legacy and successfully perform EPR spectroscopy in academic institutions worldwide. Memory is at the beginning of the New.

With regard to the new scientific cooperation possibilities of Yakov Lebedev, the political paradigm shift happened at a favorable moment, and that is the validation of high-field EPR as high-performance spectroscopic method in magnetic resonance of complex systems. The growing appreciation is mirrored also by the rising number of research groups in Europe, the US and Japan, dedicated to the development and application of high-field EPR spectroscopy. This was made possible by increased financial support from national and international funding agencies. The European Union, for example, supported the Human Capital and Mobility (HCM) project "High-Field EPR: Technology and Applications" (coordinator J. Schmidt, Leiden, 1993–1996); strong support was granted by the DFG (Deutsche Forschungsgemeinschaft) through the Priority Program "High-Field EPR in Biology, Chemistry and Physics" (coordinator K. Möbius, Berlin, 1998–2004). These initiatives acted like seeding programs for the rapid development of high-field EPR spectroscopy in Europe, including Israel and Russia.

Our cooperation and friendship with Ya. S. Lebedev reached kind of a peak when he was honored with the Zavoisky Award 1994, and shared it with K. Möbius (Berlin) and J. R. Norris (Chicago).

The picture (Fig. 1) shows Yakov Lebedev and Klaus Möbius at the Conference Dinner after the 1994 Zavoisky Award ceremony in Kazan. The guests are seated at tables lavishly loaded with food and drink. Later at the evening, in a relaxed state, the guests at that table talked about their favorite books, books they would read over and over again. Without hesitation, Yakov Lebedev said *The Master and Margarita* (Мастер и Маргарита) by Mikhail Bulgakov. And he explained why this was his favorite book: First, because it is a great Russian novel, but with a truly Faustian complex of themes, a journey through the ages; second, because it is a great satire about living and dying under an omnipresent dictatorial system with an all-pervading dogmatic bureaucracy; third, because it shows that narrow-mindedness of censorship of ideas does not last in the long run, just as the Inquisition did not last in the long run. "Manuscripts don't burn".

If Mikhail Bulgakov had not become world-famous through The Master and Margarita, he would certainly have made it by this minimal aphorism of only three words, Manuscripts don't burn. Writers return, and burnt manuscripts resurrect miraculously. The Master and Margarita is now considered one of the best satires of the time of dogmatically ruled Soviet Union.

Fig. 1 Conference Dinner in Kazan after the award ceremony of the 1994 Zavoisky Prize; the guests are distributed around the tables, among them Yakov Lebedev and Klaus Möbius together with their wives Tanya (left side) and Uta (right side)

"Censorship is the younger of two nefarious sisters, the elder is called Inquisition" ("Die Zensur ist die jüngere von zwei schändlichen Schwestern, die ältere heißt Inquisition", Johann N. Nestroy, 1848) murmered K. M. And Yakov Lebedev continued that, to make a living, Bulgakow started working as a correspondent and columnist for newspapers. Bulgakov's grotesque depictions of everyday life in the young Soviet Union often have fantastic or absurd features—a typical way of exercising social criticism in the Russian literature since Gogol. And indeed, Bulgakov was best known for his humor and penetrating satire. Between 1922 and 1926, he wrote several satirical theater plays. The most significant features of Bulgakov's satire were a skillful blending of fantastic and realistic elements, grotesque situations, and a concern with fundamental ethical issues. Because of this mixture of realism and humor, Bulgakov's works enjoyed great popularity in the USSR of the mid-1920s, but their trenchant criticism of Soviet bureaucracy and power structure was increasingly unacceptable to the authorities. They reacted with relentless censorship and a ban on publication. By 1929, all Bulgakov's plays had disappeared from the theaters' repertoire, and Bulgakov had lost all hope of getting anything printed or even getting any work at all. "In 1929, my destruction as a writer was completed," Bulgakov wrote in a letter.

If there were any gleams of hope for him during this period, they owed it to Elena Sergeevna Shilovskaya. Bulgakov met her in 1929, and married her in 1932 as his third wife. Mikhail Bulgakov was also her third husband. For both of them, it was the great love. She is the shining example for the figure of Margarita in the novel. Until March 10, 1940, when Bulgakov, suffering from great pain and gradual blindness, died of kidney sclerosis, two tormented people experienced their all-embracing love. Without his wife Elena Sergeevna, he would hardly have endured his lonely struggle for so long. She managed to keep their house open for friends during the worst years of hunger. In the days of the fatal illness, when he was almost blind, Bulgakov dictated the last pages of his masterpiece to his wife, he corrected it again and again. But the printing permission was denied to the work for more than 25 years.

Finally, after severe cuts by USSR censorship, the work was published as a follow-up in the literary magazine "Moskva" in November 1966. Its circulation of 150,000 copies was sold in a short time during this period. Actually, it was Mikhail Bulgakov's widow Elena Sergeevna who did accomplish this. She was plagued by predicaments of death (she died in July 1970 at the age of 76) and was afraid that the banned manuscript of The Master and Margarita would be forgotten forever after her death. She had been able to personally persuade the then Chairman (1959–1977) of the Union of Writers of the USSR, Konstantin Alexandrovich Fedin, to agree to publication—but he insisted that this would be possible only under the condition that for her part she agreed to substantial deletions in the text. Only under great pain did she agree to this extortion.

Yakov Lebedev told this moving story almost shyly, with a deep, melodious voice, calmly and without agitation, but with great persuasion, as we knew him talking from scientific discussions.

Many admirers of Mikhail Bulgakov read the novel within a short time and were able to recite long passages from it. Group readings were organized. The novel was discussed in public and it became clear to everyone that the text had been severely

mutilated by the censorship. Those parts cut out by the censorship were extrapolated in different versions, multiplied with typewriters and secretly distributed as Samizdat. The uncut version of "Мастер и Маргарита" appeared in book form for the first time only in 1973.

The novel depicts in an allegorical and satirical way the life in Moscow at that time. The second main theme of the novel is linked to human values such as good and evil, God and devil, life and death. The ultimate salvation of all (and only) those who accept help even from the devil, is central to this part of the book. It includes the story of the Master and his beloved Margarita, who are reunited after a long separation by Voland, the devil. Importantly, some chapters of this part contain elaborations on the Passion story about Pontius Pilate during the last days of Jesus Christ, who is referred to in the story by his Hebrew name Yeshua. The Pontius Pilate story deviates strongly from the historical biblical text; but it was completely deleted by the censorship.

In the novel The Master and Margarita, the Roman procurator Pilate is a man plagued by migraines who gives in to political pressure from the Jewish High Priest Caiaphas and condemns Yeshua to death, but later bitterly regrets this. The story of Pilate is a novel within a novel, and spans four chapters of The Master and Margarita. That inner novel about Pilate is the work of the "Master", an artist living in Moscow who suffers greatly from censorship and is forcibly put into a madhouse because of his provocative Pilate novel. Since his beloved Margarita makes a pact with Voland, the devil frees the Master and also restores his Pilate novel (which the Master had previously burned). At first, the accused Yeshua appears to Pilate as an ordinary Jewish self-proclaimed prophet, of whom there were numerous examples in Jerusalem at the time. When he asks him about his prophetic message, Yeshua says that a kingdom of truth will come in which violence is no longer necessary. At this point, the interview changes, it goes from a routine interrogation between the procurator and the prisoner to a personal conversation, in which even Pilate's headache disappears. Pilate is fascinated by Yeshua's message and wants to keep him around him. That is why he refuses to pass the death sentence demanded by the Jewish High Council. But the High Priest Caiaphas threatens him with political consequences and so Pilate believes he is forced to condemn Yeshua. However, this decision later robs him of sleep: he torments himself and regrets his cowardice, repeating over and over again the sentence "Cowardice is the worst of all sins". In the fantastic epilogue of the novel, the Master and Pilate meet—and the Master frees Pilate after 2000 years from the penance and remorse he had to suffer, and Pilate is reunited with the itinerant preacher Yeshua.

Therefore, we see that Mikhail Bulgakov's Pilate figure is a subordinate ruler of a totalitarian state who, fearing for his career, makes decisions that he personally does not approve of; and he functions as an image for the Russian regime 2000 years later. Yeshua, who (like the biblical Jesus) speaks of peace, truth and justice, stands in sharp contrast to Pilate, but is clearly the superior figure at the end of the book. It is clear: Pilate was conceived by Bulgakov as an allegory for a Soviet functionary, and one must read Yeshua's utopia of an empire of truth and justice, where violence is no longer necessary, as a utopia for Russia.

With a smile, Yakov Lebedev told that also he had tried his hand with interpolations of the missing parts of Bulgakov's novel as it was first printed. Even with good success, he said in all modesty, in particular when extrapolating the missing Pontius Pilate story.

And he added that in Moscow he occasionally passes by a discreet tombstone with the inscription: "Writer Mikhail Afanasevich Bulgakov 1891–1940, Elena Sergeevna Bulgakova 1893–1970" at Moscow's central cemetery, the Novodevichy Cemetery (reserved for prominent persons only), when he visits the graves of his parents, Sergey Alexeevich Lebedev and his wife Alice. His stepfather and stepmother, to be exact. Sergey Alexeevich Lebedev (1902–1974) is highly honored as Creator of USSR Electronic Computers, both of the analogue and digital machines. He was a great scientist and a brilliant organizer of large-scale electronic computer projects during war and post-war Soviet Union. And a great human being.

And Yakov Lebedev also said that the sepulchral stone at his father's grave is of unconventional design, made of stacked granite blocks, one of them with a hole in the front side, a hole of an unorthodox shape. For insiders, it is clear: The hole represents a hysteresis loop, the reversible magnetization curve of a ferromagnetic substance in response to a reversible external magnetic field. It describes a bistable state behavior—an effect that was used in the early years of computer technology to store digital bits in a core memory by magnetic diode switches.

In the subsequent discussion, Yakov Lebedev was asked: "You said that your stepfather and stepmother are buried at Novodevichy Cemetery, not your real parents? Would you mind to explain?" He turned to K. M. and said: "You know my story, would you mind to tell it?"

And K. M. replied that he remembers that Yakov drove him one late afternoon in Moscow to the Novodevichy Cemetery to show him the grave of his father Sergey Alekseevich Lebedev. It was in June 1991, at the occasion of a Symposium to remember the 60th anniversary of foundation of the N.N. Semenov Institute of Chemical Physics to which Yakov Lebedev had invited him. And it was the 50th anniversary of Nazi Germany's invasion of USSR. Operation Barbarossa was the code name for the vigorous attack of the Soviet Union by the German Wehrmacht on 22 June 1941—which ultimately fueled the Second World War.

And K. M. remembered that they had just returned from an unforgettable lunch in the country summer house of the Lebedev family near Moscow, where three generations of family members and their friends had come together to commemorate the victims of the Nazi invasion. Yakov Lebedev had introduced him as his colleague and friend from Germany. Clearly, this was not an easy situation, for all participants. But it was wonderfully dissolved by the eldest at the table, he himself a Russian soldier at the time, offering a thoughtful and warm welcome toast to "Yakov's friend from the other Germany".

Afterwards, Yakov told K. M. that late Sergey Alekseevich Lebedev was not his "biological" father but his stepfather, who had adopted him, and in whose family he grew up in Moscow. Yakov's real father, Boris Solomonovitch Grunfeld, was killed during the Second World War, and his real mother had died from cancer when he was about fifteen. His family had lived in Kiev at that time, it consisted of the grandmother and several children; they were trapped in very bad conditions, indeed. But

the family of Yakov's best school friend—which was the family of Sergey Alekseevich Lebedev—had recognized him as a very talented young man and had proposed to adopt him. And Yakov agreed. They had to explain to Yakov's grandmother that they plan to move from Kiev to Moscow, where Sergey Alekseevich Lebedev had been offered a new mathematical and engineering task area with excellent opportunities for research and development in computer science. And in Moscow, the "very talented young man" would have the best chances for his higher education. The proposal was accepted, and after a short time Sergey Alekseevich Lebedev's family, now enlarged by young Yakov, had settled down in Moscow. In 1953, Sergey Alekseevich Lebedev was elected full member of the Academy of Sciences of USSR.

One of Yakov's distinctive features was the joy and satisfaction of attending international scientific conferences. What he valued so much was to meet friends and colleagues, to present his own results to a knowledgeable audience and to get to know the results of his scientific competitors, to cultivate an open exchange of ideas and experiences, and to experience new worlds of thought in their historical context. To his delight, after the paradigm shift in the 1990s, he was invited more often to such conferences and research fellowships in Europe and the United States, as an example to Berlin, at several occasions, the last time in June 1996:

It was the mini-symposium "Magnetic Resonance Studies of Photochemical and Photobiological Systems", taking place in the historic Magnus Haus, in Berlin, on 8 June 1996, organized by Wolfgang Lubitz on the occasion of K. M.'s 60th birthday. An impressive cross-section of EPR spectroscopists and X-ray crystallographers from photosynthesis research have met in this baroque building. Since the eighteenth century, famous physicists and mathematicians have enriched here, in this building, the cultural heritage of Europe at large. Among the more than 60 participants of the mini-symposium were George Feher, Giovanni Giacometti, Arnold Hoff, Melvin Klein, Harry Kurreck, Yakov Lebedev, Haim Levanon, Wolfgang Lubitz, Maria-Elisabeth Michel-Beyerle, Klaus Möbius, Pier Luigi Nordio, Kev Salikhov, and Dietmar Stehlik (sadly, nine of these thirteen attendees listed have passed away since then). Heated discussions followed each lecture presentation; they were continued during coffee breaks and the buffet dinner. More and more, the discussions revolved around political issues initiated by the new situation since November 1989, the expected new cultural opportunities and unexpected political, social and economic difficulties following the end of the German division and the lifting of the Iron Curtain across Europe.

And Yakov Lebedev was happy to be in Berlin in such a time of new hopes, after the Berlin Wall had collapsed. And he was happy to discuss this with his colleagues and friends—and to chat about other historic peculiarities of Berlin in the time before, during and after World War II. For instance: how did German scientists, famous or not so famous, cope with the new political situation in the rising fascist "Third Reich" since 1933? And he understood the often controversially discussed answers. Most of them had the common pretext that the German scientists reacted either indifferently, supportive, cowardly, or bravely opposing—the full range. Probably in this order, with strongly decreasing numbers. Rather similar to what had

happened in the other countries under dictatorial regimes of that time or, sad but probably realistic, under dictatorial regimes of all times.

And Yakov Lebedev was interested in learning about the latest state of historical research on the Nazi German "Uranium Project", which, as is well known, was located in Berlin-Dahlem, in the "Dahlem Oxford" as the Berliners are proud to point out, where so many German Nobel Prize winners had their institutes of the Kaiser Wilhelm Gesellschaft (now Max Planck Society), for example Werner Heisenberg, Max von Laue, Otto Warburg. Was the construction of a German nuclear bomb really the goal set by the Wehrmacht? There in Dahlem, where today the Free University of Berlin has its home-base?

Currently, the assessment of the speculations on whether the German nuclear scientists were working in Dahlem on developing a nuclear bomb is that the Uranium program dwindled into establishing a nuclear chain reaction in natural uranium in a reactor with heavy water as neutron moderator, the Uranmaschine. And even this reactor failed to get critical for a nuclear chain reaction. Fortunately, it failed, one must say, and most Germans agree on this assessment. Thus, no German "Project Manhattan" existed. This historic fact was also unveiled by the "Farm Hall transcripts"; they were declassified by the British authorities as late as 1992. They represent a spectacular new source of information about the inner views of leading German scientists during the Nazi period.

The Farm Hall transcripts are the results of a secret operation by the British and American forces—codename Operation Epsilon—near the end of World War II. Their aim was to detain top German scientists who were thought to have worked on Nazi Germany's nuclear program. The scientists were captured between early May and end of June, 1945. Subsequently, ten of them were interned at Farm Hall, a Georgian country house in England, near Cambridge. This Club of Ten in Farm Hall housed Erich Bagge, Kurt Diebner, Walther Gerlach, Otto Hahn, Paul Harteck, Werner Heisenberg, Horst Korsching, Max von Laue, Carl Friedrich von Weizsäcker, and Karl Wirtz. They stayed there rather comfortably, as privileged prisoners of war, for 6 months, from the beginning of July, 1945 to the beginning of January, 1946. The British and American Secret Service officers bugged Farm Hall—with the goal to determine how close Nazi Germany had been to constructing an atomic bomb by tapping day and night their conversations. By capturing the major players in German nuclear physics, the British and Americans had kept them out of the hands of the Russian—and French—allies.

The recently published Farm Hall transcripts were known only by a few of the participants of the 1996 mini-symposium, and hotly discussed accordingly. Yakov Lebedev added that the Soviet Army also had caught quite a number of prominent German nuclear physicists and chemists and integrated them into the USSR postwar nuclear bomb program. Among the luminaries were Manfred von Ardenne, Gustav Hertz, and Peter Thiessen. The German research contributions undoubtedly accelerated the USSR nuclear program by several years. And, thus, enhanced the Soviet stature on the world's Cold War stage.

And then we remember Yakov Lebedev saying something like this: "At present we witness a gradual change of political paradigms, away from the East–West confrontation towards a peaceful coexistence of different political and social systems.

Towards a just world and an intact environment." This is a huge challenge, also for scientists. "We ought to be happy to live just now and are able to contribute to achieve such goals. At least, I try to think along such optimistic lines." But then he added that sometimes he was scared to death: "Do we really still have time for options to choose? And I hear me say: Too late. What shall we do?"

In September 1996, the EPR community was informed that Professor Yakov Sergeevich Lebedev, Head of the Department of Kinetics and Catalysis of the N.N. Semenov Institute of Chemical Physics of the Russian Academy of Sciences, died on September 25, 1996, after his heroic but futile fight against cancer. We have lost our dear colleague, a great scientist and a wonderful friend. He was a man of intellectual honesty and deep humanity, of reliability and friendship. He took care—even in the extremely difficult times after the collapse of the Soviet Union—of his co-workers in the N. N. Semenov Institute in Moscow, in particular of the young scientists there. He tried hard to keep his group working as a center of excellence. For this to achieve, he joined cooperation projects on high-field EPR spectroscopy with the Free University Berlin (research groups of Klaus Möbius and Harry Kurreck) and the University of Leiden (research group of Jan Schmidt). These cooperation projects have made it possible to finance sustainable and very productive research stays of former co-workers of Yakov Lebedev, for instance Alexander Dubinskii in Berlin and Oleg Poluektov in Leiden.

1.2 Yakov Lebedev, as a Co-worker

The end of the Iron-curtain confrontation between East and West enabled K. M. in Berlin and Yakov Lebedev in Moscow to successfully apply for joint research grants from the Volkswagen Foundation in Germany and the German Research Foundation (DFG) to fund multifrequency EPR and ENDOR experiments on mechano-chemically and photo-chemically generated organic radicals and radical pairs. Harry Kurreck from the Department of Chemistry of the Free University Berlin joined these cooperation projects; he was a leading expert in the investigation of the multistep electron-transfer routes in covalently linked porphyrin–quinone dyads, triads and tetrads, which mimic the photosynthetic chromophore chains. His ambitious goal was to develop strategies for synthesizing porphyrin–quinone donor–acceptor model complexes with high quantum yield of light-driven charge separation. He was also interested in methods, alternative to photoexcitation, for generating charge-separated radical pairs, such as tribochemical methods [4]. Luckily, since several years, Yakov Lebedev was successfully studying tribochemical methods by EPR and optical spectroscopy.

Tribochemistry generally deals with the chemical reactions that are initiated by mechanical energy input through friction that occur, for example, between the surfaces of sliding objects or between insufficiently lubricated metallic parts of engines—or during grinding of crystallites of various mixtures of solid chemical compounds. The precise nature of the chemical reactions is not well understood. And even the causes which allow the reactions to get started and proceed are still subject of speculation.

Thus, tribochemistry includes specific reactions that occur only under rubbing conditions as well as reactions that would occur independently under the local temperatures and pressures in the immediate vicinity of the contact region. Tribochemical reaction play a crucial role in surface technology [5] in the study of wear by micro-breaking or friction corrosion. Basically, breaking in the micrometer range is a process in which new surfaces are created by separating the bonds between atoms or molecules. This separation can be facilitated by chemical action (e.g., corrosion) or made more difficult (e.g., by lubrication oils). Occasionally, such reactions can be desired, e.g., the tribochemical reaction when lighting matches. Wear and corrosion are processes in more or less all existing surfaces of material, and surfaces are, of course, found on all samples or components.

The science, engineering and technological aspects of tribology in all its breadth and scope is a still flourishing field of current fundamental and applied research. The latest developments in tribology include traditional areas such as tribochemistry and tribophysics, but have opened hot issues such as nano-tribology and bio-tribology [6].

Many of the major challenges facing today's biomolecular sciences are related to synthesize biomimetic molecular complexes which are tailor-made to carry out or catalyze optimized chemical processes such as solar-energy conversion and hydrogen-based fuels for electro-mechanical engines. In this field, vital progress is being made by studying Nature's solutions of related problems for living organisms during their evolution.

In the literature, two possible tribochemistry mechanisms are discussed: (i) the mechanically induced chemistry at fresh nascent surfaces, e.g., electron emission; (ii) the thermally induced chemistry at the asperity tips due to local high flash temperatures and plasma formation. Various kinds of particles are emitted while one solid structure slides against another solid structure, for instance, surfaces or crystallites of micro- or nano-scale materials. These emitted particles are electrons, negative and positive ions, atoms, free radicals, and molecules. Some of the particles are in excited states, some emit photons in the visible (triboluminescence). The particle emission phenomena are generally called "triboemission" and, apparently, they are of particular interest for generating excited materials in chemistry and physics. It has been postulated that locally a triboplasma is formed, generated at a sliding contact and its vicinity due to the input of tribomechanical energy. Triboplasma is a highly ionized neutral gas, in which the charge of electrons is balanced by the charge of positive ions [7].

We want to emphasize that understanding atomic-scale wear is crucial also to avoid device failure due to wear and tear under friction of sliding surfaces. Generally, atomic-scale wear differs from macroscale wear, because chemical reactions and interactions at the friction interface are dominant in atomic-scale tribological behaviors, instead of macroscale properties, such as material strength and hardness [8].

Against that background, Yakov Lebedev's tribochemical approach to produce, with high yield, organic triplet-state radical pairs by grinding polycrystalline mixtures of porphyrin donors and quinone acceptors was very exciting. At the N.N. Semenov Institute of Chemical Physics in Moscow, 140 GHz high-field

EPR spectroscopy allowed Lebedev's group to determine the absolute sign of the triplet-state zero-field splitting parameter D by means of thermal spin polarization already at $T = 4$ K and, thereby, discriminate between triplet-state molecules and biradical pairs.

The enhanced low-temperature electron-spin polarization at high Zeeman fields allows to extract the absolute sign of the zero-field splitting parameter, D, of a two-spin system and thereby distinguish between a biradical and a triplet state—provided the sample temperature becomes comparable with the Zeeman temperature. For 140 GHz/5 T EPR, the Zeeman temperature, $T_Z = g\ \mu_B\ B_0/k_B$, (g: electron g-factor, μ_B: Bohr magneton, B_0: Zeeman magnetic field; k_B: Boltzmann constant), is approx. 6.5 K, i.e., already at liquid–helium temperatures the thermal spin polarization at $T < T_Z$ is sufficiently large to predominantly populate the lowest spin level, $m_S = -1$. This results in observable asymmetries of the powder EPR line shapes that are indicative of the sign of D [9]. At $T >> T_Z$, the characteristic triplet powder EPR spectrum (see Fig. 2) is symmetric at its low- and high-field sides and, hence, contains no information of the sign of D. At $T < T_Z$, the Boltzmann distribution leads to increased populations of the low-energy levels, resulting in asymmetric line shapes from which the absolute sign of D can be directly read off. Thermal spin polarization as a means to determine the absolute sign of D in high-spin systems has been used at a variety of EPR frequencies, for example at 9.5 GHz ($T_Z \approx 0.4$ K), at 95 GHz ($T_Z \approx 4$ K), 140 GHz ($T_Z \approx 6.5$ K), 360 GHz ($T_Z \approx 15.5$ K) [9].

In the following, we will summarize our first joint publication with Yakov Lebedev et al. on mechanochemically induced radical-pair formation in porphyrin–quinone and related donor–acceptor mixtures and compare the results with photochemically induced radical-pair formation of the same compounds [9]. It is noteworthy that the mechanochemical activation of polycrystalline mixtures of porphyrins and quinones

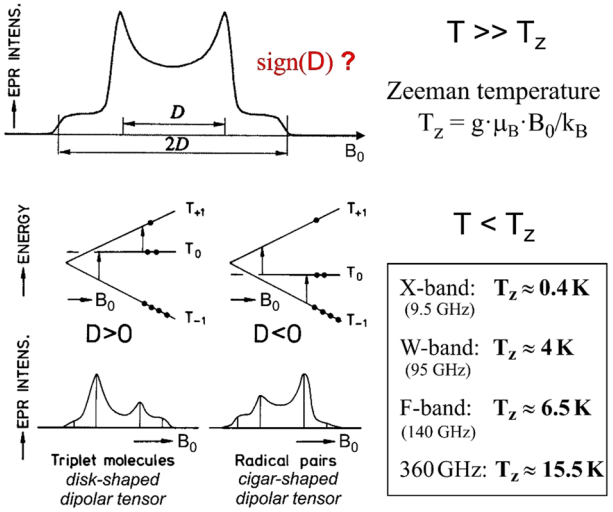

Fig. 2 Enhanced thermal spin polarization by high-field EPR, taking mechanically generated radical pairs in a donor–acceptor mixture as example. For details and original references, see [9]

produces large concentrations of triplet-state donor molecules as well as triplet-state donor–acceptor radical pairs with unusual stability in the solid-state matrix. The achieved concentrations of triplet species correspond to a conversion of as much as 1% of the initial porphyrin and quinone molecules into the stabilized radical pairs.

High-field/high-frequency (2 mm band) EPR experiments performed in Moscow revealed that below 10 K significant electron-spin polarization occurs from which the absolute sign of the zero-field splitting parameters D can be determined. They appeared to be positive ($D > 0$) in the case of tribochemically generated donor–acceptor radical pairs—in contrast to photochemically produced donor–acceptor radical pairs, for which the point-dipole approximation was confirmed to hold resulting in $D < 0$. To explain the experimental results, a matrix stabilization mechanism of exciplexes in the course of mechanochemically initiated electron (or hydrogen) transfer was postulated.

Now, we will discuss this work in some more depth, but for the experimental and theoretical details, we refer to the original publication [9]. Radical pairs (RPs) produced by light-induced electron transfer in porphyrin–quinones (P–Q) and similar donor–acceptor (D–A) complexes were very topical in the 1990s [10–19]—and continue to be so—nowadays even more so in view of the intensified efforts to cope with the global-warming climate catastrophe by means of high-efficiency solar-energy conversion. For instance, by applying Nature's strategies to optimize the primary electron-transfer mechanisms of photosynthesis [20–23]. For example, in the years between the 1990s and the 2010s, special attention was given to tailor-made porphyrin–quinone dyads and triads with either covalent bonds or hydrogen bonds between the donor and acceptor units, one of the compelling benefits was the fixed molecular position of D and A units at a controllable distance and mutual orientation [19, 20].

A non-standard way for the preparation of mixed solids in the excited state is the mechanical activation of crystallites of mixtures of suitable compounds by mechanical pressure with shearing deformation of surfaces [24]. As has been established for decades, chemical and physico-chemical reactions, under the heading "tribochemistry", can be initiated by applying mechanical energy to the system. Mechanical activation can result in numerous reactions including dislocations in crystal lattices, vibrational and even electronic excitations. Although known for a long time, the mechanisms of energy exchange processes and their quantitative description have remained widely unclear. This is not surprising, since crushing a crystal or a microcrystalline powder in a mortar represents a fairly indeterminate procedure in which elastic, plastic and fracture processes will come into play resulting in local high stresses and temperatures accompanied by shock waves and molecular reactions. It has been estimated [24] that mechanically induced dislocations of atoms and molecular fragments in the solid can store energy in excess of 10 eV which could trigger the emission of visible light ("triboluminescence").

In the present study, mechanical activation was achieved by grinding mixed micro-crystallite powders of Zn-tetraphenylporphyrin (Zn-TPP) and, for instance, substituted benzoquinone (about 1:1 v/v) in an agate mortar; the grinding was carried out at room temperature with a small addition of water to the powders to prevent electrostatic charging. After a chosen period of grinding (maximum RP yield

was obtained after about 6 min), the sample was dried and transferred to the EPR spectrometer. Whether the grinding was performed in an oxygen containing or an oxygen-free atmosphere had no noticeable effect on the RP generation process. In a first step, the kinetics of mechanochemical generation of radical pairs was systematically studied. The RP concentration was measured from the intensity of the EPR spectra. The high-field/high-frequency measurements were performed in Moscow with a home-built F-band (2 mm) spectrometer [25] using a home-built gas-flow system to control the sample temperature in the range 4.2–300 K.

As a typical example, the X-band (3 cm) EPR spectra of powdered Zn-TPP with benzoquinone, recorded after 6 min of grinding, are shown in Fig. 3. The observed four-peak lineshape of the $\Delta m_S = \pm 1$ EPR transitions in the field region around 310 mT (trace (a)) is indicative of axially symmetric systems with an $S = 1$ electron spin state; it is, therefore, attributed to radical pairs (or localized triplet molecules) with an axially symmetric zero-field splitting tensor. This assignment is corroborated by the observation of a narrow "half-field" EPR spectrum around 150 mT (see Fig. 3) since the appearance of this "forbidden" $\Delta m_S = \pm 2$ spectrum is characteristic for a triplet spin system in random orientation [26].

The EPR signals (bl and b2 in Fig. 3) in the central part of the $\Delta m_S = \pm 1$ spectrum originate from mono-radicals ($S = 1/2$), most probably from semiquinone ($Q^{\bullet -}$) anion radicals and Zn-TPP ($P^{\bullet +}$) cation radicals. While such stable mono-radicals, after mechanochemical excitation, are observed quite commonly, the formation of triplet-state RPs is, to the best of our knowledge, observed for the first time.

The kinetics of accumulation of radical pairs with grinding time always shows an induction period followed by a maximum at a grinding time of about 6 min.

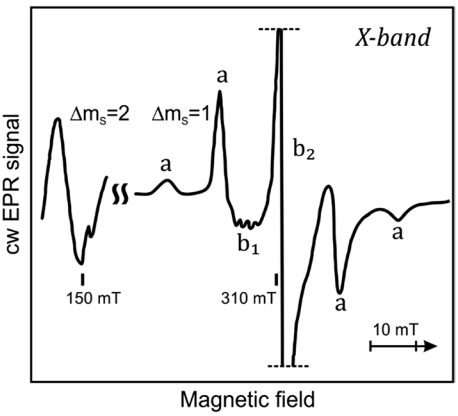

Fig. 3 First-derivative X-band (3 cm) room-temperature cw EPR spectra of a mechanically activated mixture of Zinc-tetraphenylporphyrin (Zn-TPP) with 3,5-di-tert-butyl-1,2-benzoquinone (Q) after 6 min of grinding in an agate mortar at room temperature. $\Delta m_S = \pm 1$ transitions of axially symmetric triplet state radical pairs (**a**) and of isolated mono-radicals (**b**1 and **b**2) are observed in the field region around 310 mT. In the half-field region around 150 mT the EPR spectrum of the "forbidden" transition $\Delta m_S = \pm 2$ of the triplet-state RP is shown (with 10×higher amplification). The ratio of the doubly integrated intensities, $A(\Delta m_S = 2)/A(\Delta m_S = 1) = 0.05 \pm 0.02$ is equal, within experimental error, to the ratio (D/B_0^2), as is indicative for triplet-state systems [26]

The first, typically autocatalytic, fraction of the kinetics may be related to that part of the grinding process that provides large friction interfaces of the microcrystals. At long grinding times the concentration of RPs drops, probably because of the destruction of the newly formed mixed crystals in which the RPs are stabilized. Consequently, there exists an optimum grinding time at which the maximum RP corresponds to a conversion of as much as 1% of the initial Zn-TPP and Q molecules into the stabilized radical pairs. The concentration of the doublet radical species changes only little during decay of the RPs. We conclude that RPs disappear mostly by charge recombination or by quenching of the triplet state by hydrogen atom transfer (hydrogen abstraction) and not by dissociation into the two mono-radical species. From an inspection of the data, we are tempted to suggest that electron and/or proton transfer or hydrogen abstraction are responsible for the mechanochemical generation of RPs. This suggestion is based on the fact that the RP generation ceases if the transfer channel is blocked either by prereduction or shielding of the quinone acceptor.

A definite proof that the observed EPR spectra belong to radical pairs or localized triplet molecules can be obtained by investigating spin polarization effects at low temperatures to extract the absolute sign of the zero-field splitting parameter, D. If the sample temperature T is low enough to fulfill the condition $T < T_Z = g\ \mu_B\ B_0/k_B$ which, for F-band EPR, corresponds to a Zeeman temperature $T_Z \approx 6.5$ K (see above), already at liquid-helium temperatures, the thermal spin polarization is sufficiently large to predominantly populate the lowest spin level, $m_S = -1$, and the EPR spectra of RPs become asymmetric.

An example of high-field/low-temperature EPR spectra ($\Delta m_S = \pm 1$, lines z and z'; x, y and x',y') of mechanically generated RPs is shown in Fig. 4. The asymmetry in the intensities of the $T_{-1} \rightarrow T_0$ and $T_0 \rightarrow T_{+1}$ transitions is clearly observed. This asymmetry justifies our assumption that the mechanically generated species are two-electron spin systems. Furthermore, the sign of the zero-field splitting parameter D appears to be positive (see above). This finding is rather unexpected, since for RPs with delocalized unpaired spins over the two mono-radical subunits, a negative sign of D is usually observed as long as the dipole–dipole approximation holds [27]. For delocalized triplet RPs, the situation is different from one-molecule localized triplet states for which both cases, $D > 0$ or $D < 0$, frequently

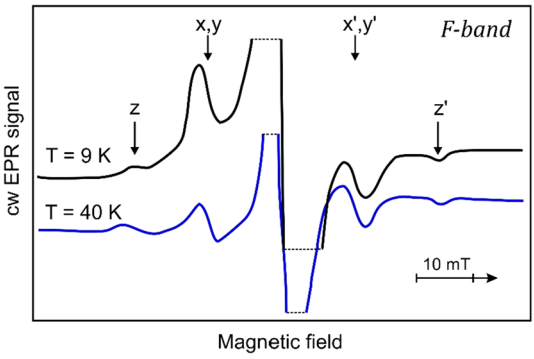

Fig. 4 First-derivative F-band (2 mm) low-temperature cw EPR spectra ($\Delta m_S = \pm 1$) of a mechanically generated radical pair in a *D–A* mixture (3,6-di-tert-butyl-catechol + 3,6-di-tert-butyl-1,2 benzoquinone), demonstrating that significant thermal spin polarization effects become observable already below 10 K. For details, see [9]

occur depending on whether the triplet electron-spin distribution is disc-like (oblate, i.e., axially compressed electron distribution) or cigar-like (prolate, i.e., axially elongated electron distribution) with respect to the main symmetry axis (see, for instance, [28]).

Thermal polarization experiments on triplet molecules had been performed earlier at 4 K and sub-helium temperature and X-band frequencies [29, 30], but not with RPs. Moreover, when working at $T < 1$ K, microwave saturation problems might render EPR spectra of systems with weak spin–lattice relaxation completely undetectable. In the present work, we demonstrate the possibility of studying thermal spin polarization effects in radical pairs at high magnetic fields at $T > 4$ K, and thereby easily determine the absolute sign of D by cw EPR, as was explained above.

To further corroborate this result of $D > 0$, we compared the experimentally determined sign of D of mechanochemically generated RPs with that of RPs generated in the traditional photochemical way. For that purpose, we used the quinone–hydroquinone donor–acceptor pairs since the photochemical yield of zinc TPP–quinone pairs decreases strongly at temperatures below the soft glass region. The comparison of the data shows that the mechanically generated RPs are always much more stable and have a "wrong", i.e., positive, sign of the zero-field splitting parameter. The "normal" negative sign of D was observed, however, for all photochemically generated pairs and for stable biradicals prepared by chemical synthesis.

We conclude and allow ourselves some speculations: the mechanochemically generated radical pairs are much more stable than those prepared by photoexcitation of similar *D–A* pairs in mixed crystals or solid solutions. The high-field/low-temperature EPR experiments show that in photochemically generated RPs the sign of the zero-field splitting D is always negative (as expected), while for mechanochemically generated RPs the zero-field splitting D is always positive (not expected).

The latter result suggests that the observed EPR spectra have to be attributed to some unusual triplet state aggregates. We postulate that these aggregates are some sort of "super-cooled" exciplexes, in analogy to jet-cooled photo-excitated intermediates. It is well established that mechanical activation of solids can produce sites of high local temperature initiating the formation of excited molecular states, followed by "tribo-induced" luminescence, charge transfer, etc. [24]. This mechanical activation can also result in a sharp acceleration of diffusion processes and phase transitions. The resulting chemical conversion is known to be similar to photo-irradiation-induced and high-energy-radiation-induced molecular conversion processes. From that point of view, the formation of radical and/or charge-transfer pairs, such as those observed here and in [31], is not surprising. What is surprising, however, is the large difference in lifetime and spectral properties of triplet states generated either mechanochemically or photochemically.

We speculate that the reason for the unusual stability could be that exciplex molecules $D^{\bullet+}A^{\bullet-}$ (charge-separated RPs) or $D^{\bullet}A^{\bullet}$ (neutral RPs), after being generated, are quickly built into a new crystalline lattice instantaneously formed by the mechanical activation. In this host lattice, the RPs adopt an energetically favorable arrangement, so that for the backward reaction to occur a large reorganization energy would be

required, i.e., this back reaction would be strongly retarded or even blocked by the new solid soft-matrix environment.

It is generally accepted that mechanical molecular activation occurs by the action of ultrasonic shock waves, which are created in micro-crystalline contact areas of sliding surfaces under tribochemical pressure [24]. Hence, the postulated model implies that, in the given contact site of molecular dimensions, the mechanical perturbation appears only for an ultra-short time in the picosecond range (the order of the molecular dimensions divided by the speed of sound). While most molecules can be mechanically excited and still move freely in the soft-solid matrix, some DA exciplexes might be formed which are immediately frozen into a local "new" solid matrix environment the moment the excitation zone has passed by. Thus, on a picosecond time scale, unusual exciplex intermediates may be stabilized by the mechanochemical activation. In the course of photolytic excitation, on the other hand, *D* and *A* stay fixed as individual molecules in the "old" crystalline lattice. In such a case, the unperturbed surrounding prevents formation of energetically favorable exciplexes which, evidently, do not correspond to the minimum energy of the "old" crystalline unit cell.

From the above considerations, we conclude that the observed EPR spectra of tribochemically excited *D–A* complexes cannot be attributed to ordinary RPs with the two unpaired electrons distributed over well-separated molecular frames. Instead, we have to assume that by mechanochemical activation trapping of triplet-state molecular complexes occurs in which the two electron-density clouds essentially overlap.

We realize, of course, that many questions remain open and many aspects of our interpretation of mechanochemically generated radical pairs and triplet molecules need further corroboration.

For this to accomplish, we had planned a series of additional multi-frequency/multi-resonance experiments on tribochemically generated radical pairs and we expected that there will be a long way to go for Yakov Lebedev and his new cooperation partners in the West after the changes of political paradigms in the East. On that way, a new joint research project was established between Moscow, Leiden and Berlin, specifically between the groups of Yakov Lebedev, Jan Schmidt and Klaus Möbius. It deals with the magnetic properties of metal–quinone high-spin complexes prepared by solid-state mechano-activation and liquid-state chemical synthesis. In the comparative study, high-field and low-temperature EPR and ENDOR techniques have been applied [32]. In the following, a brief summary of the results from this work will be given:

The magnetic properties of polyradical complexes containing diamagnetic metal ions have attracted considerable attention. Recently, it has been shown that such complexes can be prepared in a simple solid-state synthesis by a mechanically activated reaction between powdered metals and organic acceptor molecules [33–35]. Among the interesting aspects of these complexes is the magnetic interaction between the spin centers attached to the central metal ion and the possibility of spin alignment and organic ferromagnetism. 2 years earlier, we had demonstrated that EPR spectroscopy at very high frequency and low temperature is particularly well suited for studying such complexes with spin angular momentum $S > 1/2$, because the effect of thermal spin polarization can be observed already at liquid-helium

temperatures causing a high-field/low-field distortion of the lineshape of the EPR spectra (see above). By analyzing the lineshape, information can be obtained about the absolute sign and value of the electron dipole–dipole interaction (the zero-field splitting (ZFS) parameter, D). For porphyrin–quinone donor–acceptor complexes, it was found that in photochemically generated RPs the sign of the zero-field splitting D is always negative (as expected), while for mechanochemically generated RPs the zero-field splitting D is always positive, as is not expected [9].

For a qualitative explanation of these findings, it was assumed that "mechanolysis" (i.e., grinding of powdered donor–acceptor mixtures or the action of elastic waves) induces electron and/or proton transfer in the local surrounding quasi-liquid. This quasi-liquid exists locally for an ultra-short time allowing the most stable configuration of triplet intermediates to be produced. It will have a spin–spin interaction different from that of radical pairs generated by photoinduced proton transfer between partners in their fixed positions in doped crystals or glassy solutions. In this model the effect of mechanolysis of solid mixtures should resemble that of liquid-phase reactions with subsequent fast "freezing out" of the intermediate reaction products. Thus, the same properties might be expected for complexes generated mechano-chemically in a soft solid phase as for complexes synthesized in liquid-phase reactions provided the species produced in solution are sufficiently long lived.

In the present study on the spin–spin and exchange interactions within the complexes tribochemically formed within solid mixtures of quinones and metals, continuous wave (cw) and pulsed EPR as well as electron nuclear double resonance (ENDOR) spectroscopy were used, predominantly at high fields/high microwave and radio frequencies and at low temperature, to take advantage of the thermal polarization effect (see above). We compare the properties of metal–organic bi- and triradical complexes (triplet, $S = 1$, and quartet, $S = 3/2$, states) prepared by mechanical activation and by traditional liquid-phase chemical reactions of metal amalgams with quinones. As the solid mixtures of quinones the metals, M = Al, Ga, In, Cd, Sn, and Zn were investigated. The magnetic-resonance parameters and the observed thermal spin polarization provided evidence for the identity of the magnetic complexes produced in solutions and by solid-state mechanochemical treatment. In particular, the presence of ground-state triplet and quartet species could be demonstrated in both cases. In addition, the magnetic exchange and electron–electron dipole–dipole spin interaction parameters were evaluated, their comparison provided unique information about the electron spin configurations and intramolecular interactions.

The concentration, N, of triplet- or quartet-state species was determined at room temperature from the integral EPR absorption (doubly integrated EPR spectra) relative to the integral EPR absorption of a standard reference sample containing stable mono-radicals (doublet state, $S = 1/2$). Consideration was given to the dependence of the total EPR signal intensity, A, on the spin quantum number [36], which is different for the standard radical and for the high-spin complexes:

$$A \propto N \cdot (g \cdot \mu_B)^2 \cdot B_0 \cdot (k_B \cdot T)^{-1},$$

where $k_B \cdot T$ is the thermal energy; the other quantities had been introduced already (see above).

The EPR experiments were performed at Moscow, Leiden and Berlin using both commercial instrumentation (9.5 GHz) and home-built high-field spectrometers operating at 95 GHz [37, 38]. ENDOR experiments were carried out with laboratory-built instrumentation both at 9.5 GHz using cw excitation [39] and 95 GHz using pulsed excitation [37].

The wealth of results obtained in this comprehensive EPR/ENDOR study showed that at high field and low temperature the paramagnetic quinone–metal complexes created in solution by chemical reaction and in solids by mechanochemical action are characterized by the same magnetic-resonance parameters. The sign of the dipolar constant D was found to be negative for species with $S=1$ and positive for species with $S=3/2$. The experiments show that for these complexes, the equilibrium polarization of the spectral components agrees with an $S=3/2$ species rather than an $S=1$ species. ENDOR signals of the ^{27}Al nuclei and also other magnetic metal nuclei have been observed to support the suggested structure of the respective complex. Furthermore, the exchange parameters were evaluated for the Ga and Al complexes in diluted frozen solution. The results agree with the concept that the mechanochemical production of the complexes is similar to that in the liquid-phase reaction in combination with fast freezing or trapping of the products in the course of the tribochemical process.

Knowledge of the sign of D allowed us to assign the canonical peaks XX, YY, ZZ in the EPR spectrum, at high and low field, to the transition between the sublevels of the lowest electron-spin state. Apart from the thermal polarization method described above, ENDOR spectroscopy also enables this assignment.

If an EPR transition connects the states $|S, m_S>$ and $|S, m_S+1>$, the ENDOR frequencies for nuclear transitions within these manifolds are

$$\nu_{\mathrm{ENDOR}} = \nu_0 + m_S \cdot A_{ZZ} \text{ and } \nu_{\mathrm{ENDOR}} = \nu_0 + (m_S + 1)A_{ZZ},$$

where ν_0, is the Larmor frequency of the nucleus in the external field B_0 and A_{ZZ} is a principal component of the hyperfine interaction (HFI) tensor.

For systems with $S>1/2$, EPR transitions can be selected with both m_S and (m_S+1) of the same sign, i.e., ENDOR lines appear separated from each other on one side of the free nuclear Larmor frequency ν_0, at higher or lower frequency, depending on the sign of the HFI constant A_{ZZ}. Thus, if the sign of D is known, then the position of the ENDOR lines allows us to determine the sign of the hyperfine-interaction constants directly.

For instance, radical dimers with well-separated partners (e.g., radical pairs and biradicals) are characterized by a negative D. The EPR canonical peak at the lowest field position (the low-field "parallel" or Z-peak) and the high-field "perpendicular" or X-, Y-peaks (which for axial symmetry of the triplet molecule will coincide) correspond to the transition between the spin states ($|S, m_S>$), namely: $|1, -1> \leftrightarrow |1, 0>$, for which the ENDOR spectrum consists of the one dominant line at ν_0 from the $|1, 0>$ manifold and lines at frequencies $\nu_{\mathrm{ENDOR}} = \nu_0 + A_{ZZ}/2$ from the $|1, -1>$ manifold, i.e., positive HFIs correspond to a positive difference $(\nu_{\mathrm{ENDOR}} - \nu_0)$, see [26].

For molecular triplets with delocalized spins (e.g., photo-excitated aromatics) and radical trimers, a positive sign of D is expected, and the transition $|1,-1> \leftrightarrow |1,0>$ can be selected at the high-field parallel Z-peak or at the low-field perpendicular X-, Y-peak. From doing ENDOR on those transitions, the change of sign of D is accompanied by a change of sign of the difference $(\nu_{\mathrm{ENDOR}} - \nu_{\mathrm{o}})$. Thus, there are the two cases, either the sign of D is known but the sign of the HFI constant has to be determined, or the sign of D has to be determined, but the HFI constant is already known including its sign. In both cases, the corresponding line can be assigned in the ENDOR spectrum, and the sign problem can be solved. The "spin gymnastics" necessary for this to do is described in detail in [32], and we refer the reader to this work for further information.

We conclude the high-frequency and low-temperature EPR and ENDOR experiments on the metal–quinone complexes show that their production by mechanochemical action or by liquid-phase reactions leads to the same diradical and triradical species. They exhibit exactly the same magnetic-resonance parameters regardless of the method of generation. For all complexes described in this study, it is found that the high-spin state ($S=1$ for the diradicals and $S=3/2$ for the triradicals) is the lowest, i.e. there is a ferromagnetic coupling within the complexes. The sign of the dipolar coupling constant is $D>0$ for the triradical complexes and $D<0$ for the diradical complexes, which is in agreement with theoretical predictions.

The work described here appeared in the literature in 1996; it was this year when Yakov Lebedev died, at the height of his creative powers. How sad that he had to leave his family and friends so early, and so many ideas and unfinished projects behind him. We are still remembering our colleague and friend Yakov Lebedev with great esteem.

2 EPR and Pulsed-Laser Studies of Protein–Matrix Interactions in Biocatalysis

In this Review, we will summarize a few of our studies, based on high-field EPR, FTIR and fast-laser optical absorption spectroscopies, related to protein–matrix interactions and to the coupling between conformational protein dynamics and its electron-transfer function. To unravel the intimate association between solvent dynamics, internal protein motions and function, we focused on photosynthetic reaction center complexes incorporated into glassy matrices formed by the disaccharides trehalose or sucrose. The confinement of these membrane proteins within saccharide amorphous solid matrices has a twofold interest. First, by controlling the residual water content of the glassy system, the conformational dynamics of the embedded protein can be finely regulated at room temperature leading, under extreme dehydration, to a dramatic retardation of internal protein motions [40, 41] (see Sect. 2.2.1). Due to this extreme and simple tunability, it becomes, therefore, possible to investigate at room temperature the role of protein dynamics in specific catalytic events, avoiding the freezing of the protein to cryogenic temperatures to reduce internal protein motions. The low-temperature approach, which has been used in a number of fundamental studies on function–dynamics coupling (e.g., [42–45], has, however,

some drawbacks, related to the use of cryosolvents as, e.g., glycerol, employed to prevent the formation of ice crystals harmful to the protein integrity. Cosolvents, in fact, besides inducing subtle structural alterations in the native protein structure [46] lead, at cryogenic temperatures, to the formation of an amorphous solid matrix, making difficult to disentangle genuine temperature effects from those due to the increased rigidity of the protein environment. On the contrary, the room temperature incorporation of the protein into a glassy matrix formed by trehalose, can be considered a kind of "soft" confinement, in that it minimally perturbs the native structural configuration of the protein, as shown for two different reaction center complexes by high-field EPR spectroscopy [47, 48] (see Sects. 2.2.1 and 2.2.2). Among the many advantages of trehalose–protein glassy matrices, it has to be mentioned that the incorporation into extensively dehydrated trehalose glasses promotes a tremendous thermodynamic stabilization of the incorporated protein, preventing its thermal denaturation at room (and even higher) temperatures for periods as long as several months [49].

The extraordinary bioprotective capabilities of trehalose, bring us to the second motivation for the strong interest in disaccharide–protein glassy systems. Indeed, the use of trehalose glassy matrices in the study of biocatalysis and conformational dynamics of carboxymyoglobin, pioneered by the works of Eaton [50, 51] and Cordone and coworkers [52, 53], was originally inspired by the natural phenomenon of anhydrobiosis, in which the biopreservation properties of disaccharide glasses are deeply involved (see Sect. 2.1). Several organisms, including plants, yeast, nematodes and tardigrades, are able to survive extremely harsh, adverse environmental conditions, as almost complete water loss and high temperatures, by entering reversibly a state of suspended metabolism, called anhydrobiosis or cryptobiosis [54]. Most anhydrobiotic organisms, in response to desiccation and heat stress, synthesize massive amounts of disaccharides (mainly trehalose and/or sucrose) resulting in the formation of "biological glasses" which embed and fully preserve cellular components, enabling a state of suspended animation [55]. Following rehydration, even after very long periods of drought and extreme temperatures, as typical of hot desert climates, anhydrobiotes resume their metabolism. The so-called "resurrection plants", as *Selaginella lepidophylla*, are emblematic of this anhydrobiotic behavior.

In the study of matrix–protein interactions, particularly when using as model membrane-proteins photosynthetic reaction centers (bacterial reaction center, Photosystem I, Photosystem II), the combination of high-field EPR, FTIR and time resolved-laser optical absorption spectroscopies proved to be optimal in providing complementary information in terms of structure, dynamics and composition of the system. Since the photocatalytic activity of photosynthetic reaction centers involves the formation of cofactor ion radicals as well as charge-separated radical pairs (see Sects. 2.2.1, 2.2.2), high-field EPR at W-band (95 GHz, 3.4 T) is ideal in detecting the transient states of electron donor and acceptor cofactors with the required sensitivity and time resolution, because of the high resonance frequency [3]. Remarkably, light-induced electron transfer within the reaction center results, for donor and acceptor cofactors, also in absorption changes in the visible and NIR spectral range (see e.g., [56, 57]), thus allowing for an independent detection of charge-separation and -recombination events by laser

time-resolved optical absorption spectroscopy. Since the sample requirements for optical and EPR measurements are different, for instance in terms of concentration and paramagnetic perturbation, the agreement between electron transfer kinetics detected by EPR and optical spectroscopy is of particular significance.

High-field EPR offers additionally powerful tools to obtain structural and dynamical information both on the reaction center cofactors and on the embedding matrix. W-band transient EPR (TR-EPR) signals from the spin-correlated radical pair, produced by charge separation between the primary donor and acceptor cofactors, are in fact sensitive to the geometry of the cofactor pair [58]; they can, therefore, reveal possible alterations in the cofactor configuration due to incorporation of the reaction center protein into the dehydrated matrix. Additionally, in bacterial reaction centers, dynamical information is conveyed by the T_2 relaxation times of the primary photo-reduced quinone acceptor and their anisotropy, measured by ESE-detected high-field EPR, which sensitively probes the librational fluctuations of the semiquinone anion in its binding pocket [59], and possible alterations in the cofactor local dynamics due to matrix interactions. Finally, high-field EPR of nitroxide spin probes, either site-specifically attached to the protein or dissolved in the amorphous disaccharide-reaction center matrix, can be used to retrieve information on the hydrogen-bonding properties of the matrix, and specifically on the structural and dynamical homogeneity or heterogeneity of the nitroxide microenvironment. The EPR spectrum is in fact very sensitive to the rotational motion of the nitroxide probe, because the time-scale of its dynamics determines the extent of averaging of the magnetic interaction anisotropies [60].

As mentioned above, the content of residual water of the glass is an important parameter, in that it finely tunes the degree of immobilization of the matrix-embedded protein. The hydration level of the system can be strictly controlled by an isopiestic approach based on the equilibration of the matrix with an atmosphere of definite relative humidity in the presence of different saturated salt solutions [61]. The residual water content can be conveniently determined by FTIR spectroscopy of the water combination band appearing around 5150 cm^{-1}. The area below this band has been proven in fact to be proportional to the water concentration with an absorptivity coefficient independent of the presence of cosolvents, of the physical state of the water sample (solid or liquid), and therefore on the extent of hydrogen bonding [61]. At variance, the association band of water, around 2130 cm^{-1}, due to its intermolecular character, mirrors the interaction of water molecules with their neighbors. The band is attributed to the combination of bending and libration modes [62]. Since these modes are extremely dependent on the molecule's microenvironment, the association band of water, in binary or ternary systems at low water content, becomes structured, due to the vibrational coupling with non-water hydrogen-bonding groups [63, 64]. As a consequence, the band can provide qualitative information on the structural and dynamical organization of the water–disaccharide–protein matrix, complementing the picture emerging from the lineshape analysis of the nitroxide radical EPR spectrum.

In the following sub-chapter, we will shortly overview some aspects of anhydrobiosis, focusing on the nature of the protein–disaccharide interactions and on

the molecular mechanisms which have been proposed to explain saccharide-based biopreservation.

2.1 Anhydrobiosis—Life Without Water Enabled by Proteins Embedded in Trehalose Soft Matrices

Water is an essential component of life, primarily to ensure metabolism, and the vast majority of organisms will die upon complete drying. For most plants and several animals only specialized structures, which characterize a specific phase of their life cycle, such as encysted embryos in crustaceans or seeds or pollen in vascular plants [65], are able to tolerate an almost complete removal of water. However, several organisms (epitomized by resurrection plants as cushion mosses, rotifers, and tardigrades) have developed the ability to withstand a severe water deficit in any phase of their life cycle, and in their apparently unspecialized, vegetative tissues [54]. These species (anhydrobiotes), upon removal of intracellular water, survive as desiccated material, entering a state of suspended life. The period of arrested animation and metabolism can last as long as decades, or centuries, and, when normal water availability is restored in the environment, they resume metabolic activity and life. Anhydrobiotes are distributed among the three domains of life—Archaea, Bacteria, and Eukarya [66].

The intriguing phenomenon of *anhydrobiosis* is known since a long time. It was discovered in 1702 by Antonie van Leeuwenhoek (1632–1723) from Delft, who was the first to describe "animalcules" (most likely rotifers), found in dry dust from a roof gutter, which, when rehydrated, surprisingly resumed animation. Going through cycles of draught and rehydration, van Leeuwenhoek observed, with his single-lens microscopes, that the phenomenon was reproducible, even following desiccation periods lasting for many months [67]. Interestingly, about 70 years after van Leeuwenhoek's discovery, Lazzaro Spallanzani (1729–1799) from Bologna revisited the phenomenon of anhydrobiosis of rotifers. Astonishingly ahead of his times, he established the essentials of anhydrobiosis, i.e., that rotifers did not retain water and stopped all life processes upon desiccation. At variance with van Leeuwenhoek, who believed that anhydrobiotic species (rotifers) were protected by a kind of impermeable coating, avoiding any evaporation of water from the organism, Spallanzani realized that in the anhydrobiotic state rotifers were indeed extensively dehydrated and that they underwent a transition to a fragile solid, that could be splintered like a "salt particle". This qualitative observation, reported in 1776 in the "Opuscoli di Fisica Animale e Vegetabile" ("Tracts on the natural history of animals and plants"), anticipated the current concept that, upon desiccation, anhydrobiotic organisms undergo a glass transition [68].

Glass formation has been unequivocally demonstrated to exist in dry systems in vivo and to be closely associated to subcellular stabilization in the dry state. An emblematic example is provided by the African chironomid *Polypedilum vanderplanki*, which can be considered the largest multicellular animal capable of anhydrobiosis. An elegant study by Sakurai and coworkers [69], by combining differential scanning calorimetry and FTIR spectroscopy, showed that the anhydrobiotic

larvae of *Polypedilum vanderplanki* survive extreme dehydration by forming a biological glass, i.e., a supersaturated liquid with the mechanical properties of a solid that prevents the crystallization of cellular solutes. Additionally, optical and FTIR imaging revealed that as larvae dehydrate, they synthesize and accumulate large amounts of trehalose, uniformly distributed throughout the dehydrated body, confirming the essential role of this disaccharide in vitrification and consequently in successful anhydrobiosis. Studies in vivo have indeed led to a widespread consensus that the building of stable intracellular glasses by many anhydrobiotic organisms is made possible by the accumulation of disaccharides (mainly trehalose and sucrose), which, in some organisms, may act in combination with the synthesis of highly hydrophilic, intrinsically disordered proteins, as "late embryonic abundant" (LEA) proteins [70], or "cytosolic abundant heat soluble" (CAHS) proteins in tardigrades [71]. Currently, there is a particular interest for research on the dynamics and interactions of intrinsically disordered proteins involved in the regulation of key cellular signaling pathways. Modern biochemical and biophysical techniques are being used to probe the mechanisms by which intrinsically disordered regions of cellular proteins achieve synergetic advantages by interacting with structured protein domains for regulating their biological functions.

The essential role played in anhydrobiosis by trehalose and sucrose has triggered a profusion of in vitro studies, focused upon the physico-chemical properties of amorphous matrices formed by disaccharide and macromolecules, aimed, on one side, to exploit the technological potential of their extraordinary effectiveness in protecting and stabilizing biostructures, and, on the other side, to grasp the underlying molecular mechanisms and interactions. The former studies have translated into many useful and new applications in the fields of pharmacology, biotechnology and biomedicine [72, 73]. As an example, stabilization of an increasing number of therapeutic proteins [74], available for the treatment of cancers, diabetes, or brain diseases, relies on sugar-based glassy matrices [75, 76]. As to the latter studies, in spite of the considerable efforts devoted to unraveling the mechanisms of disaccharide stabilizing effects on macromolecules at the atomistic level, no clear definitive scenario has emerged, and a number of questions remain open to a lively debate.

In particular, the structure and dynamics of glassy matrices constituted by proteins and disaccharide have received a wide interest. Extensive experimental work, employing a wide range of spectroscopic and thermodynamic approaches, such as FTIR [77], Raman [78], neutron and X-ray scattering [53, 79, 80], EPR [47], differential scanning calorimetry [81, 82], and theoretical investigations, based on molecular dynamics simulations [83–85], have led to the generally accepted idea that a tight dynamic coupling is set up between the embedded protein and the sugar matrix when the residual water content is reduced. This coupling entails that internal motions of the protein, which fluctuates over a large ensemble of hierarchically organized conformational sub-states [86], are governed by the dynamics of the water–matrix system. As a result of stiffening of the glassy system induced by dehydration, the protein conformational dynamics is, therefore, expected to be strongly inhibited, thus retarding, or even precluding, on a long time-frame, protein unfolding and denaturation. What is at present still unclear is the precise nature of

the interactions responsible for the tight dynamical protein–matrix coupling and the underlying structural organization of the system.

During the last decades, different hypotheses have been articulated, in which different interactions are considered to play a determinant role in protein stabilization. The "vitrification" or "high viscosity hypothesis" [87] assumes that the extremely high viscosity of the glassy sugar matrices causes by itself a dramatic slowing of the internal protein dynamics. Since unfolding requires molecular mobility of the protein, vitrification, which also minimizes the rate of detrimental chemical reactions, is considered sufficient to prevent structural damages and protein denaturation. In this respect, the glass-transition temperature of the sugar matrix, T_g, at the specific hydration of the matrix in which the protein is incorporated and stored, becomes the critical parameter, because the glass relaxation processes of the glassy matrix (see below), i.e., the internal mobility of the system, are expected to scale with the difference between the storage temperature and T_g. Notably, trehalose–water systems exhibit a significantly higher T_g at all water contents as compared to other similar saccharide–water mixtures [88]. This feature has been put in relation with the superior efficacy of trehalose in protein stabilization, as compared to other saccharides (e.g., maltose, fructose, sucrose). However, further studies have provided experimental evidences that carbohydrates, such as maltodextrin, with T_g values considerably higher than those of trehalose, are less effective in stabilizing proteins [89], and that, in general, the high macro-viscosity of sugar glasses is not sufficient to assure stabilization of the dehydrated system [90–92]. These findings have an in vivo counterpart, since a number of species exist with seeds and pollen that cannot survive water removal, although their cytoplasm transforms into glass in the dry state [93]. These observations suggest that the glassy state is necessary but not sufficient to ensure a good protein stabilizing environment, and that additional factors must be taken into account, as for instance direct interactions between the stabilizing co-solute and the protein.

The most direct interaction would be the formation, upon water removal, of hydrogen bonds between the protein and the sugar of the glassy matrix, as postulated by the "water replacement hypothesis". According to this model [94], the bound sugar molecules would in fact replace the water molecules of the hydration shell, thus preserving the hydrogen bond interactions which are thought to determine the native protein conformation. That such a simple, direct, sugar–protein interaction occurs with high probability and can play a role in anhydrobiotic protein stabilization has been, however, questioned on the basis of thermodynamical considerations [95], experimental results [96, 97], and molecular dynamics simulations [85, 98]. These studies have led to propose a different scenario ("water entrapment" or "preferential hydration" model) [96, 99–101], in which disaccharide molecules are essentially excluded from the protein surface. The native protein hydration shell, rather than replaced, would be maintained, at least partially, and would mediate the dynamical coupling between the protein and the sugar matrix.

It should be noticed that the above described models are not mutually exclusive, in the sense that the protein–matrix interactions postulated by them could in principle coexist and contribute to a different, but significant extent to condition the protein conformational dynamics. A synthesis has been attempted by proposing a model

("anchorage model") which incorporates and combines features from the three hypotheses [102]. The model retains from the "water replacement" hypothesis the idea that hydrogen bonding is the prevailing interaction responsible for the dynamical protein–matrix coupling, but assumes that such interaction involves mainly the hydration shell of the protein (a feature shared with the "preferential hydration" hypothesis), which is assumed to connect via multiple bonds surface amino-acid groups of the protein with sugar molecules in the matrix, while trehalose molecules make few direct hydrogen bonds to the protein. Stable hydrogen bonds are also assumed to bridge, upon desiccation, disaccharide molecules in the bulky matrix, which will be stiffened, and, being dynamically coupled to the protein through its hydration layer, will give rise to a highly integrated glassy system locking the protein surface and determining its extraordinary stabilization. The immobilization of the protein is thus determined by an extended, highly connected network of hydrogen bonds, which is expected to become progressively more rigid as the content of residual water is decreased.

The conformational locking of protein dynamics within trehalose glasses, although very effective, can be regarded as a "soft confinement" [103], being mediated by the hydration shell of the protein, which, as we will see in Sects. 2.2.1 and 2.2.2, gently preserves and stabilizes the native protein structure, minimizing perturbations of the protein spatial configuration. Interestingly, an infrared vibrational-echo study performed in myoglobin has indicated that fixing the protein surface topology by a solid external matrix dramatically hinders also internal protein structural fluctuations [104]. In line with this conclusion, and with a tight dynamical coupling between the protein and its hydration layer, molecular dynamics simulations performed in aqueous solution of ribonuclease A, showed that, when the translations of water molecules in the hydration shell were turned off, atomic fluctuations were strongly reduced throughout the entire protein [105]. More recently, surface and core dynamics of a small globular protein have been studied in parallel through a combination of isotope labeling and neutron scattering [106]. Consistent with the assumption of the "anchorage model", it has been found that dynamics probed in the interior of the protein and at the surface exhibit comparable behavior as a function of temperature and hydration.

The "anchorage model" was proposed on the basis of molecular dynamics simulations performed on systems formed by trehalose and carboxymyoglobin at low water content; they showed that the amplitude of the nonharmonic motions of protein atoms, stemming from the interconversion among high tier conformational substates [107], are reduced with respect to hydrated systems [83], and that the fraction of water molecules of the protein hydration shell involved in multiple hydrogen bonds with both surface groups of the protein and matrix sugar molecules, increases by decreasing the water content, implying a progressively tighter dynamical coupling between the trehalose matrix and the "anchored" protein [98]. These views have been supported by many experimental results obtained by FTIR spectroscopy [77, 108], spectrally resolved infrared stimulated vibrational-echo spectroscopy [109], neutron scattering combined with molecular dynamics [85, 99], EPR spectroscopy [47, 48, 110], and time-resolved optical absorption spectroscopy [49, 102, 111–113].

The "vitrification hypothesis" ascribes the protein immobilization capability of disaccharide–protein matrices to the inhibition of the dynamics of the sugar-glass which is governed by the α dielectric relaxation time, τ_α. For a homogeneous medium, τ_α can be thought of as the reorganization time of the material on the molecular scale [114, 115]. Cicerone et al. [92] have challenged the existence of a simple correlation between the α dielectric relaxation time and the biopreservation by disaccharide glasses, observing that protein stability within sugar glasses rather correlates with high-frequency β relaxation processes. High-frequency dielectric relaxations in glasses are characterized by two distinct time scales: fast β relaxations, with times in the picosecond time scale, are related to exploration of the molecular cage of neighbors, while the slower, Johari–Goldstein β relaxations, taking place on time-scales of microseconds to milliseconds, are considered to reflect small amplitude intermolecular motions [116–118]. The correlation found between the retardation of protein dynamics and β relaxation times of the embedding glass is consistent with the notion that local protein motions, such as those involving amino-acidic sidechains, are "slaved" to the high-frequency β dynamics of the protein hydration shell [119].

The tight coupling with fast β fluctuations of the glass puts into play the well-established spatial heterogeneity in the structure and dynamics of super-cooled liquids and glasses [115, 120]. Remarkably, in fact, glass inhomogeneities, involving for instance local stiffness and elastic constant, are thought to occur on a spatial scale comparable to that of the protein [120, 121]. Such inhomogeneities are therefore expected to impact significantly the local conformational degrees of freedom of the protein. High-field W-band EPR spectroscopy of nitroxide radicals is a powerful tool in investigating the structural and dynamical homogeneity or inhomogeneity of glassy matrices at the molecular scale (see Sect. 2.2). By this approach, we have found, in agreement with the above considerations, that homogeneity/inhomogeneity in the local dynamics of a disaccharide glassy matrix is a critical parameter in determining the degree of protein immobilization, providing a plausible explanation for the different efficacy and modalities of trehalose and sucrose matrices in protein stabilization (see Sect. 2.2.1).

2.2 High-Field EPR and Fast-Laser Spectroscopy of H-Bond Interactions in Membrane Proteins

In the present Review on studies of protein–matrix interactions between disaccharides and membrane protein complexes, we focus on high-field EPR spectroscopy (we define "high-field/high-frequency" as at least one order of magnitude higher than used in conventional X-band EPR, 9.5 GHz/0.34 T), FTIR spectroscopy as well as on fast and ultrafast laser spectroscopy. The excitation sources in these spectroscopic methods are operated either in cw (continuous wave) mode or in pulse mode.

In time-resolved optical or EPR spectroscopy, ultrashort-pulse or short-pulse lasers are used to study molecular dynamics, structural changes or charge-recombination kinetics in different time windows with scales ranging from hundred femtoseconds to hundreds of picoseconds, from ten nanoseconds to several microseconds.

Vastly different spectroscopic methods are applied, spanning vastly different time scales and photon energy ranges, to examine the dynamics of charge carriers, atoms, and molecules, probing, for example, characteristic molecular bond vibrations of various functional groups in organic and bioorganic molecules. Or measuring the kinetics of $P^{\bullet+}Q^{\bullet-}$ charge recombination of light-induced donor–acceptor radical pairs in photosynthetic electron-transfer reactions either by optical or EPR methods. This was achieved, for example, by optical laser absorption spectroscopy monitored at 422 nm [122] with an apparatus of laboratory design in Bologna [102]. Pulsed photoexcitation was provided by a frequency-doubled Nd:YAG laser that delivered 150 mJ pulses of 7 ns width. From 2 to 25 kinetic signals were averaged, depending on the sample, with a dark adaptation of at least 1 min between successive single photoexcitations. In measurements performed on Photosystem I and Photosystem II samples, the frequency-doubled Nd:YAG laser was used to pump a sulforhodamine B dye cavity emitting at 587 nm, and the transient absorbance changes of $P^{\bullet+}$ were measured at 820 nm [48].

FTIR absorption measurements were performed at 297 K using a commercial Fourier transform spectrometer; using in the mid-IR range (7000–1000 cm^{-1}) a standard high-intensity ceramic source, when extended to the NIR region (15,000–2200 cm^{-1}), using a halogen lamp source and replacing the beam splitter and the exit interferometer window with adequate components. The spectra were recorded with a resolution of 4 cm^{-1}, accumulating 10^2 or 10^3 scans per spectrum depending on the signal-to-noise ratio. The content of residual water in the sugar matrices used in the FTIR measurements was estimated from the area under the $(\nu_2+\nu_3)$ combination band of water around 1940 nm, essentially as described in [61]. The area under this band can be taken to be proportional to the water concentration, being unaffected by cosolvents, by the physical aggregation state of the sample and, in particular, by the extent of hydrogen bonding (see [61] and references therein).

Specifically, in ultra-fast optical laser work on matrix hydrogen-bonding effects in membrane proteins, pump-probe laser spectroscopy in the time domain from 100 fs to 600 ps as well as time-resolved absorption spectrometry at 480 nm and 830 nm with time resolution > 10 ns were used. In this way, characteristic factors governing guest–host interactions could be measured to elucidate the effect of trehalose glassy matrix on the light-induced forward electron-transfer kinetics of the formation of primary and secondary donor and acceptor ion radicals and radical pairs in RC complexes of non-oxygenic and oxygenic photosynthesis. In the femtosecond laser photolysis work, transient absorption spectra were measured using a femtosecond pump setup coupled to a supercontinuum probe setup of laboratory design in Moscow.

The occurrence of paramagnetic intermediates in electron-transfer reactions such as the light-induced radical ions of donors and acceptors, enables the use of EPR spectroscopy and its electron-nuclear and electron–electron double-resonance variants to extend and complement the results of optical spectroscopy with the aim to obtain a better understanding of protein–matrix interactions on the atomic and molecular level. In principle, EPR is a promising spectroscopic technique to study both stable and transient radicals or radical-pair intermediates. In practice, however, for large spin systems in solid-state disordered matrix environments, standard

X-band EPR (9.5 GHz, 0.34 T) soon reaches its resolution limits for useful information on magnetic interaction parameters and molecular orientations, which is hidden under inhomogeneously broadened EPR lines. By going to higher and higher magnetic fields and microwave frequencies, for example, to W-band EPR at (95 GHz, 3.4 T), at least five important features, (i), (ii)–(v), are emerging from the EPR spectra (see, for instance, [2, 3, 123, 124]): (i) enhanced spectral resolution; (ii) enhanced orientational selectivity; (iii) enhanced low-temperature electron-spin polarization; (iv) enhanced detection sensitivity for restricted-volume samples such as membrane proteins; (v) enhanced sensitivity for probing fast motional dynamics, that is, high-frequency EPR acts as a faster "snapshot" recorder for molecular motion than low-frequency EPR.

*A*d (i): with increasing external magnetic field the field-dependent spin interactions (electron Zeeman interaction, nuclear Zeeman interaction) in the spin Hamiltonian are separated from the field-independent ones (hyperfine and quadrupolar interactions, spin–spin interactions).

Ad (ii): enhanced orientation selectivity by high-field EPR on randomly oriented spin systems becomes essential for organic radicals with only small g-anisotropy (see Fig. 5). If in disordered powder-type samples the anisotropy of the leading spin interaction is larger than the inhomogeneous linewidth, the canonical orientations (g_{xx}, g_{yy}, g_{zz}) of the dominating Zeeman interaction tensor can be resolved. As a consequence, single-crystal like information on the hyperfine interactions can be extracted by performing orientation-selective ENDOR (electron–nuclear double resonance) at the magnetic field values of resolved spectral features. In case of transition-metal complexes, the hyperfine anisotropy of the metal ion may provide this orientation selectivity from the entire orientational distribution of the molecules.

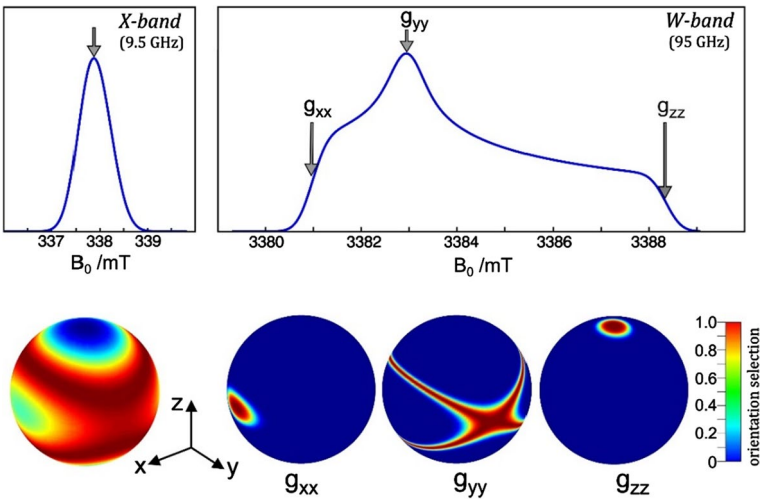

Fig. 5 Enhanced orientational selectivity by high-field EPR, taking the anion radical of the ubiquinone acceptor cofactor, $Q_A^{\bullet -}$, in frozen-solution bacterial photosynthetic reaction centers as example. Standard X-band (9.5 GHz) EPR spectra are compared with W-band (95 GHz) EPR spectra. For details, see [3]

Ad (iii): The enhanced low-temperature electron-spin polarization at high Zeeman fields allows to extract the absolute sign of the zero-field splitting parameter, D, of a two-spin system like a biradical or triplet state (for details, see Sect. 1.2).

Ad (iv): The absolute EPR sensitivity is defined by the minimum detectable number of spins in the sample, N_{min}; the relative (or concentration) sensitivity is given by $N_{\mathrm{min}}/V_{\mathrm{S}}$, i.e., is scaled by sample volume, V_{S}. This is limited by the amount of sample that can be introduced into the cavity of high-field EPR spectrometers which, of course, is usually significantly smaller than standard X-band cavities. Thus, if the amount of sample available is limited like in high-purity protein preparations, the sensitivity of high-field EPR can be superior, with respect to X-band EPR, by orders of magnitude. Under certain experimental conditions, for constant incident microwave power and unsaturated EPR lines, one obtains theoretical expressions for the absolute sensitivity, $N_{\mathrm{min}} \propto \omega_0^{-9/2}$, and for the relative sensitivity, $N_{\mathrm{min}}/V_S \propto \omega_0^{-3/2}$ (where ω_0 is the spin-resonance frequency; see the detailed sensitivity discussions in [3]).

Ad (v): the faster "snapshot" capability for complex motional dynamics with increasing EPR frequency can be used in a multifrequency continuous-wave (cw) EPR approach at the same temperature to probe fast internal modes of motion and to discriminate them from the slow restricted motion of a macromolecule in solution. In high-frequency cw EPR spectra, slow motions appear to be frozen out, whereas fast motions dominate the observed spectral lineshape.

The W-band EPR measurements were performed with a laboratory-built spectrometer (first in Berlin, since 2010 continued in Mülheim) [3, 38, 125–128] operating in both cw and pulsed modes of microwave excitation. For different EPR experiments, it was necessary to construct different types of microwave cavities with optimized sensitivity and time-resolution performances: For cw EPR experiments a gold-plated bronze cylindrical TE_{011} cavity was used (loaded quality factor $Q_{\mathrm{L}} = 2400$ of the empty cavity. For pulsed EPR experiments applying $\pi/2$-pulses and π-pulses, for which the highest possible microwave field B_1 at the sample position is required, a special TE_{011} cavity with high Q is used. The cavity body was machined from pure gold (99.9%) to minimize resistive losses in the cavity walls. A room-temperature unloaded $Q_{\mathrm{U}} = 7400$ was measured without sample. The overall time resolution of the W-band pulse EPR spectrometer was measured to be better than 10 ns·when using the fully available excitation mw power. For direct-detection W-band time-resolved (transient) EPR (TR-EPR) measurements, the time resolution of the heterodyne detection channel of about 2 ns and the short ringing time of the EPR cavity of about 6 ns provide an overall time resolution that is an order of magnitude higher than for X-band TR-EPR. For optical sample irradiation, the light was guided to the center of the cavity through a quartz fiber of 0.8 mm diameter. The electron transfer was initiated by singlet excitation of the primary donor in bacterial reaction centers at 532 nm using a frequency-doubled Nd:YAG laser which was self-assembled from various commercial components (5 ns pulse length, 1–10 Hz repetition rate, 0.5 mJ/pulse on the sample surface) or at 690 nm using a cw diode laser (25 mW output, 10 mW on the sample surface).

In Fig. 6, the EPR experiments on laser-pulse generated radicals and radical pairs are summarized showing the microwave (mw) and radiofrequency (rf) irradiation

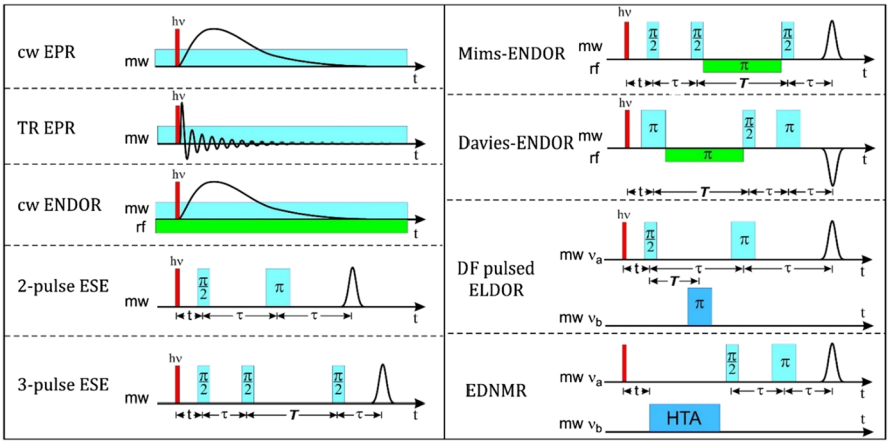

Fig. 6 Microwave (mw) and radio-frequency (rf) cw and pulse irradiation schemes of various time-resolved EPR techniques. For photochemical EPR applications, the initial laser excitation pulse hν starts the photo-reaction creating paramagnetic intermediates. *cw* continuous wave, *TR* transient, *ENDOR* electron–nuclear double resonance, *ESE* electron spin echo, *DF* dual frequency pulsed ELDOR, *PELDOR* pulsed electron–electron double resonance, also called DEER, *EDNMR* ELDOR-detected NMR, HTA (high turning angle pulse). Adapted from [129]

schemes of a variety of cw and pulse high-field EPR techniques that are dealt with in this Review (for stable paramagnetic systems, the laser pulse is, of course, omitted).

A rich variety of microwave pulse sequences and sophisticated experimental setups is found in more recent text books, for example those by Arthur Schweiger and Gunnar Jeschke [130]; Oleg Grinberg and Larry Berliner [2], Klaus Möbius and Anton Savitsky [3], and in the recent EPR compendium edited by Daniella Goldfarb and Stefan Stoll [131].

2.2.1 Bacterial Reaction Centers

The photosynthetic reaction center (RC) from the purple bacterium *Rhodobacter* (*R.*) *sphaeroides* is an integral membrane pigment–protein complex that catalyzes the primary photochemical events of photosynthesis. It initiates the conversion of solar energy into chemical-free energy by promoting a sequence of intra-protein electron-transfer reactions which leads to the separation of electrical charge over a ~ 30 Å distance across the membrane. The RC protein is composed of three subunits, called L, M, and H. The scaffold formed by the first two subunits binds non-covalently the following cofactors: four bacteriochlorophylls (BChl), two bacteriopheophytins (BPh), two quinones, and a non-heme iron in the form of Fe^{2+}. As depicted in Fig. 7a, the bacteriochlorin molecules and quinones (Q_A and Q_B) are organized into two symmetrical branches, approximately related by a twofold rotation axis which connects the special bacteriochlorophyll pair P_{865} with the Fe^{2+} ion (for reviews, see [132, 133]).

Despite this symmetrical arrangement, electrons are transferred only along the branch of cofactors most closely associated with the L subunit (the so-called L or

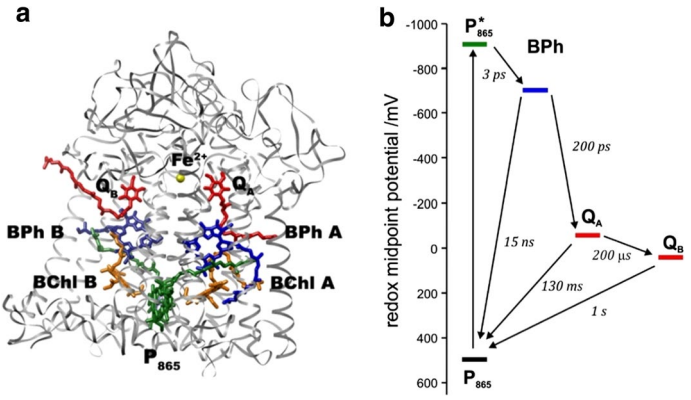

Fig. 7 **a** X-ray structure of the reaction center from *Rhodobacter* (*R.*) *sphaeroides* R-26. **b** Energy and kinetic diagram of the excited and charge-separated states involved in the RC electron transfer reactions. Both forward electron transfer and recombination time constants at room temperature are given. Information was taken from references [132–136]

A branch). As schematized in Fig. 7b, light absorption results in the excitation of the bacteriochlorophyll pair P_{865}, which serves as the primary electron donor, and within a few picoseconds delivers an electron, via the interposed monomeric bacteriochlorophyll, to the bacteriopheophytin (BPh A). This is followed by electron transfer to the primary quinone acceptor, Q_A, in approximately 200 ps, and, subsequently to the secondary quinone, Q_B, within ~ 200 µs. The quantum yield of this charge-separation process is essentially one. In RCs that lack a quinone at the secondary acceptor site Q_B, the electron on the photo-reduced $Q_A^{\bullet -}$ recombines with the hole on $P^{\bullet +}$ by direct electron tunneling with a rate constant of approximately 10 s^{-1}. Recombination from the secondary quinone Q_B proceeds predominantly by thermal repopulation of $Q_A^{\bullet -}$ with a time constant of ~ 1 s.

If myoglobin has been considered the archetypal model system in the study of function–dynamics relationships in soluble proteins ("Myoglobin: The hydrogen atom of biology", as stated by Frauenfelder et al. [137]), the bacterial photosynthetic reaction center can be regarded as the paradigmatic model protein when analogous problems are discussed in membrane proteins. The RC conformational dynamics is strictly interwoven with most of the electron transfer processes that take place within the RC over different time scales, from the initial charge-separation steps occurring in picoseconds [138] to charge recombination processes regulated by the slow rearrangement of large RC domains during adaptations to continuous illumination [139]. In our studies on the bacterial RC incorporated into glassy disaccharide matrices, we focused on two specific electron transfer events, which are closely associated with or governed by the RC conformational dynamics, i.e., the forward electron transfer from the primary $Q_A^{\bullet -}$ to the secondary quinone acceptor Q_B, and the recombination of the electron on the primary photo-reduced quinone $Q_A^{\bullet -}$ with the electron hole on the primary photoxidized donor $P^{\bullet +}$.

A benchmark study by Kleinfeld et al. [44], which compared the kinetics of these two electron transfer processes in RC frozen at cryogenic temperatures in the dark

or under continuous strong actinic illumination, paved the way for the exploration of the RC energy landscape, underlying its conformational dynamics. It was found that when RCs were frozen in the dark at temperatures $T < 200$ K, the electron transfer from $Q_A^{\bullet -}$ to Q_B was arrested, while it persisted if RCs were frozen under illumination at cryogenic temperatures. This was taken as indicating that the RC complex could be trapped at cryogenic temperatures in a dark-adapted and in a light-adapted conformation, only the latter being competent for electron transfer to the terminal quinone acceptor Q_B. A subsequent investigation revealed that at room temperature the rate of $Q_A^{\bullet -}$-to-Q_B electron transfer was independent of the associated redox free energy change, demonstrating a conformationally-gated electron transfer process. Direct evidence for light-induced structural changes has been provided by high-resolution X-ray data collected in dark- and light-adapted RCs frozen at cryogenic temperatures [140]. A major difference between the dark and light conformations was in the position of Q_B itself, which, in the structure of the RC cooled under illumination was found 2.7 Å closer to Q_A and twisted by 180° around the isoprene chain, as compared to the protein frozen in the dark. Whether the movement of Q_B from the distal to the proximal site represents the electron gate, or other events (like dielectric responses of amino-acid side chains, internal proton movements, and changes in the hydrogen bonding pattern) play a determinant role in the gating mechanisms, is still controversial [141–145]. It is, however, clear, from a number of wild-type and mutant RC structures (see [46, 146–149] and references therein) that Q_B can occupy at least two different positions, and that a quite complex energy landscape, leading to a correspondingly complex dynamics, is associated with electron transfer to the secondary quinone acceptor.

A second electron-transfer process, whose kinetics has provided basic information on the RC conformational dynamics, is the recombination of the primary charge-separated state $P^{\bullet +}Q_A^{\bullet -}$ following a short flash of light, observable in RCs deprived of the secondary quinone acceptor Q_B. Kleinfeld et al. [44] have shown that this electron transfer event is accelerated by a factor of ~ 5, as compared to room temperature, when RCs are frozen to 77 K in the dark, whereas it is significantly slowed down in RCs cooled under continuous illumination. Interestingly, in both cases, kinetics exhibit at low temperature a strongly non-exponential, distributed character, which was interpreted as reflecting the trapping of the RC over a large ensemble of lower tier conformational sub-states, each characterized by a different rate constant for charge recombination. At room temperature, the rapid sub-states interconversion, leads to averaging of free energy barriers on the time scale of charge recombination, resulting in a single rate constant, i.e., monoexponential recombination kinetics. The low temperature behavior observed by Kleinfeld et al. [44] indicates that the stability of the primary charge-separated state $P^{\bullet +}Q_A^{\bullet -}$ differs significantly in the dark- and light-adapted RC conformations, and suggests that, in response to the electric field generation, the RC-solvent system undergoes at physiological temperature a dielectric relaxation stabilizing charge separation. The dependence upon temperature (5–300 K) and illumination protocol of $P^{\bullet +}Q_A^{\bullet -}$ recombination kinetics has been subsequently revisited by Nienhaus and co-workers in a series of systematic studies performed in native [45] and genetically modified [150] RCs, suspended in water-glycerol, or confined in a sol–gel matrix [151]. Results could be adequately analyzed

in terms of a quantum mechanical spin-boson model. Essentially, to account for the coupling between electron transfer and RC dynamics, the model conveys protein-solvent conformational relaxations and inter-substate fluctuations into a unique parameter, i.e., the free energy gap between the charge separated $P^{\bullet+}Q_A^{\bullet-}$ and neutral PQ_A states, which can be mapped on a conformational coordinate, describing the diffusive internal motions of the RC, i.e., the relaxation of the RC from the dark- to the light-adapted conformations. It is assumed that at room temperature, following light-induced charge separation, the RC light-adapts by relaxing adiabatically along the free energy profile of the $P^{\bullet+}Q_A^{\bullet-}$ state, through solvation of the altered charge distribution. This diffusive relaxation results in a decrease of the free energy gap between the $P^{\bullet+}Q_A^{\bullet-}$ and PQ_A states, which is reflected in a slowing of charge recombination, i.e., in stabilization of the primary charge-separation. Additionally, at physiological temperature, the system has sufficient thermal energy to sample rapidly the distribution of conformational sub-states, thus averaging rate constant heterogeneity on the time scale of charge recombination. Relaxation from the dark- to the light-adapted conformations and thermal fluctuations give rise, therefore, to the relatively slow (lifetime of about 100 ms) and exponential recombination kinetics (see Fig. 7b). In contrast to this, when RCs are cooled in the dark at temperatures between 250 and 150 K, both thermal averaging and relaxation to the light-adapted state are hampered, and a faster and strongly non-exponential $P^{\bullet+}Q_A^{\bullet-}$ recombination kinetics is observed. The kinetic analysis of recombination kinetics following a laser pulse provides, therefore, a convenient, endogenous probe of RC dynamics on the time scale of 10^{-3}–10^{-1} s.

Incorporation of the RC into trehalose glassy matrices at low water content has deep effects, both on $Q_A^{\bullet-}$-to-Q_B electron transfer and on the kinetics of $P^{\bullet+}Q_A^{\bullet-}$ recombination, which mimic at room temperature the behavior observed when RCs are frozen in the dark at cryogenic temperatures, in water–glycerol systems. $Q_A^{\bullet-}$-to-Q_B electron transfer is reversibly inhibited upon reducing the content of residual water in the trehalose matrix below 0.07 g of water per g of dry matrix [112]. In the following, we will express the matrix hydration level as mass of water per mass of dry matrix, since this evaluation allows a meaningful comparison of the overall hydration in glasses which differ in the molar ratio between the disaccharide and the protein, or in the chemical nature of the disaccharide. In evaluating the mass of dry matrix, we have included the disaccharide, the RC (with a molecular mass of 100 kDa), a detergent belt surrounding the RC, formed by 289 molecules of lauryldimethylamine N-oxide (LDAO) per RC [61], and the free LDAO molecules. The inhibition of $Q_A^{\bullet-}$-to-Q_B electron transfer is inhomogeneous, involving two RC sub-populations: one (active) in which electron transfer is slowed, but still successfully competes with $P^{\bullet+}Q_A^{\bullet-}$ recombination, the other (inactive) in which the electron is not transferred to Q_B. The fraction of the latter sub-population increases upon dehydration, and electron transfer appears to be completely blocked in glasses still relatively hydrated (0.04 g of water per g of dry matrix). The effects described above are fully consistent with a conformational gate, and indicate that the conformational transition which controls electron transfer is strongly enslaved to the dynamics of the trehalose matrix. Remarkably, a complete inhibition of $Q_A^{\bullet-}$-to-Q_B electron transfer

is attained at contents of residual water, at which the kinetics of $P^{\bullet+}Q_A^{\bullet-}$ recombination is still unaffected (see below).

The inhibition of the terminal forward electron transfer step in moderately dehydrated trehalose glasses has been observed also in Photosystem I (PS I), a photosynthetic reaction center characterized by a much higher structural and functional complexity (see Sect. 2.2.2). This common response to the dehydration of the trehalose matrix is consistent with the "anchorage model" (see Sect. 2.1). If the inhibition of protein internal dynamics is brought about by the locking of the protein surface to the glassy matrix, we expect in fact that the conformational dynamics of protein regions closer to the protein–matrix interface will be more effectively and primarily inhibited, even in matrices "softened" by a significant content of residual water. Only upon further dehydration, the stronger dynamical constraints introduced at the surface of the protein complex by the development of a more rigid hydrogen bond network, will propagate more deeply within the large protein complex through residue–residue and protein–cofactor interactions, retarding the conformational dynamics of the inner regions. The internal rigidity of the protein complex is therefore predicted to be tuned and differentially shaped by the hydration of the trehalose glass.

When the hydration of the trehalose glass is progressively reduced below ~ 0.04 g of water per g of dry matrix, the kinetics of $P^{\bullet+}Q_A^{\bullet-}$ recombination become progressively faster and non-exponential [111], resembling those observed in RCs frozen in the dark at cryogenic temperatures. Kinetic traces of $P^{\bullet+}Q_A^{\bullet-}$ recombination after a nanosecond laser pulse, recorded by time-resolved optical absorption spectroscopy, have been analyzed by assuming that the distribution of rate constants k is well approximated by a Gamma distribution [111]. This choice implies that the kinetics are fitted to a power-law decay, i.e.,

$$N(t) = \int_0^\infty p(k)\exp(-kt)\mathrm{d}k = \left(1 + \frac{\sigma^2}{< k >}t\right)^{-<k>^2/\sigma^2}, \quad (1)$$

where $N(t)$ is the survival probability of the $P^{\bullet+}Q_A^{\bullet-}$ state at time t after the photoactivating light pulse, $<k>$ is the average rate constant, and σ is the width of the rate distribution.

Figure 8 collects $<k>$ and σ values obtained in a number of RC-embedding trehalose glasses, characterized by different trehalose-to-RC molar ratios, as a function of the residual hydration of the glassy matrices. Dehydration of the matrix below ~ 0.04 g of water per g of dry protein leads to a steep increase in both the average rate constant $<k>$ and width σ of the rate constant distribution

The values of $<k>$ and σ obtained in the driest glasses at room temperature are quite comparable to those measured in RCs cooled in the dark below 60 K in a water–glycerol mixture [45]. Notably, the broadening of the rate distribution function observed upon extensive dehydration of the trehalose matrix is even larger than that induced by freezing the RC at cryogenic temperatures [45]. Based on this similarity, it was inferred that, upon reducing the water content of the matrix below a threshold value, the relaxation from the dark- to the light-adapted state of the RC, as well as the interconversion between conformational sub-states, are progressively

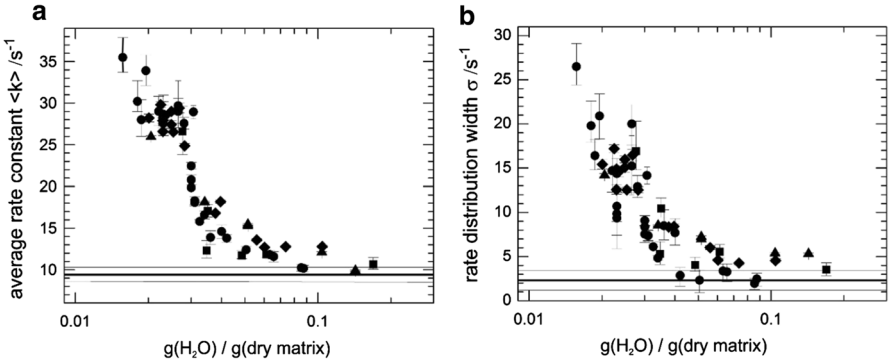

Fig. 8 Average rate constant, $<k>$ (**a**), and width, σ (**b**), of the rate distribution function which governs the kinetics of $P^{\cdot+}Q_A^{\cdot-}$ recombination in trehalose glasses incorporating the bacterial reaction center purified from *R. sphaeroides* R26. Both parameters are shown as a function of the content of residual water of the glassy matrix, expressed as mass of water per mass of dry matrix (see text for details). Different symbols correspond to different molar ratios (trehalose/RC): 1.5×10^4 (squares, data from [111]), 10^4 (circles, data from [102, 113]), 5×10^3 (diamonds, data from [110]), 5×10^2 (triangles, data from [152]). Thick horizontal lines correspond to values measured in solution. The vertical bars and thin horizontal lines indicate confidence intervals within two standard deviations

retarded. The rate distribution function experimentally obtained at room temperature in the driest glasses was in quantitative agreement with that calculated from the dynamical model of Nienhaus and coworkers [45], assuming that both sub-state interconversion and relaxation are inhibited on the time scale of the electron transfer reaction [111]. It was concluded that the RC dynamics involved in these processes was essentially arrested on the time scale of $P^{\cdot+}Q_A^{\cdot-}$ recombination.

The results summarized in Fig. 8 are in line with the expectations of the "anchorage model". Noteworthy, the hydration threshold below which the RC dynamics is progressively inhibited does not coincide with the glass transition: At residual water contents between 0.2 and 0.04 g of water per g of dry protein, no significant increase in $<k>$ and σ is found, notwithstanding the glassy state of the solid matrix. Therefore, an extremely high viscosity of the RC embedding matrix is not sufficient, per se, to retard significantly the RC internal dynamics. The remarkable sensitivity of $<k>$ and σ to the hydration state of the matrix is fully consistent with the notion, central to the "anchorage model", that below a threshold value of hydration, a growing fraction of the residual protein hydration shell is involved in a hydrogen-bond network, which, at the matrix–protein interface, connects exposed amino-acid residues and sugar molecules. Such a network, extending over the whole trehalose matrix, anchors the protein dynamics to the strongly restricted dynamics of the trehalose glass.

Figure 8 includes data obtained in glasses characterized by different trehalose/RC molar ratios, varied between 5.0×10^2 and 1.5×10^4. Within the experimental error, the dependence of $<k>$ and σ upon the content of residual water of the matrix appears unique, i.e., independent of the protein concentration within the glassy matrix. This is a distinctive feature of dehydrated trehalose matrices, which, as revealed by high-field EPR of a nitroxide radical incorporated into the matrix (see

below), can be put in relation with the unique capability of trehalose, as compared to other disaccharides like sucrose, to form, under extensive dehydration, an essentially homogeneous glassy matrix, independently of the concentration of the embedded protein.

The interpretation of the above described results (Fig. 8) in terms of the dynamical model introduced by Nienhaus and coworkers and of the "anchorage model" has received strong support by a high-field EPR study of RC-embedding trehalose matrices [47], which additionally provided insights at the molecular level on the dynamics involved in RC conformational relaxation. The kinetics of $P^{\bullet+}Q_A^{\bullet-}$ recombination in dehydrated matrices, probed in parallel by transient EPR absorption and by laser optical spectroscopy, were found fully consistent: an unprecedented agreement for such profoundly different spectroscopic approaches.

Continuous-wave EPR and electron spin echo (ESE) analyses of the flash-induced $P^{\bullet+}$ and $Q_A^{\bullet-}$ radical ions and of the spin correlated $P^{\bullet+}Q_A^{\bullet-}$ radical pairs, performed at room temperature or 150 K, indicated that the incorporation of the RC into the dehydrated trehalose matrix did not perturb the molecular configuration of the radical pair [47]. This finding is of particular relevance: it shows in fact that the RC, although "immobilized", is "softly confined" by the sugar glass, since the native cofactor geometry is preserved, both at room and cryogenic temperature. This is at variance with glasses formed at low temperature in the presence of cryo-solvents, like ethylene glycol or glycerol, which were found by X-ray crystallography to displace significantly the secondary quinone Q_B [46]. The observation that the distance and relative orientation of the $P^{\bullet+}Q_A^{\bullet-}$ radical pair is not affected by incorporation into a dehydrated trehalose glass excludes also that the acceleration observed in $P^{\bullet+}Q_A^{\bullet-}$ recombination (see Fig. 8) is due to a change of the electronic coupling term, which is expected to be highly sensitive to the distance and relative orientation of the redox cofactors involved in electron tunneling [153, 154]. It rather indicates that, in agreement with the model proposed by Nienhaus and coworkers, the increase of $<k>$ induced by matrix dehydration is a genuine dynamical effect.

Furthermore, essentially the same field dependence of the transverse relaxation time T_2 was found when the RC was embedded at room temperature in a trehalose or in a polymeric (polyvinyl alcohol) matrix, or dispersed in a glycerol/water system at 150 K. It was inferred that the local librational dynamics and hydrogen bonding of Q_A in its binding site [59] do not contribute to the conformational relaxation of the RC, which stabilizes the primary charge-separated state. All in all, the results of this EPR investigation suggest that the RC dynamics affected by incorporation into the dehydrated trehalose glass involves mostly structural rearrangements of the protein/solvent system. In agreement with these conclusions, small-scale conformational changes localized at the side chains of specific RC residues, in the proximity of $P^{\bullet+}$ or $Q_A^{\bullet-}$ cofactors [155–157], as well as the dielectric response of water molecules weakly bound to the RC [158, 159] have been proposed to be responsible of the RC conformational light adaptation.

Since macro-viscosity of the glassy matrix does not appear to be the critical parameter determining the immobilization of the embedded protein (see also Sect. 2.1), whatever model adopted ("water replacement", "preferential hydration"

or "anchorage model"), specific disaccharide–water and disaccharide–protein interactions, as well as the structural and dynamic characteristics of the matrix at the molecular scale, must clearly play a central role in the mechanisms of bioprotection, i.e., in inhibiting the protein conformational dynamics. In this respect, the comparison between glassy matrices formed by two homologous disaccharides, such as trehalose and sucrose, in terms of bioprotective capabilities and structural organization, is expected to provide important information for understanding the molecular details of protein–matrix structural and dynamical coupling.

Trehalose amorphous matrices exhibit a superior efficacy in preserving structural and functional integrity of many different soluble proteins under low water content and high temperature [91, 160–163]. A tighter protein–matrix dynamic coupling has been evidenced in trehalose-glasses than in sucrose-glasses by FTIR studies performed on carboxy-myoglobin (MbCO) incorporated into water–disaccharides amorphous systems [164, 165]. Consistently, molecular dynamic simulations showed that the internal motions of MbCO were less inhibited in sucrose as compared to trehalose systems of comparable water content [84]. The peculiarity of trehalose matrices in protein immobilization was even more evident in the case of the bacterial reaction center. When the kinetics of $P^{\bullet+}Q_A^{\bullet-}$ recombination was analyzed comparatively in RCs embedded in trehalose glasses and amorphous sucrose matrices, characterized by a high (10^4) sugar-to-RC molar ratio, sucrose, in contrast to trehalose, was found essentially ineffective in blocking the relaxation from the dark- to the light-adapted RC conformation, as well as thermal fluctuations among conformational sub-states [102]. Additionally, sucrose glasses were also scarcely effective, as compared to trehalose matrices, in preventing thermal denaturation. To explain the extremely weak dynamical coupling between the RC and the sucrose matrix, it was proposed that, under extensive dehydration, a kind of protein-matrix "nanophase separation" took place, implying the onset of structural inhomogeneities within the glassy sucrose matrix at low water content [102].

This suggestion received strong support by the results of a more recent study [166], in which the structural and dynamical features of binary trehalose–water and sucrose–water matrices, at well-defined hydration, were probed by means of high-field W band EPR, using a perdeuterated nitroxide radical as an electron-spin probe dispersed into the glasses. Analysis of the EPR spectrum of the probe has shown that, within the dehydrated trehalose glass equilibrated at a relative humidity, $r = 11\%$, the nitroxide probe is homogeneously distributed and immobilized to an extent comparable to that observed at cryogenic temperatures.

In contrast to this, deconvolution of the nitroxide EPR spectrum recorded in the sucrose–water matrix at the same hydration level, has revealed three contributions, stemming from nitroxide radical sub-populations exposed to substantially differing microenvironments: the first component, accounting for approximately 30% of the nitroxide population, corresponds to an amorphous matrix domain which immobilizes the nitroxide guest molecules, similar to what was observed in the trehalose glass; the second contribution, containing ~ 20% of the probe molecules, reflects a matrix domain rich in water, in which the guest molecule has gained a considerable mobility; the third contribution originates in a fraction of nitroxide radicals at very high local concentration in a highly hydrated domain. The sucrose matrix, at low

water content, displays, therefore, a high structural and dynamical heterogeneity. This result is confirmed by the FTIR analysis of the spectral evolution of the water-association band (see Sect. 2.2) with the hydration level of the matrices [166]. The finding that a large fraction of the guest molecules in the sucrose matrix appears to be "nanophase separated" in a highly hydrated domain, and that another domain of the sucrose matrix contains diluted guest molecules significantly mobilized by residual water, suggests a reasonable explanation for the dynamical decoupling observed in RC-sucrose-water systems between the RC and the disaccharide matrix [102].

To test and further explore the relevance of structural homogeneity/heterogeneity of disaccharide glasses in determining protein–matrix coupling/uncoupling, the EPR approach summarized above has been extended to ternary RC–water–trehalose and RC–water–sucrose systems. This study [110], combining high-field EPR with the analysis of $P^{\bullet+}Q_A^{\bullet-}$ recombination kinetics based on laser optical spectroscopy, has disclosed a more complex scenario, in which the protein concentration within the sucrose matrix appears to play a critical role in determining protein–matrix coupling/uncoupling.

Figure 9a compares room-temperature W-band cw EPR spectra of perdeuterated nitroxide radicals dispersed into sucrose–RC matrices, characterized by sugar/RC molar ratios m of 10^3, 5×10^3 and 10^4, with the spectrum acquired in a trehalose-RC glass, with $m = 10^4$. To attain a common dehydration level, all samples have been equilibrated at the relative humidity $r = 11\%$, by exposure to a saturated solution of LiCl [61]. The spectra in the trehalose–RC glass and in the sucrose–RC matrix at high protein concentration ($m = 10^3$) exhibit the characteristic high-field lineshape predicted for a homogeneous distribution of immobilized nitroxide radicals. The spectra are clearly resolved into three B_0 regions, corresponding to the principal values of the g-tensor (g_{xx}, g_{yy} and g_{zz}). The nitrogen ^{14}N hyperfine splitting into line triplets ($I(^{14}N) = 1$) is distinctly observed in the g_{yy} and g_{zz} region.

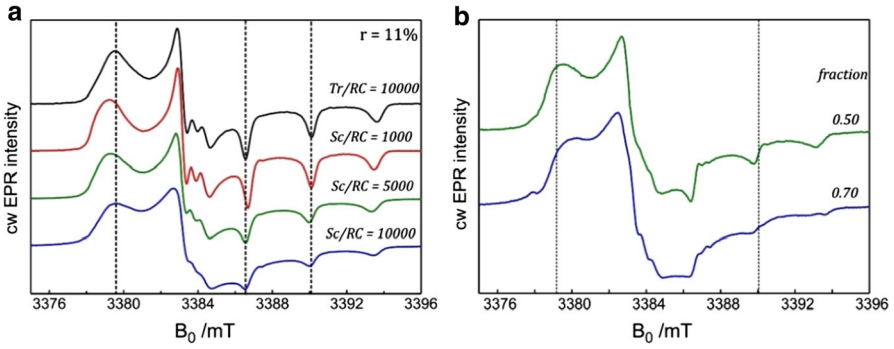

Fig. 9 **a** W-band cw EPR spectra of a perdeuterated nitroxide radical recorded at 293 K in trehalose (Tr)-RC and sucrose (Sc)-RC matrices characterized by different sugar/RC molar ratios, as indicated in the figure labels. **b** Deconvolution results of the EPR spectra measured in the sucrose-RC matrices with a sugar/RC molar ratio $m = 5 \times 10^3$ (green) and $m = 10^4$ (blue). The properly normalized spectrum recorded in the sucrose-RC matrix with $m = 10^3$ has been subtracted from the spectra with higher molar ratios. The relative integral weights of the deconvoluted EPR spectra of high-mobility nitroxide fractions are given at the respective spectra. For details, see [110] (color figure online)

The homogeneity of the nitroxide radical microenvironment in these matrices is quantitatively demonstrated by the fact that a single set of magnetic interaction parameters (g_{ii} and A_{ii}) yields an adequate simulation of the spectra. Multiparameter best fitting of the spectrum recorded in the trehalose–RC glass, obtained by numerical solution of the spin Hamiltonian, results in g- and A-tensor principal values ($g = [2.0083; 2.0059; 2.0022]$ and $A = [0.56; 0.57; 3.69]$ mT), which are essentially coincident with those obtained by analyzing the spectrum previously acquired in a trehalose-water binary matrix equilibrated at the same relative humidity [166]. This indicates that the presence of the RC protein does not perturb the local structure and dynamics of the glassy trehalose matrix, as probed by the nitroxide radical.

Unexpectedly, when the protein concentration within sucrose glassy matrices is decreased, i.e., at sugar/RC molar ratio increasing to $m = 5 \times 10^3$ and $m = 10^4$, the EPR spectrum undergoes remarkable changes, which reflect the onset of formation of heterogeneities in the nitroxide radical microenvironment, and the presence of a probe sub-population experiencing a substantially increased mobility. This appears when the spectra, acquired in the matrices with $m = 5 \times 10^3$ and $m = 10^4$, are deconvoluted by subtracting the appropriately normalized spectrum, recorded in the sucrose matrix with $m = 10^3$, which originates from the nitroxide probe immobilized within a homogeneous environment (Fig. 9b). According to the corresponding relative weights of the deconvoluted spectra, the fractional contribution of the matrix domain characterized by a high mobility increases to 0.5 and 0.7 when the sucrose/RC molar ratio is increased to 5×10^3 and 10^4.

Although both spectra measured in the trehalose–RC glass and in the sucrose–RC matrix at high protein concentration ($m = 10^3$) are typical of a nitroxide radical immobilized in a homogeneous microenvironment, a closer look reveals interesting differences (see Fig. 10): In the sucrose–RC matrix, as compared to the trehalose–RC glass, the g_{xx} spectral component is shifted to lower field values, and a lower A_{zz} value is observed. This is quantitatively confirmed by multiparameter best fitting of the spectrum measured in the sucrose–RC matrix to the numerical solution of the spin Hamiltonian, which yields $g = [2.0086; 2.0059; 2.0022]$ and $A = [0.55; 0.55; 3.53]$ mT [110]. These changes are indicative of a

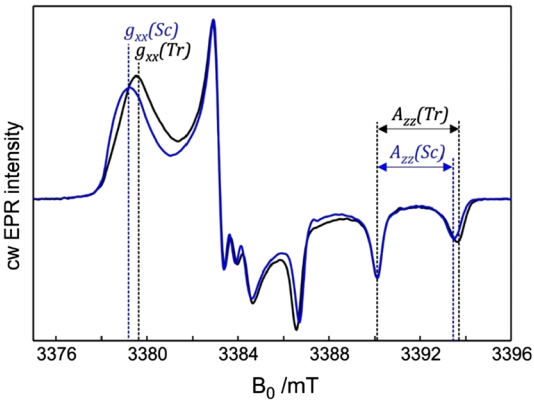

Fig. 10 Comparison between W-band cw EPR spectra of the perdeuterated nitroxide radical measured at 293 K in a trehalose-RC glass with $m = 10^4$ (black trace) and a sucrose-RC matrix with $m = 10^3$ (blue trace), equilibrated at a relative humidity $r = 11\%$. For details, see [110]

different hydrogen-bonding pattern of the nitroxide radical within the trehalose and sucrose glass, the latter matrix being characterized by a lower proticity [167]. Spectra recorded at 180 K in the amorphous RC–trehalose matrix (not shown) suggest that all nitroxide radicals involve a hydrogen bond with their environment, while the spectrum in sucrose appears to contain additional contributions from nitroxides which do not form any hydrogen bond with their environment [167].

The lower proticity detected by high-field EPR in RC–sucrose glasses is in line with the results of molecular dynamics simulations performed in binary disaccharide-water systems, which showed that sucrose forms essentially intramolecular hydrogen bonds [168–170]. It is known that in sucrose crystals glucopyranosyl and fructofuranosyl are bridged by two intramolecular H-bonds [171, 172]. Molecular dynamics simulations indicate that these intramolecular hydrogen bonds persist in concentrated solutions approaching the glass transition [173]. In sucrose, the formation of intramolecular H-bonds reduces therefore the number of sites available for intermolecular H-bonds, resulting in a lower proticity. The limited propensity of the sucrose molecule to form intermolecular hydrogen bonds is likely to be the main cause of the structural heterogeneity observed in ternary RC–water–protein matrices at low protein concentrations. Molecular dynamics simulations and experimental studies on binary disaccharide–water systems highlight additional differences between trehalose and sucrose: (a) a stronger solute–solvent interaction in trehalose; (b) a better effectiveness of trehalose in retarding water dynamics [174, 175]; (c) a stronger perturbation induced by trehalose of the tetrahedral H-bond pattern of water [176]; (d) a larger size of water clusters in sucrose as compared to trehalose; (e) a larger flexibility of trehalose, allowing it to explore a larger conformational space than sucrose. These factors could further contribute to determine the structural and dynamical heterogeneity revealed by EPR in RC–sucrose amorphous matrices.

The scenario emerging at the molecular scale from the high-field EPR analysis of sucrose–RC glasses characterized by different protein concentrations is fully consistent with the response to this parameter of the conformational dynamics of RCs embedded within sucrose amorphous matrices. Following the approach described above, which is based on the kinetic analysis of $P^{\bullet+}Q_A^{\bullet-}$ recombination monitored by time-resolved optical absorption spectroscopy, we have re-investigated the ability of sucrose amorphous matrices with different RC protein concentration to retard the RC relaxation from the dark- to the light-adapted conformation, as well as the thermal averaging between conformational sub-states.

In Fig. 11, values of the average rate constant $<k>$ (panel a) and rate distribution width σ (panel b), as a function of the content of residual water in the glasses, are shown for a series of sucrose–RC amorphous matrices, characterized by different sugar/RC molar ratios, m (i.e., 10^3, 5×10^3 and 10^4, as in the high-field EPR investigation). For the sake of comparison, results obtained in a trehalose–RC glass with $m = 5 \times 10^3$ are also included. We recall that in trehalose–RC matrices the sugar/RC ratio m does not significantly affect the dependence of $<k>$ and σ upon the hydration level of the matrix, as shown in Fig. 8 for a large range of m values (from 5.0×10^2 to 1.5×10^4): dehydrated trehalose glasses are able to block the RC conformational dynamics over a large range of embedded protein concentration.

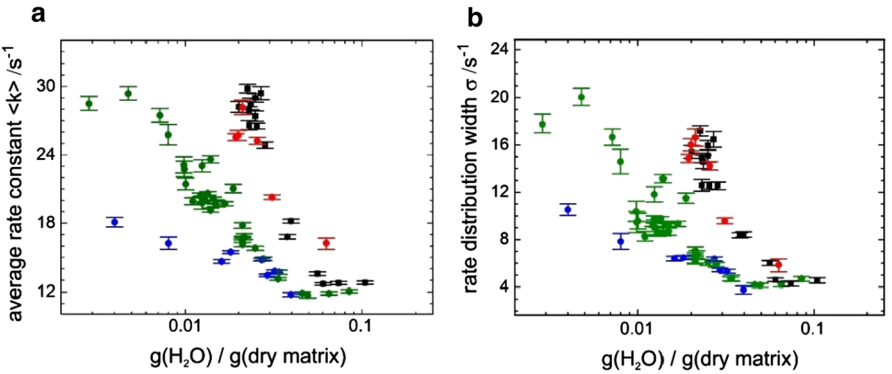

Fig. 11 The average rate constant $<k>$ (**a**) and the rate distribution width σ (**b**), obtained from kinetic analysis of $P^{\bullet+}$ $Q_A^{\bullet-}$recombination, as a function of the residual water content in sucrose-RC matrices with different sugar/protein molar ratios: $m = 10^3$ (red); $m = 5 \times 10^3$ (green); $m = 10^4$ (blue). The dependence observed in a trehalose-RC glass, at $m = 5 \times 10^3$, is also shown in black for the sake of comparison. The vertical bars represent confidence intervals within two standard deviations. For details, see [110] (color figure online)

Figure 11 demonstrates that, on the contrary, the ability of sucrose-RC matrices to inhibit the internal RC motions depend dramatically upon the protein concentration within the matrix. At low protein concentration ($m = 10^4$), both $<k>$ and σ undergo a modest increase upon decreasing the content of residual water, as compared to the behavior observed in the trehalose–RC glass. This indicates that, in agreement with our previous study [102], performed at low protein concentration, the RC conformational dynamics is scarcely hampered and, to a large extent, decoupled from the dynamics of the matrix, even under conditions of extreme dehydration. However, when the sucrose/RC molar ratio is decreased to $m = 10^3$, thus increasing the RC protein concentration by one order of magnitude, the dependences of $<k>$ and σ upon the hydration level are barely distinguishable from those found in the trehalose–RC matrix (independently of the protein concentration). At high protein concentration, therefore, the sucrose matrix blocks the RC conformational dynamics as observed in trehalose–RC matrices. Consistently, at an intermediate protein concentration ($m = 5 \times 10^3$), a reduction of the RC dynamics comparable to that in the trehalose glass can be attained also in the sucrose matrix, but only at considerably lower contents of residual water.

Interestingly, the surose/RC molar ratio was found to affect dramatically also the thermal stability of the RC embedded into the dehydrated glassy matrices. When the RC denaturation kinetics at 44 °C, studied by FT-NIR spectroscopy, was compared in sucrose matrices characterized by $m = 10^3$ and $m = 10^4$ [110], it was found, in fact, that in the latter, i.e., at low protein concentration, the RC lost its native structure on the time scale of hours, while in the former, i.e., at high protein concentration, denaturation was totally prevented even after incubation at high temperature for 1 week, as observed in trehalose glasses. It is concluded that the protein concentration modulates the ability of the dehydrated sucrose matrix to hinder not only the small-scale,

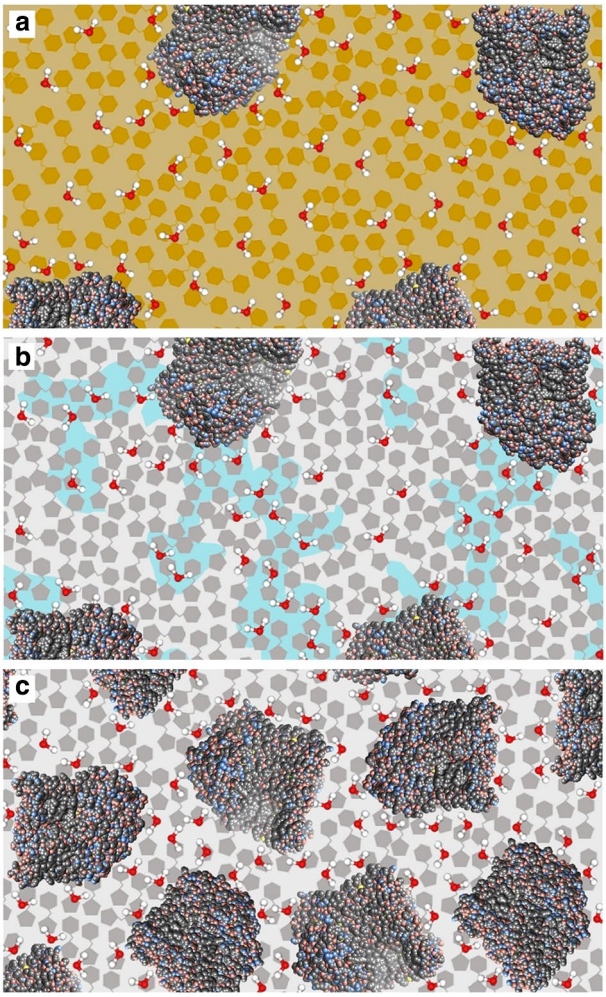

Fig. 12 Pictorial representation of the structural organization of RC-disaccharide-water amorphous matrices, for a trehalose matrix at low RC protein concentration (**a**), and sucrose matrices at low (**b**) and high (**c**) RC protein concentration. In **b** the light blue areas correspond to an amorphous sucrose phase significantly more hydrated as compared to that grey colored, as also inferred from the different density of the depicted water molecules

fast RC conformational dynamics associated with charge recombination, but also the slow, large-scale RC internal motions, which leads to unfolding and denaturation.

The switching from protein–matrix coupling to decoupling, in response to the protein concentration within the dehydrated sucrose matrix, finds a natural explanation in the light of the corresponding switching from structural and dynamical homogeneity to heterogeneity of the matrix, as revealed at the molecular scale by the high-field EPR analysis outlined above. Figure 12 offers a pictorial

representation of the structural molecular model of trehalose–RC and sucrose–RC glassy matrices, obtained by combining the information provided by EPR and time-resolved optical spectroscopies. The scheme incorporates basic assumptions of the "anchorage model" of disaccharide bioprotection, which accounts well for the relationships observed between the structural organization of the different matrices and the dynamics of the incorporated protein.

The chemical structures of the two disaccharides trehalose and sucrose as well as the chemical structure of the perdeuterated nitroxide radical used are shown below:

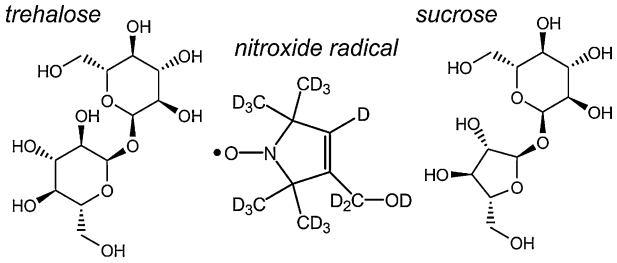

In Fig. 12, it is schematically visualized that in the dehydrated trehalose-RC matrix (panel a) the RC is strongly immobilized within a structurally and dynamically homogeneous sugar matrix. Even under extensive dehydration, the protein hydration shell is partially retained and bridges, through multiple hydrogen bonds, amino-acid side chains of the protein surface with OH groups of trehalose molecules of the matrix. A few direct protein–trehalose interaction contribute to reduce the protein backbone flexibility [177]. Residual water molecules connect by hydrogen bonding also trehalose molecules within the bulk sugar matrix, thus forming an extended, continuous network of H-bonds, which stiffens the whole matrix, tightly coupling the internal motional degrees of freedom of the embedded protein to those of the rigid trehalose–water matrix. Such a structural organization of the homogeneous trehalose–RC matrix, which appears to be independent of the protein concentration within the matrix, results in a dramatic hindering of the RC conformational dynamics. A different scenario characterizes the sucrose–RC matrix at low RC protein concentration (panel b). The rigidity of the sucrose molecule, due to its intramolecular H-bonds, and its low propensity to form intermolecular H-bonds with nearby groups, lead, in this case, to a structural and dynamical heterogeneity of the amorphous matrix, which includes, besides rigid sugar domains with low water content, which mimic the organization of the dehydrated trehalose matrix, large, more flexible regions with a higher water content, which are in contact with the RC protein. These more hydrated regions disrupt the rigid amorphous sucrose phase, while connecting large areas of the RC protein surface, which gains a considerable flexibility. As a result, the protein–matrix dynamical coupling is drastically weakened and the RC conformational dynamics is only marginally inhibited, notwithstanding the large macro-viscosity of the glassy system. When the protein concentration within the sucrose matrix is significantly increased (panel c) the development of sucrose clusters embedded into a more hydrated and mobile sucrose phase is disturbed, and

sucrose molecules, most of which interact with the residual hydration shell of the protein, are forced to hydrogen bond with exposed protein residues. Under these conditions, the formation of an extended homogeneous H-bond network, which incorporates the embedded RC protein, is favored, thus restoring a tight dynamical coupling between the matrix and the RC protein.

The rearrangement of the structure and H-bonding pattern of the sucrose matrix in response to a change in the RC protein concentration appears to be reasonable, when the average distance between nearby proteins within the matrix is evaluated in the light of the sugar/RC ratio and of the volume of the RC–detergent complex. A rough estimate [110] yields average inter-protein distances of about 85 Å and 15 Å for sucrose–RC matrices with a sugar/RC molar ratio of 10^4 and 10^3, respectively. The latter distance entails that the space interposed between adjacent proteins be filled by only a few layers of sucrose molecules. This configuration is therefore well compatible with the idea that, at high protein concentration, the overall homogeneous structural organization of the matrix is largely governed by (water-mediated) sucrose–protein interactions.

Summarizing, the studies performed on trehalose and sucrose matrices using the bacterial RC as a model protein, point to a general molecular mechanism of disaccharide bioprotection, in which the long-range H-bond connectivity within the protein-water-disaccharide matrix plays a critical role by determining the degree of protein–matrix dynamical coupling. The peculiar bioprotective capabilities of trehalose, as compared to other disaccharides, appear to stem from its propensity to form, under very different conditions, a homogeneous, extended H-bond network encompassing, at low water contents, the whole protein–water–sugar glass. At the same time, the capability of sucrose matrices to hinder protein conformational dynamics at high protein concentration, can explain why in vivo large amounts of this disaccharide are expressed by anhydrobiotic higher plants. It is tempting to speculate that the high sensitivity of the structure and dynamics of sucrose matrices to the concentration of the embedded protein is involved in activating/deactivating protein function during anhydrobiotic cycles.

2.2.2 Photosystem I (PS I)

The pigment–protein complex of Photosystem I (PS I) is one of the crucial components of the photosynthetic electron-transfer chain in thylakoid membranes of oxygenic organisms [178]. The PS I complex catalyzes the light-driven electron transfer (ET) from external donor proteins plastocyanin and/or cytochrome c_6 to ferredoxin and/or flavodoxin.

The three-dimensional structure of the trimeric form of PS I from the thermophilic cyanobacterium *Thermosynechococcus elongatus* has been obtained by X-ray structural analysis with 2.5 Å resolution [179]. Each monomer has a molecular weight of ~ 330 kDa and contains 12 protein subunits and ~ 130 cofactors (96 chlorophyll (Chl) *a*, 22 β-carotene, three [4Fe–4S] clusters, two phylloquinone (PhQ), and four lipid molecules). PS°I also contains 201 water molecules and a calcium ion. Two transmembrane subunits PsaA and PsaB compose a C_2-symmetrical heterodimeric core complex containing most of the electron-transfer cofactors.

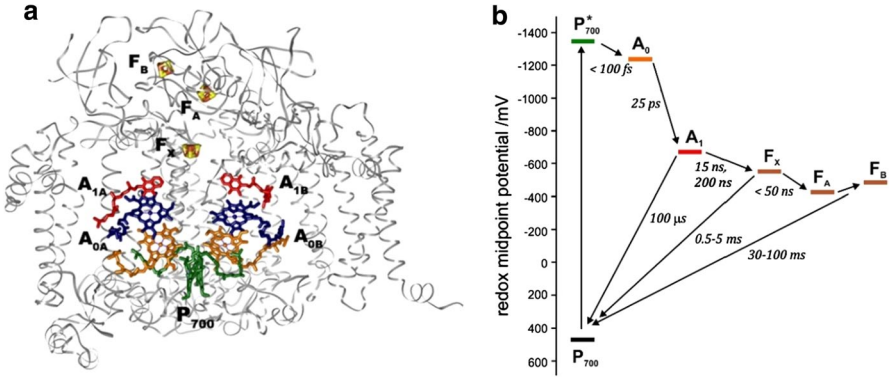

Fig. 13 **a** Structure of Photosystem I (PS I). **b** Energy diagram and time constants of forward electron-transfer and recombination reactions in PS I. Information was taken from [180, 181] and references therein

The electron-transfer chain of PS I consists of the Chl dimer (Chl *a*/Chl *a*') P_{700}, A_0 (pairs of Chl molecules designated as Chl_{2A}/Chl_{3A} and Chl_{2B}/Chl_{3B}), A_1 (phylloquinone molecules designated as A_{1A}/A_{1B}), and 4Fe–4S clusters F_X, F_A, and F_B (see Fig. 13a).

It is known that electron transfer in PS I occurs through both branches of the redox cofactors from P_{700} to F_X, but the degree of asymmetry of this transfer and the factors that govern it are not yet completely understood [182, 183].

As mentioned above, out of 96 Chl molecules, 6 are involved in electron-transfer and are located near the contact surfaces of the PsaA and PsaB subunits. The chlorophyll dimer P_{700} consists of the two Chl *a* molecules (Chl_{1A}= Chl *a*' and Chl_{1B} = Chl *a*) whose porphyrin planes are parallel to each other (at an average distance of 3.6 Å) and perpendicular to the membrane plane. The spatial localization of the other two molecules of Chl *a* (Chl_{2A}/Chl_{2B}) roughly corresponds to the localization of the two molecules of monomeric bacteriochlorophyll in the RC of purple bacteria, and the two additional molecules of Chl *a* (Chl_{3A} and Chl_{3B}) are arranged in a manner similar to the two molecules of bacteriopheophytin in the RC of purple bacteria [184, 185]. The planes of the porphyrin rings of Chl_{2A} (Chl_{2B}) and Chl_{3A} (Chl_{3B}) molecules are parallel (with a distance of 3.9 Å), but they are slightly more shifted relative to each other than Chl_{1A} and Chl_{1B}. The mutual arrangement and relatively close distance between the central Mg^{2+} atoms of Chl_{2A} and Chl_{3A}, and Chl_{2B} and Chl_{3B} (8.7 Å and 8.2 Å, respectively) imply the possibility of significant interaction between these pairs of Chl *a* molecules.

Recently, it was shown that after preferential excitation of P_{700} by a femtosecond laser flash, formation of the primary radical pair $P_{700}^{\cdot+}A_0^{\cdot-}$ occurs within 100 fs [186], followed by electron transfer leading to formation of $P_{700}^{\cdot+}A_1^{\cdot-}$ with a characteristic time of ~ 25 ps [180, 186]. Subsequent electron-transfer reactions from A_{1A} and A_{1B} to F_X take place with characteristic times of ~ 200 and ~ 20 ns, respectively [187, 188]. This is followed by electron transfer from F_X to the terminal iron-sulfur clusters, F_A and F_B, within 200 ns and further to water-soluble

native acceptors ferredoxin or flavodoxin. Photooxidized P_{700} is reduced by plastocyanin or cytochrome c_6, returning all the cofactors of PS I back to their initial state [178]. In the absence of external donors and acceptors, the electron recombines with $P_{700}^{\bullet+}$ from intra-protein electron acceptors. The electron on $[F_A/F_B]^{\bullet-}$ recombines with the hole on $P_{700}^{\bullet+}$ with a time constant of 30–100 ms. Charge recombination from the $P_{700}^{\bullet+}F_X^{\bullet-}$ also takes place under certain condition and occurs within a time of 0.5–5 ms [180, 189]; and in PS I cores lacking iron-sulfur clusters, the lifetimes of charge recombination between $A_1^{\bullet-}$ and $P_{700}^{\bullet+}$ were found to be ~ 10 µs and ~ 150 µs [190, 191]. The rates of forward and backward electron transfer are indicated in Fig. 13b [180, 181].

Earlier studies have described the effect of temperature on certain forward and backward electron-transfer reactions in PS I. It was shown that at cryogenic temperatures more than 60–70% of RCs exhibited irreversible charge transfer on successive laser flashes [192]. The remaining 30–40% of RCs showed distributed recombination lifetimes ranging from 120 µs to 500 ms. Later it was demonstrated that at temperatures below 150 K, forward ET was blocked at the level of A_1 in ~ 45%, and at the level of F_X in ~ 20% [193]. Recently, the kinetic and thermodynamic effects of temperature, from 310 to 4 K, for PS I complexes in a water-glycerol glassy matrix was studied [194]. The charge-recombination kinetics from the terminal F_A/F_B clusters significantly slowed upon temperature decrease from 310 to 200 K. At temperatures between 200 and 150 K, an abrupt increase in the rate of charge recombination from seconds to milliseconds occurred. This behavior was ascribed to the arrest of forward ET to the terminal 4Fe–4S clusters at the glass transition temperature of the water–glycerol mixture due to the restriction of the protein conformational mobility. In this temperature range, a sharp decrease of the slow recombination from F_A/F_B at the expense of the increase of faster recombination from F_X and A_1 was observed. Note also that the charge recombination from the iron–sulfur clusters at temperatures between 150 and 200 K was significantly heterogeneous, whereas below 150 K, the kinetics became almost temperature-independent.

As was pointed out in Sect. 2.2.1, incorporation of the bacterial RC into dry trehalose glassy matrices at room temperature had deep effects on the kinetics of charge recombination between the photo-reduced primary quinone acceptor Q_A and the photo-oxidized primary donor *P*, which mimicked the behavior observed at cryogenic temperatures in water–glycerol systems. It was concluded that the protein dynamics involved in these processes was significantly arrested on the time scale of $P^{\bullet+}Q_A^{\bullet-}$ recombination. A similar approach was applied to study the effect of desiccation in dry trehalose matrix on the kinetics of electron transfer in the more sophisticated pigment–protein system, the PS I complex from cyanobacteria *Synechocystis* sp. PCC 6803 [48].

In this work, the coupling between electron transfer (ET) and protein-solvent dynamics by incorporating PS I at room temperature into trehalose glasses at different hydration levels was studied (see Fig. 14). The decay kinetics of the $P_{700}^{\bullet+}$ reduction after the laser flash in solution and in trehalose matrix at 63% of relative humidity (*r*) was dominated by a slow kinetic component centered at $\tau \approx 100$ ms (phase 5), which is due to recombination from the $P_{700}^{\bullet+\circ}[F_A/F_B]^{\bullet-}$ state. The minor components with lifetime ~ 3 ms (phase 2) and ~ 0.1 ms (phase 1) were attributed to

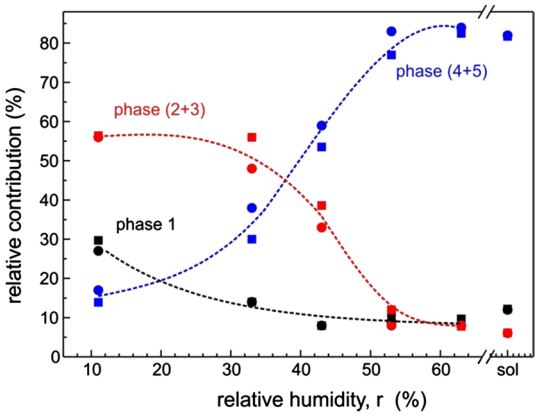

Fig. 14 Relative contribution to charge recombination of the different kinetic phases of $P_{700}^{\cdot+}$ reduction in PS I as a function of the relative humidity *r*. The label sol stands for solution. The relative contributions of the fastest phase (phase 1) are represented by black symbols. Red symbols correspond to the sum of the normalized areas of phases 2 and 3; blue symbols represent the sum of the relative contribution of phases 4 and 5. Dashed lines are drawn through the experimental points to guide the eye. For details, see [48]

the small fractions of PS I complexes, lacking terminal F_A/F_B clusters and all three 4Fe–4S clusters (F_X, F_A and F_B), see Fig. 14. At $r<53\%$ and lower, phase 5 split into two phases 4 and 5 (mean lifetimes 80 and 360 ms at this r value), which were both ascribed to the back reaction from the $[F_A/F_B]^{\cdot-}$ state.

The overall evolution of the lifetime distribution in the trehalose glass suggests that dehydration of the matrix causes a progressive arrest of forward ET to F_A/F_B in an increasing fraction of the PS I, as shown by the decrease in the contribution to the back reaction of the slowest phases (4 and 5). The increasing contribution, at $r<43\%$, of the faster phases suggests that, at lower content of residual water, also the forward electron transfer to F_X is blocked in an increasing PS I sub-population.

The kinetic phases attributed to the recombination from the $P_{700}^{\cdot+}F_X^{\cdot-}$ state (phases 2 and 3 with mean lifetimes of ~ 2 and ~ 10 ms at $r<43\%$, respectively) demonstrate a complex response to dehydration. At the lowest humidity, $r=11\%$, the contribution of the fastest phase 1 (lifetime ~ 0.1 ms) significantly increases [48].

The time resolution in the experiments, described above was limited to ≥ 30 µs; therefore, no information was available for forward ET from $A_{1A}^{\cdot-}$ or $A_{1B}^{\cdot-}$ to F_X or for charge-recombination reactions involving $A_0^{\cdot-}$ and $P_{700}^{\cdot+}$ or $A_{1B}^{\cdot-}$ and $P_{700}^{\cdot+}$. A subsequent study focused on the initial steps of charge separation and forward electron transfer including A_0, A_{1A} and A_{1B}. It was shown that ET is altered at each step beyond that of primary charge separation between P_{700} and A_0 [195, 196]. The femtosecond pump-probe laser spectroscopy demonstrated that the kinetics of formation of the primary P_{700} demonstrated that the kinetics of formation of the primary $P_{700}^{\cdot+}A_0^{\cdot-}$ and the secondary $P_{700}^{\cdot+}A_1^{\cdot-}$ radical pairs in trehalose matrix at $r=11\%$ was not affected, but the quantum yield of the secondary electron transfer $P_{700}^{\cdot+}A_0^{\cdot-}\rightarrow P_{700}^{\cdot+}A_1^{\cdot-}$ was decreased to ~ 80% [195].

The forward ET was monitored by measuring the kinetics of the $A_1^{\bullet-}$ decay kinetics at a wavelength 480 nm, reflecting the electrochromic shift of carotenoid molecules located at the vicinity of A_{1A} and A_{1B} sites. The comparison of kinetics measured at 480 nm and the kinetics at 830 nm (which reports on the $P_{700}/P_{700}^{\bullet+}$ redox transitions) allowed to separate forward ET behavior $A_{1A}^{\bullet-} \rightarrow F_X$ and $A_{1B}^{\bullet-} \rightarrow F_X$ from the backward ET, $A_{1A}^{\bullet-} \rightarrow P_{700}^{\bullet+}$ and $A_{1B}^{\bullet-} \rightarrow P_{700}^{\bullet+}$. It was demonstrated that the forward ET from $A_{1A}^{\bullet-}$ to F_X in trehalose-embedded PS I is slowed down from 200 ns to 13 µs, while ET from $A_{1B}^{\bullet-}$ to F_X is slowed from 20 to ~ 100 ns [196]. The ~ 10 µs and ~ 150 µs components in liquid PS I are assigned to recombination between $A_{1B}^{\bullet-}$ and $P_{700}^{\bullet+}$ and between $A_{1A}^{\bullet-}$ and $P_{700}^{\bullet+}$, respectively, and are only marginally slowed down in trehalose-embedded PS I.

Note that while the lifetimes of the $P_{700}^{\bullet+}A_0^{\bullet-}$ and the $P_{700}^{\bullet+}A_{1A}^{\bullet-}/A_{1B}^{\bullet-}$ recombination reactions are almost identical in liquid PS I and trehalose-embedded PS I, the $P_{700}^{\bullet+}F_X^{\bullet-}$ and the $P_{700}^{\bullet+}/[F_A/F_B]^{\bullet-}$ recombination kinetics are significantly slower in trehalose than in liquid PS I. It is also noticeable that the lifetimes of the forward electron transfer reactions from $A_{1B}^{\bullet-}$ to F_X slow from 17 to 80 ns, while the ET from $A_{1A}^{\bullet-}$ to F_X slow from 227 ns to 13 µs in the liquid state compared to trehalose embedded PS I.

The unique feature in this protein domain is the presence of five water molecules in the space between A_{1A} and F_X and the presence of six hexagonally arranged water molecules in the space between A_{1B} and F_X [197]. If removal of the water molecule(s) from either of these intra-protein pools occurs upon dehydration of PS I in trehalose, the redox potential of the quinones and/or the reorganization energy of the reactions involving the quinones would most likely change. Therefore, at some level of dehydration, the rate of recombination would exceed the rate of forward ET resulting in a lower quantum yield. We also suggest that the degree of removal of water from the two pools would not be the same; this would explain why the rate of forward ET from $A_{1B}^{\bullet-}$ to F_X is slowed by a factor of 4, whereas the rate of forward ET from $A_{1A}^{\bullet-}$ to F_X is slowed by a factor of 57. Moreover, because charge recombination from the F_X, F_B and F_A, 4Fe–4S clusters occurs by backward ET to the A_{1A} and A_{1B} quinones [198, 199], the lifetimes of these reactions would also be affected by the specific removal of water from the sites in the vicinity of A_{1A} and A_{1B}.

It is interesting to compare the effects of a low temperature water–glycerol mixture with desiccation in trehalose glassy matrix at room temperature, which both restrict protein conformational mobility. A number of similarities are apparent in the charge recombination kinetics of PS I immobilized in glycerol glass at 170 K [193, 194] and trehalose glass at 298 K [48, 195, 196]. The slowing of ET in the trehalose and glycerol mixtures could be caused by similar physical processes that take place within and around the protein globule upon glass transition of the surrounding medium. As described above, the temperature at which a sudden change of recombination kinetics in glycerol solution occurs (~ 170 K) corresponds to the glass transition temperature of 75% water–glycerol solution [200]. Room temperature (298 K) seems to be below the glass transition temperature for a 10% water–trehalose mixture, but above the glass transition temperature for the 30% water–trehalose mixture [201]; thus, the process of dehydration also drives the solution through the glass transition process.

As discussed in the previous sections, high-field W-band EPR spectroscopy is distinguished from standard X-band EPR by providing valuable high-resolution information on the structural and dynamical organization of binary disaccharide–water systems even in the amorphous solid state. Analysis of the room-temperature EPR spectrum of a nitroxide radical dissolved in a dehydrated trehalose matrix, equilibrated at $r = 11\%$, has demonstrated that upon extensive dehydration trehalose forms a highly homogeneous amorphous phase in which the residual water and hosted nitroxide molecules are uniformly distributed. Additionally, it has been shown that the rotational mobility of the guest nitroxide probe is dramatically restricted at room temperature (RT), to an extent comparable to that observed at cryogenic temperatures ($T < 150$ K). The incorporation of a protein within the trehalose glass can in principle perturb the structural and dynamical characteristics of the matrix, e.g., by affecting its homogeneity, particularly in the case of a large integral membrane protein, such as the trimeric PS I (PS I(tr)) surrounded by its detergent belt. Therefore, we have compared the W-band EPR spectra of perdeuterated nitroxide radicals dispersed in dehydrated trehalose matrices in the absence and in the presence of embedded complexes, PS I(tr), varying the sugar/protein molar ratio.

From the results of this experiment, we infer that the incorporation of PS I does not perturb the homogeneous structural organization of the trehalose matrix in terms of distribution of the hosted spin-probe and residual water molecules. The lineshape of the EPR signals of the nitroxide spin probe does not change significantly at the different molar ratios trehalose/PS°I(tr). This shows that in the tested range, the molar ratio has no effect on the microenvironment of the hosted spin probe and its rotational dynamics. Summarizing the structural and dynamical characterization of trehalose-PS I glassy matrices by EPR, we conclude that the inclusion of the large trimeric PS I complex in the solid trehalose matrix does not perturb significantly the hydration state as well as the structural and dynamical organization of the homogeneous trehalose glass at $r = 11\%$ over a wide range of PS I concentrations [48].

A second point we have addressed concerns the reverse side of the mutual protein-matrix interaction discussed so far, i.e., the possibility that the extensively dehydrated, stiff trehalose matrix perturbs in turn the structure of the PS I complex, altering in particular distances and relative orientations of its cofactors. Obviously, such structural matrix effects would be relevant for the kinetics of electron-transfer processes. The structural configuration of two key cofactors of the PS I complex, i.e., the primary donor P_{700} and the quinone acceptor A_1, can be conveniently probed by examining the spin-polarized EPR spectrum of the transient radical pair created in the pure singlet electronic state by a laser flash and taken before thermalization of the spin system has occurred, i.e., before Boltzmann equilibrium of the spin populations has been reached. Electron spin polarization can be observed by transient EPR (TR EPR) methods (see Fig. 6) provided the lifetime of the radical pair and/or the electron spin–lattice relaxation times of the individual pair partners are long enough compared to the EPR detection time. This polarization phenomenon is well accounted for by the "correlated-coupled-radical-pairs" (CCRP) model [58, 202]. In solid amorphous samples, the transient EPR lineshape, which is determined by the magnitude and sign of the dipolar coupling of the two electron spins, is sensitive to

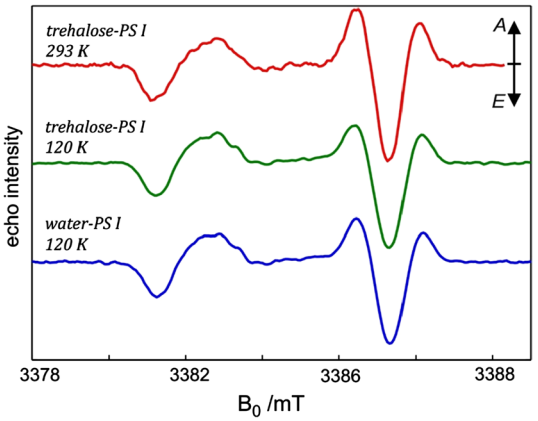

Fig. 15 Field-swept echo-detected W-band EPR signals (TR-EPR) of the spin-correlated $P_{700}^{+}A_1^{-}$ radical pair in dark-adapted PS I complexes, embedded in trehalose glassy matrices and dissolved in water. The spectra were recorded 400 ns after a 532 nm laser flash using a Hahn echo pulse sequence with π/2 pulse length of 30 ns and inter-pulse delay of 150 ns. The signals were acquired at both 293 K (upper spectrum) and 120 K (middle spectrum), as well as in water at 120 K (lower spectrum). The trehalose-protein matrix was characterized by a trehalose/PS I(tr) molar ratio of $m = 1.0 \cdot 10^5$. The A_1^{-} contribution to the spectrum is at the low-field side (higher g values than the P_{700}^{+} contribution). **A** stands for absorptive and **E** for emissive type of spin polarization. For details, see [48]

the relative orientation and distance of the radical-pair partners. A lineshape analysis reveals, therefore, these important structural parameters of the donor–acceptor spin system.

In Fig. 15, the W-band EPR spectra of the spin-correlated radical pair $P_{700}^{+}A_1^{-}$, as measured in a dehydrated trehalose-PS I matrix at 293 K and 120 K, are compared with the spectrum recorded in an aqueous buffer solution of PS I frozen at 120 K. The three spectra are essentially identical, revealing that the structural configuration of the transient radical pair does not change significantly upon solvation in the different matrices embedding the PS I complex. This conclusion is in line with the results of our previous study of bacterial RCs which had shown the absence of matrix effects on the EPR spectrum of the spin-correlated $P_{865}^{+}Q_A^{-}$ radical pair generated by pulsed light excitation of bacterial RCs embedded in trehalose glasses [47].

Taken together, these EPR observations suggest that in photosystems of different size and complexity regarding subunit composition and oligomeric organization, the molecular configuration of the cofactors involved in the primary processes of charge separation is not significantly distorted by incorporation into trehalose glass, even under extensive dehydration.

Dry trehalose–PS I glasses, equilibrated at $r = 11\%$ and characterized by m values in the 10^4–10^5 range, represent a homogeneous amorphous system which is well defined in terms of hydration. Remarkably, the embedded PS I complexes fully retain their photoactivity at RT and preserve it for long periods of time (at least for two months).

The kinetics of $P_{700}^{\cdot+}$ decay after pulsed photoexcitation are also independent of the protein concentration in the glassy matrix over the m range examined. The described trehalose–protein system appears, therefore, to be well suited for investigating the effects of matrix hydration on the kinetics of charge-recombination processes. The hydration state of the matrix is known to govern the dynamical properties of the glassy system. Such hydration effects largely modulate the protein–matrix coupling and, therefore, are important for protein function.

2.2.3 Local-Water Sensing in Proteins

The behavior of soft matter, such as protein complexes dissolved in aqueous saccharide matrices, is largely governed, on the nanoscale, by the surface properties of its constituents [203]. This aspect is of particular importance for all biological matter, where extended molecular layers are major components, for instance, in the form of biomembranes. Surface interactions are decisive for the stability and structural organization of complex energy converters in biology, for example photosynthetic reaction centers as membrane–protein complexes in bacteria and green plants that are able to convert light energy into chemical potential.

The characteristics of surface interactions of proteins in an aqueous environment, such as interaction strength, directionality and range, as well as whether interactions are repulsive or attractive in general depend on the chemical composition of the surfaces involved, e.g., their ability to form hydrogen bonds between local water of the matrix and amino-acid sidechains of the protein (see Fig. 16).

Thus, surface interactions in aqueous environments are of great importance in biology (and also from a technological viewpoint, for instance the proper lubrication of engines). Comprehensive knowledge of the underlying physical mechanisms is

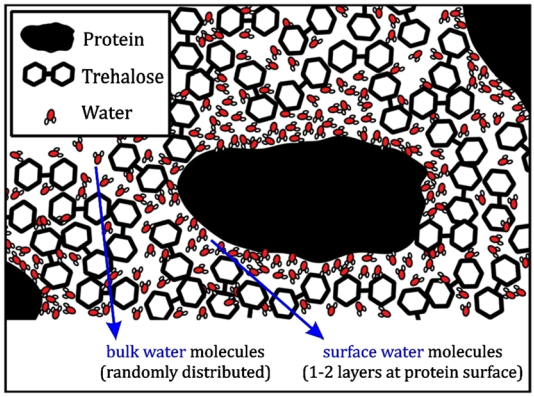

Fig. 16 Schematic structure of the protein-trehalose-water system. The preferential hydration of the protein molecules is typically one to two molecular layers of water at the protein surface (local water). The trehalose molecules and the remaining water molecules (bulk water) are almost randomly distributed between the hydrated protein molecules. There is an important functional difference between surface-bound water (local water) and bulk water. Figure adapted from [204]

thus a prerequisite to understanding numerous biological processes as well as for the rational design of surfaces exhibiting desired interaction characteristics.

In the following, we summarize a recent pulsed W-band high-field multi-resonance EPR study, such as ELDOR-detected NMR (EDNMR) and ENDOR (see Fig. 6) in conjunction with using isotope labeled water (D_2O and $H_2{}^{17}O$), to address the biologically important issue of sensing and quantifying local water in proteins embedded in trehalose matrices [205]. The photosynthetic bacterial reaction center (bRC) from *R. sphaeroides* R26 has been chosen as the model system whose 3D X-ray structure is known with atomic resolution [206]. In the bRC from *R. sphaeroides*, the photosynthetic electron-transfer cofactors, that are buried deep in the protein L- and M-subunits, are P_{865} (the "special pair" primary donor composed of two bacteriochlorophylls (BChl), two monomeric BChl's, two bacteriopheophytins (BPhe), two ubiquinone-10 acceptors (Q_A and Q_B), and a non-heme iron Fe^{2+}. In the present EPR study, the paramagnetic Fe^{2+} cofactor was replaced by diamagnetic Zn^{2+} (Zn-RC) to avoid fast electron spin relaxation. In the native bRC from *R. sphaeroides*, Q_A and Q_B form the primary and secondary electron acceptor, respectively. In the work described here, the secondary electron transfer from $Q_A^{\cdot-}$ to Q_B was blocked by using the inhibitor stigmatellin [207].

A site-specific nitroxide spin label group was attached to amino-acid site Cys156 located at the surface of the protein H-subunit. Thus, the studied bRC hosts the two native radical cofactor ions, $P_{865}^{\cdot+}$ and $Q_A^{\cdot-}$, as well as the artificial radical spin probe. The three paramagnetic reporter groups have distinctly different local environments; they serve as local spin probes to detect and characterize different types of water molecules via their specific electron-nuclear hyperfine and nuclear quadrupole interactions in isotope-labeled water (D_2O or $H_2{}^{17}O$) with either deuterons ^2H or ^{17}O nuclei when either D_2O or oxygen-17 labeled water is used.

The bRCs were equilibrated in an atmosphere of different relative humidities, r, allowing to control precisely various hydration levels of the protein. To this end, the samples were transferred into a sealed box where further dehydration of the sample occurred via controlled exposition to an atmosphere of low relative humidity over a saturated aqueous salt solution at room temperature using H_2O with natural isotope abundance. This isopiestic method of controlled sample dehydration [208] has been employed successfully both in EPR [47] and IR [61, 159, 209] studies on bRC/trehalose glasses and bRC films dehydrated in the absence of sugar. For measurements on samples equilibrated to the desired relative humidity with either D_2O or $H_2{}^{17}O$ vapor, the saturated solutions of an adequate salt [210] were prepared using the respective isotope-labeled water at room temperature. The dehydrated bRC/trehalose films contained about 0.5 mM of protein, they were then crumbled into small flakes and inserted into the W-band sample quartz capillaries (i.d. 0.6 mm). In the present study, two specific hydration levels (relative humidity, r) of bRC/trehalose glasses were obtained when using LiCl ($r = 11\%$) or NaCl ($r = 74\%$) saturated solutions [210]. For more details of the sample preparation, see [205].

In the light of the EPR results, which will be described to some detail below, we would like to emphasize already at this point that by using oxygen-17 labeled water as solvent quantitative conclusions can be made about local and bulk water distribution. Moreover, from the experiments, it also can be concluded that upon

dehydration the trehalose matrix operates as an efficient anhydrobiotic protein stabilizer. This is accomplished through selective changes of the surface solvation shell of the protein thereby leading to an increased rigidity of the hydrogen-bonding network of the trehalose–water–protein system. Changes in hydrogen-bonding patterns are known to have an impact on the global function of a biological system.

Water plays an important, if not essential part in the chemistry of life, it governs the internal dynamics of biological macromolecules, such as proteins. Unrestricted dynamics at a specific time scale is a crucial requirement for the specific biological activity of proteins, including enzyme activity, macromolecular recognition, ligand binding and participation in electron and proton transfer processes. Under physiological conditions, these macromolecules fluctuate between different conformational states [211]. Their dynamics span an enormous time range, i.e., from sub-picosecond to tens of microseconds, and include a multitude of stochastic local and collective motions, from bond vibrations to domain motions. Despite significant efforts over the past decades, our microscopic understanding of protein dynamics in gel-like aqueous matrices is still fairly rudimentary [119, 212, 213].

In functional biological systems, water is usually divided into three distinctly different classes: (i) internal water molecules that are hydrogen-bonded to specific amino-acid residues in a water pocket of the protein or are mobile along inner protein channels; they are generally of key importance for the specificity of protein function; (ii) surface (or local) water molecules in the hydration shell of the protein at the solute–solvent interface, and (iii) bulk water molecules randomly distributed in the protein matrix. Water molecules in the protein hydration layer have restricted dynamics with respect to water molecules in the bulk as shown by different spectroscopic methods which probe different dynamical ranges of molecular motion, e.g., NMR spectroscopy [214–217], dielectric spectroscopy in the microwave region [218], terahertz absorption spectroscopy [219, 220], IR spectroscopy [221, 222], and neutron spectroscopy [211]. Additionally, powerful extensions of molecular dynamics simulation techniques have been employed recently to clarify solvation dynamics of large molecules [219, 223–225].

At physiological temperatures and in typical matrices, solvated proteins fluctuate between a multitude of conformational sub-states in a rugged energy landscape that is hierarchically organized in energy tiers [226, 227]. For most proteins cooled below the glass-transition temperature (typically around 200 K), their biological function is blocked due to restricted conformational motion. The “freezing out” of conformational dynamics by lowering the temperature is thus a common strategy for studying structure–function relationships in proteins, for instance in X-ray protein crystallography. However, freezing proteins in the presence of a cryoprotectant (used to minimize freezing damage by ice crystals) is problematic, because it complicates the disentanglement of different molecular factors that influence protein dynamics such as the effect of solvent and temperature.

An elegant alternative approach is to embed the protein into amorphous matrices formed by disaccharides like trehalose [52, 111]. This allows preservation of the native protein fold during extensive protein dehydration, even at temperatures well above room temperature (see Sects. 2, 2.1, 2.2). As we mentioned above, trehalose is the most efficient sugar for bio-protection against extreme dehydration and osmotic

stress. The mechanistic details of the trehalose efficiency are still under debate (for a review, see e.g., [41]), but most likely involve a delicate interplay between several factors including the extraordinarily high glass-transition temperature (385 K) of trehalose [88], its polymorphism adopting several crystalline and amorphous states [228], its propensity for hydrogen bonding and rigidity of the dehydrated glass matrix [170]. W-band high-field EPR techniques, such as the double-resonance extensions ENDOR and EDNMR are extremely powerful for measuring small hyperfine and quadrupole couplings even in large low-symmetry biomolecules. They allowed us to quantify the accessibility of local water at various sites in bRCs that were embedded in trehalose glasses at distinct hydration levels. The advantage of EPR spectroscopy in comparison with other techniques such as THz spectroscopy and IR spectroscopy, is that site-specific information on local water of the solvation layer can be obtained with a minimum of assumptions in the spectral analysis. Employing isotope labeled water provides the necessary contrast from internal non-exchangeable water molecules [205].

The native bRC contains 5 cysteine residues which are buried within the protein domains except for cysteine 156 which is moderately solvent exposed in the H-subunit. This residue can be site-specifically spin labeled with an external paramagnetic probe molecule. We used MTSSL (1-oxyl-2,2,5,5-tetramethylpyrroline-3-methyl-methanethiosulphonate) as a common spin label [229, 230]. The nitroxide spin label provides a third paramagnetic probe within the bRC in addition to the "natural" radical ions $P_{865}^{\cdot+}$ and $Q_A^{\cdot-}$. According to the bRC protein 3D structure, the "artificial" nitroxide spin label probes the water accessibility at a very different position and in a different way as compared to the intrinsic native cofactors, P_{865} and Q_A.

Using W-band EDNMR and Davies ENDOR, it was possible to probe directly whether the dehydration of the trehalose matrix results in a changed hydration level of the inner protein core surrounding the native cofactors, $P_{865}^{\cdot+}$ and $Q_A^{\cdot-}$, and of the protein surface at the nitroxide labeled site of cysteine 156. To trace the exchange of water between the sugar matrix and the protein, the use of isotope labeled water was essential, involving both deuterium and oxygen-17 isotopes.

Here, we will restrict the discussion of these studies to $H_2{}^{17}O$ water-accessibility results obtained by W-band EDNMR and Davies ENDOR on nitroxide spin labeled bRC/trehalose samples in which ^{17}O is used as nuclear spin probe instead of ^{2}H. The respective advantages of both approaches are highlighted. Regarding technical details of the chemicals used and the EDNMR and ENDOR experiments, we refer to the original publication [205].

We continue with reporting preliminary results regarding $H_2{}^{17}O$ water-accessibility studies obtained by W-band EDNMR and Davies ENDOR on nitroxide spin labeled bRC (SL-bRC) in trehalose/water samples in which ^{17}O is used as nuclear spin probe of water molecules instead of using the conventional nuclear spin probe D. The disadvantage of the conventional deuteron spin-probe method is that in SL-bRC/trehalose glasses equilibrated with saturated solutions of salt dissolved in D_2O, unwanted H/D exchange takes place. As a result, only a qualitative comparison of local water accessibility at different sugar hydration levels could be made. To avoid unwanted H/D exchange and detect exclusively isotope-labeled water molecules, equilibration with salts prepared in $H_2{}^{17}O$ solution was performed.

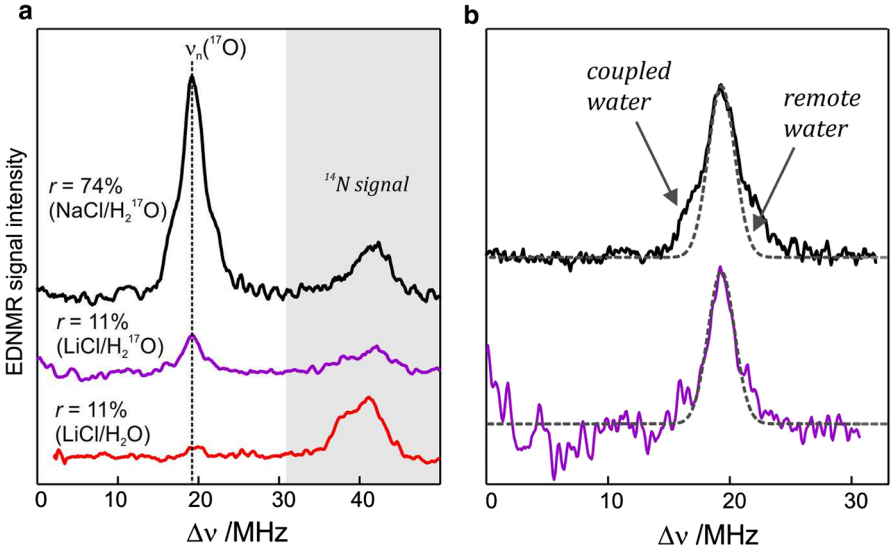

Fig. 17 **a** W-band EDNMR spectra for SL-bRC/trehalose glass samples equilibrated for 70 h at r = 74% (NaCl/$H_2{}^{17}O$) black trace; r = 11% (LiCl/$H_2{}^{17}O$) magenta trace; and r = 11% (LiCl/H_2O) red trace. EDNMR spectra are shown for $\Delta\nu < 0$ to obtain a better separation between ^{17}O and ^{14}N signal contributions. **b** The ^{17}O EDNMR spectra for r = 74% (NaCl/$H_2{}^{17}O$) (black trace) and r = 11% (LiCl/$H_2{}^{17}O$) (magenta trace) samples. The gray dashed lines show the best fit simulation of experimental recordings to a Gaussian line. For details, see [205] (color figure online)

Figure 17a, b shows ^{17}O EDNMR spectra recorded for SL-bRC/trehalose equilibrated at $r = 11\%$ (LiCl/$H_2{}^{17}O$) and $r = 74\%$ (NaCl/$H_2{}^{17}O$). In both spectra, a line centered at the ^{17}O nuclear Larmor frequency $\nu_n(^{17}O) = 19.4$ MHz and ^{14}N lines from the nitroxide nitrogen were observed. The ^{17}O line intensity at $r = 74\%$ is 6 ± 2 times larger than at $r = 11\%$. For comparison: from IR spectroscopy, this intensity ratio for ($r = 74\%$/ $r = 11\%$) was determined as 4.7 ± 0.2. This agreement within error limits is quite satisfying in view of the vastly different spectroscopic methods used for concentration measurements.

Subsequently, by means of W-band Davies ENDOR measurements, the ^{17}O hyperfine coupling constant as extracted from the EDNMR spectrum could be confirmed. In Davies ENDOR exclusively coupled water (i.e., local water) is probed since the signal from distant ^{17}O nuclei is suppressed because of the blind spot at $\nu_n(^{17}O)$ [130]. The presence of the ^{17}O line in the EDNMR spectrum of the dehydrated protein/trehalose glass ($r = 11\%$) unambiguously shows that, despite extensive dehydration and the high rigidity of the trehalose, the residual water retained in the trehalose sugar and the water on the protein surface can exchange.

We conclude and summarize this sub-chapter on local-water sensing: in the present work, pulsed high-field EPR techniques such as W-band ELDOR-detected NMR and ENDOR were used to unravel hydration-dehydration processes of bRC protein preparations embedded in trehalose matrices with carefully controlled ^2H and ^{17}O isotope-labeled water content. Specifically, the EDNMR method proved to be exceptionally sensitive in detecting hyperfine-coupled deuterium or ^{17}O nuclei

originating from D_2O or $H_2{}^{17}O$ water, respectively, which were introduced into the sugar matrix in a controlled fashion by means of the isopiestic technique.

In trehalose-embedded SL-bRC, both EDNMR and ENDOR spectra show that water molecules, detected by a nitroxide spin label that was attached to the bRC surface, are retained in the first and second solvation shell, even under extensively drying conditions ($r = 11\%$) which block the internal protein dynamics. Surface water molecules, as probed in the vicinity of the nitroxide radical, and inner water molecules, as probed in the vicinity of the ubiquinone $Q_A^{\cdot-}$ cofactor ion, exchange with water that is in equilibrium with the trehalose matrix. These observations strongly argue against the "water replacement hypothesis" of anhydrobiotic protein stabilization by trehalose sugar, which assumes that the sugar binds directly to the polar groups of the protein surface, serving as a "water substitute" upon removal of the hydration shell.

As was pointed out above, for SL-bRC, the ratio of ^{17}O EDNMR line intensities for the hydrated state to the dehydrated state reflects the number of distant water molecules in the vicinity of the nitroxide spin label, and can be compared with what is measured for the pure trehalose matrix by IR spectroscopy [166].

Thus, the scaling of the ^{17}O signal intensity follows the changes of the overall water content in the trehalose matrix. This fact is in quantitative conflict with the "water replacement hypothesis" of anhydrobiotic protein stabilization by a trehalose matrix. At the same time, the above observation weakens the applicability of the "preferential hydration hypothesis", because it does not give evidence of a preferential hydration of the protein surface in comparison to the average hydration of the whole sugar matrix. Thus, taking all arguments together, our findings appear consistent with the "anchorage hypothesis" of anhydrobiotic protein stabilization by trehalose which assumes that the trehalose matrix immobilizes the protein by locking its surface through a network of direct H-bonds between exposed protein residues and sugar molecules, as well as through indirect H-bonds mediated by bridging water molecules of the residual hydration shell. Clearly, a quantification of direct protein–trehalose *versus* water-mediated protein–matrix contacts would require the investigation of a large number of site-specifically nitroxide-labeled sites distributed over the protein surface, which was beyond the scope of the present work.

While the spectral sensitivity of EDNMR relative to ENDOR is higher by several orders of magnitude, thus making it the method of choice for EPR studies on protein complexes, the limited resolution of deuterium EDNMR using D_2O poses a disadvantage for local-water sensing in a quantitative manner. However, ^2H EDNMR is well-suited for qualitative studies, like those presented here, to determine the sugar rehydration kinetics for which no differentiation between coupled and distant water is necessary.

In case quantitative information on the different types of water present in proteins is required, ^{17}O EDNMR in combination with $H_2{}^{17}O$ should be used instead, taking advantage of the high sensitivity of the method and the possibility to resolve coupled from distant ^{17}O contributions. In this respect, W-band EDNMR in conjunction with D and/or ^{17}O isotope labeling is indeed a very strong methodology for local-water sensing.

As to the scientific and practical significance of such studies, we want to emphasize that hydration water plays a crucial role in protein dynamics and structural relaxation on all time scales. Numerous studies and their analyses suggest that changes in the amount of hydration water affect not only the protein's energy landscape but also significantly influence structural fluctuations between conformational sub-states—thereby controlling biological function. To understand the functional difference between surface-bound water and bulk water is thus a key issue for understanding and controlling biological macromolecules, including proteins and DNA, actually, right up to controlling anhydrobiotic food preservation and storage in dehydrated trehalose matrices at room temperature. Changes in water-mediated hydrogen-bonding patterns usually have a crucial impact on the global function of a biological system.

We all know of global warming with associated climate catastrophes and extreme periods of drought—and we all must act against it in all possible ways accessible to us as individuals. Apparently, water is far more than merely a solvent. Water is an active participant in the life of the cell, in fact it is the "matrix of life" [231, 232].

3 Most Recent Studies of Matrix Effects of Trehalose and Other Extremolytes

The results discussed in chapter 2 support the general conclusion that trehalose glassy matrices under controlled hydration levels represent a very valuable tool when investigating the coupling between protein conformational dynamics and function. By studying trehalose matrix effects on specific electron-transfer events performed by two different photosynthetic complexes (the bacterial RC and PS I), we have shown that the use of trehalose glasses, in conjunction with optical and EPR spectroscopy, can provide at room temperature detailed information on the interplay between internal protein motions and biocatalysis, which complement those obtainable by corresponding investigations performed at cryogenic temperatures in fully hydrated systems in the presence of glycerol. As compared to the latter classical approach, room temperature dehydrated trehalose–protein glasses exhibit essentially peculiar properties which can be used advantageously: (a) internal motions of the trehalose-embedded protein can be dramatically retarded on the time scale of the studied reaction kinetics avoiding the use of cryogenics which might perturb the protein structure; (b) even at low overall water contents of the glass, the protein retains a hydration shell, which equilibrates with the relative humidity of the sample environment, thus allowing to finely modulate the dynamics of the protein–matrix system; (c) the mutual distances and orientations of the protein cofactors involved in electron transfer are not significantly perturbed by incorporation into the trehalose glass, even under the driest conditions, leading to a severe, but "soft" conformational confinement of the incorporated protein; (d) at variance with sucrose, trehalose forms under strong dehydration a glassy matrix that is highly homogeneous on the length scale of the incorporated protein, over a very large range of sugar/protein molar ratios; (e) retardation of the protein dynamics is merely due to an increase of the energy barriers separating local minima of the protein-solvent

energy landscapes, without any change in the thermal energy of the system; on the contrary, in low-temperature studies both these factors are affected concomitantly since a glassy water–cryosolvent matrix is formed upon lowering the temperature; (f) the incorporation into a strongly dehydrated trehalose glass results in extraordinary thermal stabilization of the protein; as a consequence, even samples including labile proteins can be stored at room temperature for long periods of time (months) without undergoing thermal denaturation.

The above considerations have encouraged us to extend the use of trehalose glassy matrices to the study of the other photosystem (Photosystem II, PS II) of oxygenic photosynthesis, for which several low-temperature investigations suggest the involvement of conformational protein dynamics in electron-transfer reactions (see Sect. 3.1.1). A preliminary account of these attempts is given in Sect. 3.1.2.

The isolated photosynthetic RCs seem to be ideal systems to study the effects of protein dynamics on electron transfer. The crystal structures of all three types of RCs (PS I, PS II and bacterial RCs) at atomic resolution, the distances and orientations between redox-cofactors as well as their arrangement within the protein have been determined with fairly high accuracy. In addition, both genetic and chemical manipulations on RCs have been employed and their effects on protein structure and function are well known. Most importantly, the kinetics and thermodynamics of electron transfer have been studied in detail and their models are reasonably well understood.

Additionally, we would like to remark that the approach based on room-temperature protein incorporation into trehalose glasses, exploited by us with photosynthetic reaction centers, is expected to be also fruitful when applied, more in general, to a variety of photoactivatable protein complexes, which undergo biocatalytic reactions different from electron transfer. In this perspective, attractive systems for future investigations are flavin-binding bacterial and plant photoreceptor protein complexes, which are known to respond selectively to light activation of different wavelengths with significant conformational rearrangements [233].

Concerning the mechanisms of protein immobilization by dehydrated trehalose glasses, our results, as discussed at length in chapter 2, strongly support the "*anchorage model*" of trehalose bioprotection. In this frame, the high-field EPR studies performed on ternary disaccharide–RC–water glassy systems formed by trehalose or by sucrose, emphasize the role of specific sugar–water, water–protein and, to a minor extent, direct sugar–protein interactions in coupling the protein dynamics to that of the matrix. Such interactions are thought to result in a specific (homogeneous or heterogeneous) structural organization of the glassy matrix, which appears to be critical in determining the degree of protein/matrix dynamical coupling and consequently the extent of protein immobilization. In future experiments, we plan to test this general view by examining, in comparison with trehalose glasses, amorphous matrices formed by other low molecular weight solutes, synthesized by a variety of organisms surviving extreme environmental conditions. This large family of solutes, named osmolytes or extremolytes, are known to exert in vivo a significant bioprotective action against very high or low temperatures, desiccation, osmotic stress and other adverse conditions (see Sect. 3.2.1). The dynamical and structural information obtained by high-field EPR of nitroxide radicals dispersed into amorphous matrices

formed by the different osmolytes will be put in relation with their efficacy in inhibiting the conformational dynamics of the bacterial RC and PS I, used as model proteins. Experiments along this line are underway in our laboratories, and have primarily focused on glasses formed by the osmolytes ectoine and hydroxyectoine. Preliminary results are summarized in Sect. 3.2.2.

3.1 Photosystem II (PS II)

3.1.1 Introduction

The protein–pigment complex of Photosystem II (PS II) embedded in the thylakoid membranes of cyanobacteria and chloroplasts of algae and higher plants is an enzyme that functions as water: plastoquinone oxidoreductase. The major redox-active cofactors involved in the light-induced charge transfer reactions reside in the D_1D_2 reaction center (RC) subunits. The reducing side of the RC consists of the primary (Q_A) and secondary (Q_B) plastoquinone molecules with different properties, determined by their interaction with the protein, i.e., Q_A functions as one-electron, and Q_B as two-electron carrier [234, 235]. The water-oxidizing complex (WOC) is located at the donor side of PS II and consists of an inorganic Mn_4CaO_5 metal cluster bound to the surrounding protein matrix [236]. The two integral membrane protein subunits CP43 and CP47 associated with the PS II core, containing chlorophyll *a* and β-carotene molecules and serve as an internal antenna complex.

The capture of light excitation either by direct absorption of the RC or by energy transfer from the internal antenna initiates charge separation followed by electron transfer across the membrane. The electron transfer from the primary electron donor, a tetrameric chlorophyll complex $P_{680,}$ to the primary acceptor Q_A results in formation of an ion-radical pair ($P_{680}^{\cdot+}Q_A^{\cdot-}$) within ~ 250 ps and leads to two different chemical events: oxidation of water to molecular oxygen (after four turnovers

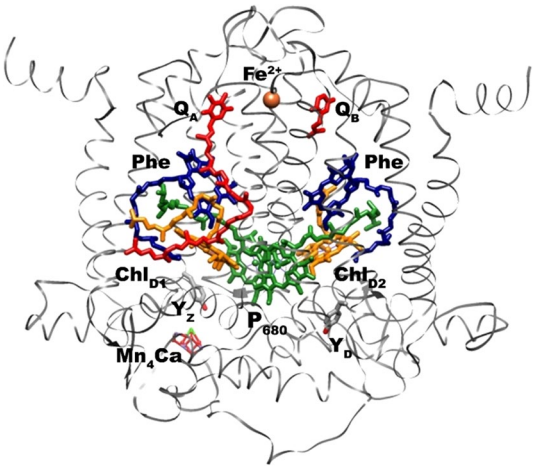

Fig. 18 Cutout from the structure of Photosystem II (PS II). The X-ray crystallographic structure of PS II from *Thermosynechococcus vulcanus* at a resolution of 1.9 Å was a milestone achievement in protein structure biology by J. R. Shen et al. [236, 240]

of PS II) and reduction of plastoquinone to plastohydroquinone in the Q_B-site (after two turnovers of PS II) (see [237–239] for details). These reactions are spatially separated and occur on different sides of the RC in the thylakoid membrane (see Fig. 18). It should be stressed that one of the difficulties in studying PS II in vitro is associated with the fragility of the oxygen-evolving complex and its high sensitivity to photo-oxidative damage.

The dimeric membrane protein (~700 kDa) is related by a C_2 axis. Major protein subunits and the location of the oxygen-evolving complex (OEC, Mn_4Ca) in the D1 protein are shown. In the literature, the OEC is also called the water–oxidizing complex (WOC). In Fig. 18 it is named "Mn_4Ca" as an abbreviation for the Mn_4CaO_5 cluster. The Mn_4CaO_5 cluster constituting the WOC is characterized in the high-resolution X-ray structure by its detailed amino acid surrounding and the four bound water molecules (W1–W4), see [240]. The Mn_4Ca cluster acts as an interface and storage device between the very fast light-reactions (picosecond time-scale) and the slow four-electron water oxidation chemistry (millisecond time-scale), bridging a kinetic gap of nine orders of magnitude [239].

The WOC represents a genuine molecular catalyst with only two sites for substrate binding, resulting in the single-product formation of O_2. The kinetics of binding changes of the oxygen evolving catalyst are well understood in terms of the S_i-state intermediates of the famous Kok cycle through the oxidation states S_0, S_1, S_2, S_3 and S_4 of the manganese–calcium complex before O_2 is released and the S_0 state is reformed, see [239, 241].

EPR spectroscopy is a highly powerful tool for determining the identity and location of water-derived species bound at or in the vicinity of the Mn_4O_5Ca cluster, specifically using W-band high-field EPR double-resonance techniques on isotope-labeled samples, in particular using $H_2{}^{17}O$ [242]. Information was achieved by means of high-field ^{17}O-EDNMR (Electron–Electron-Double-Resonance-Detected NMR, see Fig. 6) via the detection of the hyperfine and quadrupole couplings of magnetic nuclei, ^{1}H/^{2}H ($I = 1/2$, 1) or ^{17}O ($I = 5/2$), to the $S_{\text{eff}} = 1/2$ electronic states of the Kok-cycle (S_0, S_2 and S_3 oxydation states) of the Mn_4O_5Ca cluster, observing exchangeable ^{17}O "water" signals. Importantly, the induction of these ^{17}O signals, i.e., the rate with which the bulk solvent water ($H_2{}^{17}O$) exchanged with the bound Mn–^{16}O species, occurred on the same time-scale as observed in the mass spectrometry test experiment. For further details, see the [242] and also [239].

Under physiological conditions, the Mn_4CaO_5 cluster provides electron transfer from substrate water molecule to reduce the cationic radical $P_{680}{}^{\bullet+}$ via a nearby redox-active tyrosine residue Tyr161 of the D1 protein (denoted in the following as Y_Z). The electron transfer between Y_Z and $P_{680}{}^{\bullet+}$ is characterized by lifetimes in the range of 20–300 ns, depending on the S-state of the WOC [243–245]. Removal of the Mn_4CaO_5 cluster and the three extrinsic subunits PsbO, PsbP and PsbQ from the intact PS II complex results in significant retardation of the $Y_Z \rightarrow P_{680}{}^{\bullet+}$ electron transfer. The rate of Y_Z oxidation in these Mn-depleted (apo-WOC PS II) complexes shows a characteristic pH-dependence with half-lives of ~30 µs at pH 4, ~5 µs at pH 6.5 and ~180 ns above pH 8.5 [246–248] and exhibits a kinetic H/D isotope exchange effect [245, 249, 250]. It is believed that the phenolic side chain of Y_Z is most likely protonated in the reduced state and deprotonated in the oxidized

state. The transferred proton is thought to be accepted by D1-His190, which forms a hydrogen bond to Y_Z [245, 250]. The slowing down in the electron-transfer rate can be explained by the removal of the Mn_4CaO_5 cluster, which increases the accessibility of the suspension medium leading to a more hydrophilic surrounding of Y_Z. In addition, the hydrogen-bonding network may be disturbed, and pK values may be altered [248].

We have previously reported that the rates of electron-transfer reactions in PS I embedded in trehalose glassy matrix significantly change upon dehydration, and that this effect is similar to the effect observed at low temperature [48, 194, 196]. This similarity was ascribed to the restriction of conformational mobility observed both in glycerol glass at 170 K and in trehalose glass at 298 K [194]. Therefore, we studied the effect of a trehalose glassy matrix at low humidity on the kinetics of charge transfer in Mn-depleted PS II complexes, and compared it with the low temperature kinetics observed with similar PS II samples.

3.1.2 Summary of Preliminary Results on PSII/Trehalose

The preliminary results on the effect of desiccation of PS II in trehalose glassy matrix were recently presented [251]. Since the water-oxidizing complex does not operate at cryogenic temperatures (see [248] and references therein), for these experiments, we used apo-WOC PS II complexes, lacking the Mn_4CaO_5 cluster and extrinsic subunits PsbO, PsbP and PsbQ.

After nanosecond laser flash excitation the kinetics of the PS II primary donor $P_{680}^{\cdot+}$ reduction in these complexes, embedded in dry trehalose glass, was monitored by measuring the flash-induced absorption changes at 830 nm (ΔA_{830}) at relative humidity 11%. The lifetimes of the decay of two main kinetic components in solution were ~ 3 and ~ 10 μs with relative amplitudes of ~ 70 and 20%, correspondingly. These components can be assigned to electron transfer from tyrosine Y_Z to the photo-oxidized P_{680} in the Mn-depleted complexes, the lifetimes of which were shown to vary in the range of 2–20 μs for different samples [247, 252, 253].

Upon gradual dehydration in the presence of trehalose (from 73 to 11% of relative humidity), the kinetics of $P_{680}^{\cdot+}$ reduction became distributed. To analyze the complex decay kinetics, we used the Maximum Entropy method (MemExp), which calculates the experimental kinetics as a sum of a large number of exponential decays, characterized by lifetimes linearly distributed on the logarithmic scale [254]. The MemExp analysis showed that the relative contribution of the fast kinetic components decreased to ~ 45%, compared to 90% in solution [255]. In addition, the slower phases with lifetimes ~ 100 μs and ~ 1 ms appeared at the expense of faster phases. We suggested that these slower kinetic phases most probably, reflect the back reaction from the reduced primary quinone acceptor $Q_A^{\cdot-}$ to $P_{680}^{\cdot+}$ in the fraction of PSII, where the forward electron transfer $Y_Z \rightarrow P_{680}^{\cdot+}$ did not proceed.

As was previously shown, the recombination from $Q_A^{\cdot-}$ to $P_{680}^{\cdot+}$ in PS II complexes with the pre-oxidized Y_Z is temperature dependent at $T > 200$ K, and the kinetics is heterogeneous. At room temperature, it can be fitted to several

exponential components within the range of 120 µs to 5 ms [256–258]. Upon temperature lowering, the slower component accelerated and reached ~ 1 ms at $T \leq 200$ K. The yield of $P_{680}^{\cdot+}$ reduction by Y_Z decreased strongly at temperatures below 250 K, and reached about 50% at $T = 180$–190 K [248].

The slower kinetic components of the $P_{680}^{\cdot+}$ reduction observed at 11% in dry trehalose matrix accounted for 55% of the overall ΔA_{830} signal. Thus, our data are generally in line with the results observed with PS II in the glycerol-water mixture close to its glass transition temperature (180–190 K).

In conclusion, our preliminary results obtained with Mn-depleted PS II complexes embedded in a dry trehalose matrix allow to propose that the faster components (3–10 µs) are due to the forward electron transfer from Y_Z to $P_{680}^{\cdot+}$, which is sensitive to conformational constraints, while the ~ 0.1 ms and ~ 1 ms components are most probably related to charge recombination from $Q_A^{\cdot-}$ to $P_{680}^{\cdot+}$.

3.2 Extremolytes, Organic Osmolytes Protect Biological Macromolecules Against External Stress (Ectoine, Hydroxyectoine)

3.2.1 Introduction

Trehalose belongs to a vast class of solutes (termed *compatible solutes* for being non-toxic to the cell even at molar concentration) synthesized by extremophylic or extremotolerant organisms in order to face successfully extreme or detrimental environmental conditions, like osmotic stress at high salinity, very high or low temperature, extreme hydrostatic pressure, and oxygen radicals. These small molecules of low molecular weight, which include polyols (e.g., glycerol, sorbitol, mannitol), mono- and oligo-saccharides (e.g., glucose, sucrose, trehalose and glucosyl-glycerol), amino acids and derivatives (e.g., proline, glutamate, glutamine), quaternary amines (glycine and betaine), and ectoines (i.e., ectoine and hydroxyectoine), are designated *osmolytes*, being primarily accumulated by organisms able to grow at high salt concentrations to achieve osmotic balance across the cell membrane. The term *extremolytes* has been also introduced [259] to indicate organic osmolytes synthesized by extremophylic organisms.

Interestingly, several species isolated from samples taken in extreme environments, have been found to tolerate several different extrema (*polyextremophyles*). An impressive example is provided by tardigrades, i.e., micro-animals about 0.5 mm in size, colloquially known as water bears or moss piglets, close relatives of arthropodes. As a likely by-product of their anhydrobiotic capability (see Sect. 2.1), they show an extraordinary tolerance to a number of different extreme conditions: extremely low and high temperatures, from 4 to 400 K, high hydrostatic pressures up to 7.5 GPa, high radiation doses of 5000 Gy (gamma rays) and 6200 Gy (heavy ions). Additionally, in the dormant anhydrobiotic state, tardigrades can withstand desiccation for at least 10 years, resuming metabolism and animation upon rehydration. On the other hand, it is noteworthy that several osmolytes, which are typically synthesized in response to increased extracellular salinity (osmotic stress), are also

accumulated as a response to other environmental changes, such as very high or low temperatures. As an example, the osmolyte trehalose, accumulated by anhydrobiotic organisms to survive almost complete dehydration, is also synthesized in response to salt-induced osmotic stress [260–262], to high temperatures [263], and to freezing conditions [264]. The disaccharide trehalose, as shown also by in vitro studies, can therefore be considered as a universal "stress molecule", protecting biomolecules and biostructures against damages caused by high osmolarity, heat, oxidation, desiccation and freezing to cryogenic temperatures. Other osmolytes, such as ectoine and hydroxyectoine, are common compatible solutes, found in a wide range of halophilic and halotolerant bacteria, again in response to different stresses, like increased salinity and/or temperature [265]. Additionally, very often, in response to extreme conditions, a cocktail of different osmolytes is produced, the composition of which is modulated by environmental conditions.

This close association and interplay between diverse osmolytes and their capability to protect simultaneously against diverse harsh environmental conditions, which are found in vivo (polyextremophyles) and in vitro, as revealed by the wide spectrum of protective roles of some osmolytes (extremolytes), might implicate common underlying mechanisms at the molecular level. In any case, it can be reasonably expected that the comparative study of chemically different osmolytes, in relation to their bioprotective capabilities, will provide insight into the basic, finely tuned molecular strategies of the general phenomenon of bioprotection.

Among the large variety of extremolytes, we have focused on ectoine and its derivative hydroxyectoine (see Fig. 19), because these compounds, notwithstanding the obvious differences at the level of electronic structure (e.g., their zwitterionic character), appear to share several properties with trehalose. For instance, ectoine and hydroxyectoine display remarkable stabilizing capabilities towards two sensitive enzymes (lactic dehydrogenase and phosphofructokinase) with respect to freeze thawing, heat-treatment, and freeze-drying [266]. It has been additionally reported [267] that hydroxyectoine is a good glass forming compound, and that it exhibits a remarkable bioprotective effect in vitro against desiccation and heat denaturation of lactic dehydrogenase.

Quite interestingly, molecular dynamics simulations of an ectoine-water mixture, in the presence of the model protein *chymotrypsin inhibitor 2*, have shown that ectoine does not perturb the hydration shell of the protein, but retard the diffusion of water molecules at the protein surface [268]. These results are consistent with the notion that osmolytes, as it is assumed for trehalose according to the *preferential hydration hypothesis* (see Sect. 2.1), do not interact directly with macromolecules, but rather affect the solvent properties. A recent experimental study [269], based on

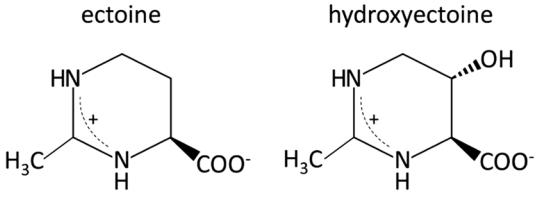

Fig. 19 Chemical structures of ectoine and hydroxyectoine

small angle neutron scattering, neutron diffraction and inelastic scattering, further supports the view that ectoine is essentially excluded from the dense hydration water layer around a model soluble protein (maltose binding protein), and suggests that ectoine perturbs the hydrogen bonding pattern of the solvent by weakening inter-water hydrogen bonding in the vicinity of the osmolyte.

In the light of these relationships, which appear to exist between many properties of ectoines and of trehalose, we have undertaken a systematic study of amorphous matrices formed by hydroxyectoine or ectoine and the bacterial reaction center (see Sect. 2.2.1), based on high-field EPR, FTIR and fast-laser spectroscopies. We aim at clarifying, by high-field EPR of a nitroxide radical dispersed into the amorphous matrices, the structural and dynamical organization of ectoine-RC matrices, in comparison with trehalose-RC glasses, with special emphasis on the proticity of these osmolytes within the respective glassy systems. We are investigating in parallel the capability of hydroxyectoine or ectoine matrices to inhibit fast, small-scale conformational dynamics of the RC, as probed by the kinetics of $P^{\bullet+}$ $Q_A^{\bullet-}$ recombination, as well as large-scale slow internal dynamics associated with unfolding, as revealed by thermal denaturation kinetics monitored by FT-NIR and visible absorption spectroscopy [49].

3.2.2 FT-NIR and Visible Absorption Spectroscopy

We anticipate in the following some preliminary results [152], which point to similarities and differences in protein–matrix interactions within glassy matrices formed by disaccharides (trehalose and sucrose) or by ectoine (and its derivative hydroxyectoine).

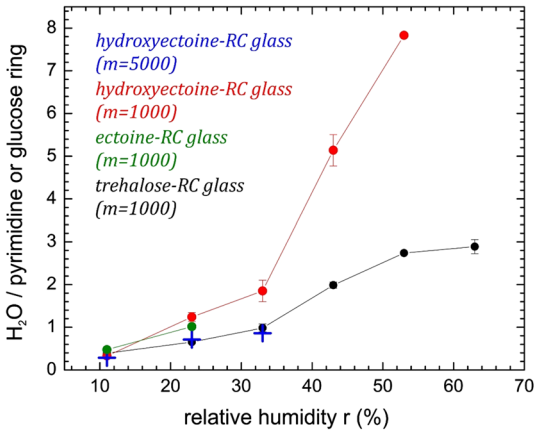

Fig. 20 Hydration isotherms at 297 K of glassy matrices incorporating the reaction center RC from *R. Sphaeroides* R-26, formed by trehalose (black symbols), ectoine (green symbols) and hydroxyectoine (red symbols), characterized by a molar ratio m between pyrimidine (one for ectoins) or glucose rings (two for trehalose) and RC equal to 10^3. Blue crosses refer to a hydroxyectoine-RC matrix with $m = 5 \times 10^3$. The content of residual water in matrices equilibrated at different values of relative humidity has been determined by FTIR spectroscopy from the area of the water combination band centered at 5150 cm^{-1}, using the absorption of the RC at 800 nm as an internal standard (see [61], for further details) (color figure online)

As to the ability of hydroxyectoine to form glasses, at variance with what was reported by Tanne and coworkers [267], we have found that binary hydroxyectoine-water systems, even upon fast dehydration under nitrogen flow, form amorphous matrices which undergo in a short time (minutes) extensive crystallization. This propensity to form crystallized areas is considerably alleviated by the incorporation of the reaction-center protein, resulting, particularly under extensive and fast dehydration (i.e., equilibration at a relative humidity $r = 11\%$), in stable ternary RC-hydroxyectoine (or ectoine)-water glassy matrices. The presence of the protein likely disturbs the establishment of a long-range order in the matrix structure. When progressively rehydrated, these glasses, at variance with trehalose matrices, exhibit, however, a high propensity to form crystallized areas, particularly in the case of ectoine. Crystallization, in turn, leads, even at room temperature, to rapid (on the time scales of hours) denaturation of the RC, as shown by the progressive loss of photochemical activity upon rehydration.

A comparison of the water sorption isotherms of the ectoine- and hydroxyectoine-RC glassy matrices with that of trehalose matrices (see Fig. 20), characterized by the same molar ratio between the glucose and pyrimidine rings and the RC, m, fixed at 10^3, indicates that hydration is similar in the driest matrices (equilibrated at a relative humidity $r = 11\%$), but becomes considerably higher in the ectoine- and hydroxyectoine-glasses when the relative humidity is increased. The higher hydration of hydroxyectoine matrices could arise from the zwitterionic character of the molecule, that makes it very polar. Interestingly, when the RC protein concentration within the hydroxyectoine is decreased (i.e., at a molar ratio m (pyrimidine rings/RC) of $\sim 5 \times 10^3$) the average water content per pyrimidine ring also decreases (compare red and blue symbols in Fig. 20). Such a behavior is readily explained by considering that the measured water content is clearly an average value, which includes water adsorbed to the hydroxyectoine bulk matrix and the water hydration shell of the protein. If the protein hydration layer is, at least partially, retained in the glass, at the higher protein concentration, the contribution of water from the hydration

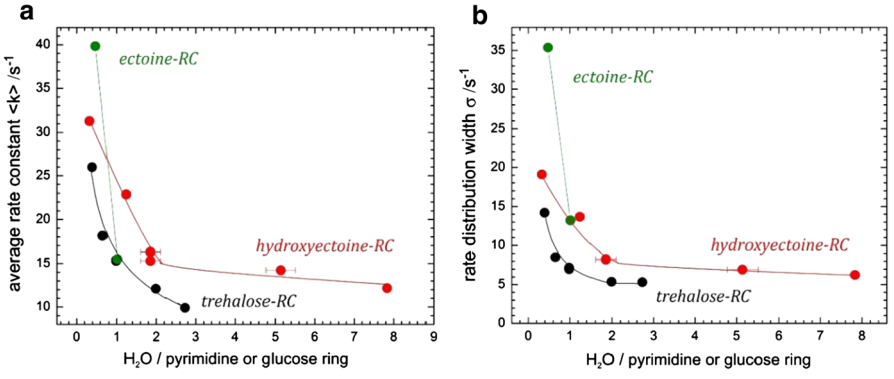

Fig. 21 Dependence of the kinetics of $P^{\bullet+}Q_A^{\bullet-}$ recombination upon the content of residual water in trehalose RC (black circles), ectoine-RC (green circles) and hydroxyectoine-RC glassy matrices (red circles), characterized by the same molar ratio between pyrimidine or glucose rings and RC, equal to 10^3. Panels **a** and **b** show the values of the average rate constant $< k >$ and rate distribution width σ, respectively (color figure online)

shell to the measured average water content is expected to be higher. This observation suggests therefore that the hydration shell of the protein is not replaced by the osmolyte (as assumed in the water replacement hypothesis), being rather in line with the preferential hydration hypothesis (see Sect. 2.1).

Kinetic analysis of $P^{\bullet+}Q_A^{\bullet-}$ recombination shows that extensively dehydrated ectoine and hydroxyectoine glasses inhibit the small-scale, short-time conformational dynamics of the RC to an extent comparable to that observed for trehalose matrices, keeping the molar ratio between glucose or pyrimidine rings and the RC fixed to 10^3 (see Fig. 21). Remarkably, the values of the average rate constant for charge recombination, $<k>$, and of the rate distribution width, σ, are systematically larger in the hydroxyectoine as compared to the trehalose matrix at any given water content. This could imply that, at comparable hydration levels, hydroxyectoine matrices are even more effective than trehalose matrices in inhibiting the RC conformational dynamics. We cannot exclude, however, that the hydroxyectoine, at variance with the trehalose matrix, perturbs slightly the RC structure, altering the configuration (distance and/or orientation) of the donor and acceptor cofactors, to an extent sufficient to affect the rate of electron transfer [154]. Or that the zwitterionic character of hydroxyectoine results in dielectric properties of the protein–matrix system which affect the reorganization energy [153] for the tunneling of the electron from $Q_A^{\bullet-}$ to $P^{\bullet+}$, in addition to the RC protein dynamics.

As mentioned in Sect. 2.2.1, thermal denaturation of the RC embedded into dried trehalose matrices is totally prevented even after weeks of incubation at 44 °C, demonstrating the extraordinary protein stabilization conferred by incorporation into trehalose glasses. A similar study of thermal denaturation kinetics, performed in comparably dried hydroxyectoine glassy matrices, has revealed a limited effectiveness in retarding RC unfolding. RC denaturation kinetics at 44 °C, obtained by FTIR and visible absorption spectroscopy approaches [49], indicate that in glassy matrices characterized by a molar ratio (hydroxyectoine/RC) of $m \approx 10^3$, the RC loses its native structure with a half-time of about 12 h, i.e., only a factor of two larger than that found in a RC film dehydrated in the absence of any excipient. When the (hydroxyectoine/RC) molar ratio is increased to 5×10^3, the half-time increases to about 40 h. In contrast ectoine matrices are totally ineffective in retarding RC denaturation, even destabilizing the RC protein as compared to a dehydrated RC-only film, in full agreement with previous studies which showed the superiority of amorphous hydroxyectoine- over ectoine-matrices in stabilizing embedded soluble model proteins [266, 267, 270].

All in all, ectoine- and hydroxyectoine-glasses display a remarkable capability of blocking, on the millisecond time-scale, protein conformational fluctuations and relaxation. However, the presence of ectoine in a dehydrated RC amorphous matrix, in contrast to trehalose, has no effect on the large-scale structural rearrangements required for protein unfolding, and hydroxyectoine-glasses can only retard large-scale dynamics to a limited extent. This failure in hampering on a long time scale the internal large-scale RC dynamics points to a looser protein–matrix dynamical coupling and/or to a softer protein-embedding matrix in hydroxyectoine as compared to trehalose glasses, in spite of the large macro-viscosity of both glassy systems. Again, high-field EPR spectroscopy of a nitroxide radical embedded in hydroxyectoine-RC

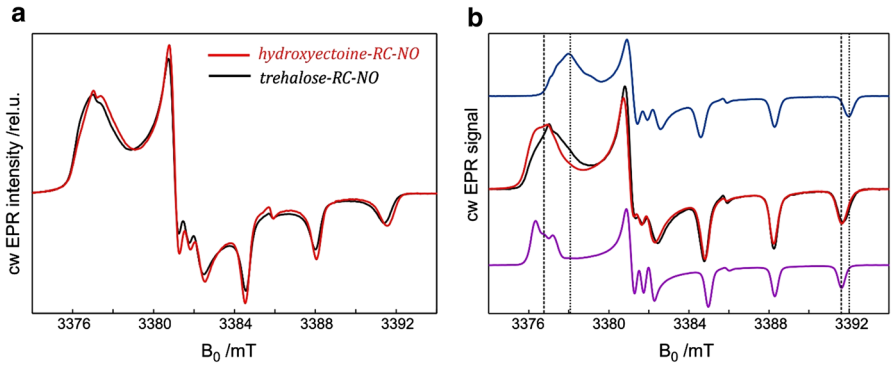

Fig. 22 Comparison between W-band cw EPR spectra of the perdeuterated nitroxide radical recorded, panel (**a**), at 293 K and in panel (**b**) at 150 K in a trehalose/RC glass with $m = 5 \times 10^3$ (black trace) and a hydroxyectoine/RC matrix with $m = 5 \times 10^3$ (red trace), equilibrated at a relative humidity $r = 11\%$. In panel (**b**), the blue and magenta traces show the 150 K W-band EPR spectra of the 1 mM nitroxide radical dissolved in H_2O/glycerol (90/10 vol%) and in *ortho*-terphenyl, respectively

matrices can provide a molecular basis for the behavior described above, yielding insights into the intermolecular hydrogen bond pattern which is expected to govern matrix dynamics.

3.2.3 EPR Spectroscopy

For the EPR measurements, in the bacterial RC from *R. sphaeroides*, the central high-spin iron Fe^{2+} of the chlorophylls was replaced by diamagnetic Zn^{2+} (Zn-RC). Figure 22a compares room-temperature W-band cw EPR spectra of perdeuterated nitroxide radicals (NO) dispersed into the hydroxyectione–RC matrix with the corresponding spectrum acquired in a trehalose–RC glass instead. To attain a common dehydration level, all samples have been equilibrated at the relative humidity $r = 11\%$, by exposure to a saturated solution of LiCl [61]. Both spectra exhibit the characteristic high-field lineshape predicted for a homogeneous distribution of well-immobilized nitroxide radicals. The spectra are clearly resolved into three B_0 regions, corresponding to the principal values of the g-tensor (g_{xx}, g_{yy} and g_{zz}); nitrogen ^{14}N hyperfine splitting into line triplets is distinctly observed in the g_{yy} and g_{zz} region. The observation of similar spectral lineshapes of both EPR spectra allows to conclude that the nitroxide probe in both samples has similar mobility and magnetic parameters. To switch off possible residual mobility contributions, the spectra taken at low temperature (150 K) were compared. Figure 22b shows the EPR spectra of both samples together with the reference spectra of the same nitroxide probe in frozen water/glycerol and *ortho*-terphenyl solutions, all recorded at 150 K. The most pronounced differences are observed in the g_{xx} spectral region. The spectral shape in this region is predominantly determined by the number and the type of hydrogen bonds that are experienced by the nitroxide radical [271]. The low-field shift of the g_{xx} component is pronounced in the hydroxyectione–RC matrix, its spectral position is practically coinciding with the magnetic field position of the g_{xx} component in

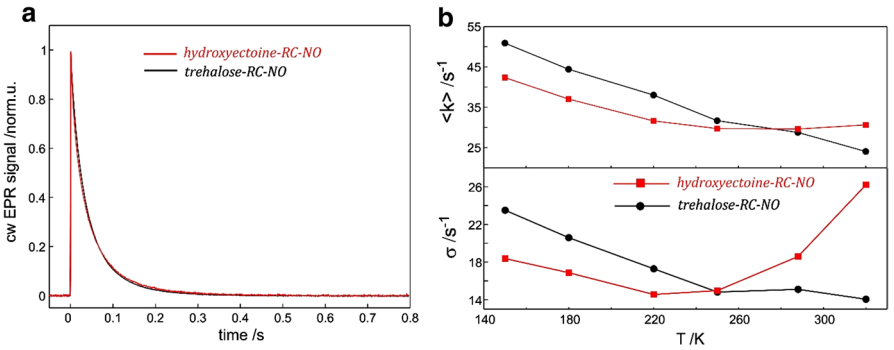

Fig. 23 **a** EPR-detected kinetics of $P^{\cdot+}_{865}Q^{\cdot-}_{A}$ recombination following a laser pulse in dark-adapted Zn-RC measured at 293 K in trehalose/RC glass (black trace) and hydroxyectoine/RC glass (red trace). **b** The temperature dependence of the average rate constant, $<k>$, and of the rate distribution width, σ, obtained from the power-law analysis of the experimental EPR kinetics. For any details, see the upcoming publication [152] (color figure online)

non-polar, non-protic *ortho*-terphenyl solution. Thus, the largest fraction of nitroxides in hydroxyectione-RC is not forming any hydrogen-bond complex, neither with water molecules nor with hydroxyectoine molecules. This is in contrast to the situation in trehalose–RC glass where the majority fraction of nitroxide radicals experience at least one H-bond, and only a small fraction of non-H-bonded complexes exists. Thus, hydroxyectoine itself is not interacting with the nitroxide directly, but is weakening nitroxide–water hydrogen bonding (see Sect. 3.2.1), i.e., is decreasing the overall proticity of the matrix.

Additionally, we conclude that the water hydration layer around the RC [269] is probably rather thin, since in a thick hydration layer the nitroxide probe molecules should have a higher mobility—which, however, is not observed in the EPR spectra acquired at room temperature or even higher temperatures.

Figure 23a shows selected EPR decay traces, due to charge recombination of $P^{\cdot+}_{865}$ and $Q^{\cdot-}_{A}$ radical ions in hydroxyectione-RC/NO and trehalose-RC/NO glasses at 293 K, respectively. They were acquired at the maximum $P^{\cdot+}_{865}$ EPR absorption using the transient-detection EPR technique with magnetic field modulation and lock-in detection. The differences between the traces are quite small. The average rate constants, $<k>$, and the rate distribution widths, σ, obtained from the power-law analysis of the EPR decay traces are in good agreement with those obtained from optical experiments. This shows that the sample dehydration conditions ($r = 11\%$) are the same for EPR and optical samples. An advantage of EPR spectroscopy is that it allows to easily measure the decay kinetics at different temperatures. Figure 23b compares the temperature dependence of the average rate constants and the rate distribution widths evaluated from EPR recordings. The behavior of the parameters is in line with what is expected for trehalose-RC samples. The temperature increase results in decrease of both $<k>$ and σ as it allows for additional restricted conformational protein dynamics leading to partial conformational relaxation of the charge-separated state $P^{\cdot+}Q_A^{\cdot-}$. The RC's incorporated in hydroxyectione show surprising results. Above about 230 K, both $<k>$ and σ start to increase. This indicates a

different mechanism of protein stabilization in hydroxyectione as compared with trehalose. For a more extended discussion, the reader is referred to an upcoming publication [152].

At the end of our Review, we would like to stress once again that the results obtained for membrane electron-transfer proteins in glassy matrices formed by chemically different organic osmolytes (trehalose, sucrose, ectoines) support a common bioprotection mechanism based on the conformational immobilization of the embedded protein complexes. The examined osmolytes, independently of their chemical structure, appear to share additionally the property of being essentially excluded from the surface of the protein, which retains, even under strongly dehydrated condition, a residual hydration shell. On the other hand, specific osmolyte-protein-water interactions, strongly conditioned by the diverse osmolyte proticity, have been shown to play an important role in determining the structure and dynamics of the entire matrix and, consequently, the osmolyte efficacy in bioprotection. These conclusions make the case for a systematic, comparative scrutiny of the numerous organic osmolytes synthesized by extremophylic and extremotolerant organisms. We expect that the spectroscopic approaches described in the present Review, combined with the use of photoexcitable model electron-transfer proteins like photosynthetic reaction centers, will contribute substantially to unravel the molecular details of in vivo bioprotection in its variety of declinations, and, at the same time, to optimally exploit glassy osmolyte matrices in the room-temperature in vitro preservation of labile biological macromolecules.

Acknowledgements Financial support from MIUR of Italy (RFO2018) is gratefully acknowledged by F. F. and G. V. This work was supported by the Russian Foundation for Basic Research (Grant 17-00-00201 to A. Yu. S.). The Max-Planck-Gesellschaft and the Cluster of Excellence RESOLV (EXC 1069), funded by the Deutsche Forschungsgemeinschaft (DFG), supported this work. K. M. gratefully acknowledges sustaining support by the Free University Berlin.

References

1. Y.S. Lebedev, in *Foundations of Modern EPR*, ed. by G.R. Eaton, S.S. Eaton, K.M. Salikhov (World Scientific, Singapore, 1998), p. 731
2. O. Grinberg, L.J. Berliner (eds.), *Very High Frequency (VHF) ESR/EPR* (Springer, New York, 2004)
3. K. Möbius, A. Savitsky, *High-Field EPR Spectroscopy on Proteins and Their Model Systems* (RSC Publishing, Cambridge, 2009)
4. S.M. Hsu, J. Zhang, Z. Yin, Tribol. Lett. **13**, 131 (2002)
5. K.-P. Müller, *Lehrbuch der Oberflächentechnik* (Vieweg, Braunschweig, 1996)
6. M. Scherge, S. Gorb, *Biological Micro- and Nanotribology, Nature's Solutions* (Springer, Berlin, 2001)
7. X. He, S.H. Kim, Langmuir **33**, 2717 (2017)
8. Y. Wang, N. Yamada, J. Xu, J. Zhang, Q. Chen, Y. Ootani, Y. Higuchi, N. Ozawa, M.-I. De Barros Bouchet, J.M. Martin, S. Mori, K. Adachi, M. Kubo, Sci. Adv. **5**, eaax9301 (2019)
9. S.D. Chemerisov, O.Y. Grinberg, D.S. Tipikin, Y.S. Lebedev, H. Kurreck, K. Möbius, Chem. Phys. Lett. **218**, 353 (1994)
10. D. Gust, T.A. Moore, Advan. Photochem. **16**, 1 (1991)
11. J. von Gersdorff, M. Huber, H. Schubert, D. Niethammer, B. Kirste, M. Plato, K. Möbius, H. Kurreck, R. Eichberger, R. Kietzmann, F. Willig, Angew. Chem. Intern. Ed. Engl. **29**, 670 (1990)

12. F. Lendzian, J. Schlüpmann, J. von Gersdorff, K. Möbius, H. Kurreck, Angew. Chem. Intern. Ed. Engl. **30**, 1461 (1991)
13. M.R. Wasielewski, Chem. Rev. **92**, 435 (1992)
14. F. Pöllinger, H. Heitele, M.E. Michel-Beyerle, C. Anders, M. Futscher, H.A. Staab, Chem. Phys. Lett. **198**, 645 (1992)
15. K. Hasharoni, H. Levanon, J. von Gersdorff, H. Kurreck, K. Möbius, J. Chem. Phys. **98**, 2916 (1993)
16. F. Lendzian, M. Huber, R.A. Isaacson, B. Endeward, M. Plato, B. Bönigk, K. Möbius, W. Lubitz, G. Feher, Biochim. Biophys. Acta **1183**, 139 (1993)
17. T.F. Prisner, A. van der Est, R. Bittl, W. Lubitz, D. Stehlik, K. Möbius, Chem. Phys. **194**, 361 (1995)
18. W. Lubitz, Phys. Chem. Chem. Phys. **4**, 5539 (2002)
19. H. Kurreck, M. Huber, Angew. Chem. Intern. Ed. Engl. **34**, 849 (1995)
20. D. Gust, T.A. Moore, A.L. Moore, Faraday Discuss. **155**, 9 (2012)
21. T.A. Faunce, W. Lubitz, A.W. Rutherford, D. MacFarlane, G.F. Moore, P. Yang, D.G. Nocera, T.A. Moore, D.H. Gregory, S. Fukuzumi, K.B. Yoon, F.A. Armstrong, M.R. Wasielewski, S. Styring, Energy Environ. Sci. **6**, 695 (2013)
22. D.R. Whang, D.H. Apaydin, Chem. Photo. Chem. **2**, 148 (2018)
23. B. Zhang, L. Sun, Chem. Soc. Rev. **48**, 2216 (2019)
24. G. Heinicke, *Tribochemistry* (Carl Hanser, Munich, 1984)
25. Y.S. Lebedev, in *Modern Pulsed and Continuous-Wave Electron Spin Resonance*, ed. by L. Kevan, M.K. Bowman (Wiley, New York, 1990), p. 365
26. N.M. Atherton, *Electron Spin Resonance, Theory and Applications* (Wiley, New York, 1973)
27. S.N. Dobryakov, G.G. Lazarev, M.V. Serdobov, Y.S. Lebedev, Mol. Phys. **36**, 877 (1978)
28. C.A. Hutchison Jr., in *The Triplet State*, ed. by A.B. Zahlan (Cambridge University Press, Cambridge, 1967), p. 63
29. A.W. Hornig, J.S. Hyde, Mol. Phys. **6**, 33 (1963)
30. R. Huber, M. Schwoerer, C. Bubeck, H. Six, Chem. Phys. Lett. **53**, 35 (1978)
31. D.S. Tipikin, G.G. Lazarev, Y.S. Lebedev, Russian. J. Phys. Chem. **67**, 159 (1993)
32. S.D. Chemerisov, G.D. Perekhodtsev, D.S. Tipikin, Ya.S. Lebedev, A.I. Prokofev, A.I. Aleksandrov, A.A. Dubinskii, K. Möbius, O.G. Poluektov, J. Schmidt, J. Chem. Soc., Faraday Trans. **92**, 1959 (1996)
33. D.S. Tipikin, Y.S. Lebedev, O.G. Poluektov, J. Schmidt, Chem. Phys. Lett. **215**, 199 (1993)
34. A.I. Aleksandrov, A.I. Prokofev, I. Yu Metlenkova, N.N. Bubnov, D.S. Tipikin, S.D. Chemerisov, G.D. Perekhodtsev, Y.S. Lebedev, Russ. J. Phys. Chem. **69**, 743 (1995)
35. A.I. Aleksandrov, A.I. Prokofev, I. Yu Metlenkova, N.N. Bubnov, D.S. Tipikin, S.D. Chemerisov, G.D. Perekhodtsev, Y.S. Lebedev, Russ. J. Phys. Chem. **70**, 25 (1996)
36. C.P. Poole Jr., *Electron Spin Resonance* (Wiley, New York, 1983)
37. R.T. Weber, J.A.J.M. Disselhorst, L.J. Prevo, J. Schmidt, WTh Wenckebach, J. Magn. Reson. **81**, 129 (1989)
38. O. Burghaus, M. Rohrer, T. Götzinger, M. Plato, K. Möbius, Meas. Sci. Technol. **3**, 765 (1992)
39. K. Möbius, M. Plato, W. Lubitz, Phys. Rev. **87**, 172 (1992)
40. L. Cordone, G. Cottone, S. Giuffrida, G. Palazzo, G. Venturoli, C. Viappiani, Biochim. Biophys. Acta, Proteins Proteomics **1749**, 252 (2005)
41. L. Cordone, G. Cottone, A. Cupane, A. Emanuele, S. Giuffrida, M. Levantino, Curr. Org. Chem. **19**, 1684 (2015)
42. R.H. Austin, K.W. Beeson, L. Eisenstein, H. Frauenfelder, I.C. Gunsalus, Biochemistry **14**, 5355 (1975)
43. R.H. Austin, A. Xie, L. van der Meer, B. Redlich, P.-A. Lindgård, H. Frauenfelder, D. Fu, Phys. Rev. Lett. **94**, 128101 (2005)
44. D. Kleinfeld, M.Y. Okamura, G. Feher, Biochemistry **23**, 5780 (1984)
45. B.H. McMahon, J.D. Muller, C.A. Wraight, G.U. Nienhaus, Biophys. J. **74**, 2567 (1998)
46. P.R. Pokkuluri, P.D. Laible, A.E. Crawford, J.F. Mayfield, M.A. Yousef, S.L. Ginell, D.K. Hanson, M. Schiffer, FEBS Lett. **560**, 171 (2004)
47. A. Savitsky, M. Malferrari, F. Francia, G. Venturoli, K. Möbius, J. Phys. Chem. B **114**, 12729 (2010)
48. M. Malferrari, A. Savitsky, M.D. Mamedov, G.E. Milanovsky, W. Lubitz, K. Möbius, AYu Semenov, G. Venturoli, Biochim. Biophys. Acta **1857**, 1440 (2016)

49. M. Malferrari, F. Francia, G. Venturoli, J. Phys. Chem. B **119**, 13600 (2015)
50. S.J. Hagen, J. Hofrichter, W.A. Eaton, Science **269**, 959 (1995)
51. S.J. Hagen, J. Hofrichter, W.A. Eaton, J. Phys. Chem. **100**, 12008 (1996)
52. L. Cordone, P. Galajda, E. Vitrano, A. Gassmann, A. Ostermann, F. Parak, Eur. Biophys. J. **27**, 173 (1998)
53. L. Cordone, M. Ferrand, E. Vitrano, G. Zaccai, Biophys. J. **76**, 1043 (1999)
54. S.J. Clegg, Comp. Biochem. Physiol. B **128**, 613 (2001)
55. L.M. Crowe, Comp. Biochem. Physiol. A **131**, 505 (2002)
56. W.W. Parson, Biochim. Biophys. Acta **153**, 248 (1968)
57. G. Feher, Photochem. Photobiol. **14**, 373 (1971)
58. D. Stehlik, C.H. Bock, J. Petersen, J. Phys. Chem. **93**, 1612 (1989)
59. A. Schnegg, M. Fuhs, M. Rohrer, W. Lubitz, T.F. Prisner, K. Möbius, J. Phys. Chem. B **106**, 9454 (2002)
60. J.H. Freed, in *Biological Magnetic Resonance*, ed. by S.R. Eaton, G.R. Eaton, L.J. Berliner, vol. 24 (Kluwer, Boston, 2005) p. 239
61. M. Malferrari, F. Francia, G. Venturoli, J. Phys. Chem. B **115**, 14732 (2011)
62. J.J. Max, C. Chapados, J. Phys. Chem. **116**, 4626 (2002)
63. S. Giuffrida, G. Cottone, L. Cordone, Phys. Chem. Chem. Phys. **19**, 4251 (2017)
64. P.K. Verma, A. Kundu, M.S. Puretz, C. Dhoonmoon, O.S. Chegwidden, C.H. Londergan, M. Cho, J. Phys. Chem. B **122**, 2587 (2018)
65. J. Ingram, D. Bartels, Annu. Rev. Plant Physiol. Plant Mol. Biol. **47**, 377 (1996)
66. P. Alpert, Integr. Comp. Biol. **45**, 685 (2005)
67. A. Tunnacliffe, J. Lapinski, Phil. Trans. R. Soc. Lond. B **358**, 1755 (2003)
68. J.H. Crowe, J.F. Carpenter, L.M. Crowe, Annu. Rev. Physiol. **60**, 73 (1998)
69. M. Sakurai, T. Furuki, K.-I. Akao, D. Tanaka, Y. Nakahara, T. Kikawada, M. Watanabe, T. Okuda, Proc. Natl. Acad. Sci. USA **105**, 5093 (2008)
70. S.C. Hand, M.A. Menze, M. Toner, L. Boswell, D. Moore, Annu. Rev. Physiol. **73**, 115 (2011)
71. T.C. Boothby, H. Tapia, A.H. Brozena, S. Piszkiewicz, A.E. Smith, A. Giovannini, L. Rebecchi, G.J. Pielak, D. Koshland, B. Goldstein, Mol. Cell **65**, 975 (2017)
72. A. Eroglu, M.J. Russo, R. Bieganski, A. Fowler, S. Cheley, H. Bayley, M. Toner, 4 Nat. Biotechnol. **18**, 163 (2000)
73. S. Ohtake, Y.J. Wang, J. Pharm. Sci. **100**, 2020 (2011)
74. D.S. Dimitrov, Methods Mol. Biol. **899**, 1 (2012)
75. M.C. Manning, D.K. Chou, B.M. Murphy, R.W. Payne, D.S. Katayama, Pharm. Res. **27**, 544 (2010)
76. M.A. Mensink, H.W. Frijlink, K. van der Voort Maarschalk, W.L.J. Hinrichs, Eur. J. Pharm. Biopharm. **114**, 288 (2017)
77. S. Giuffrida, G. Cottone, F. Librizzi, L. Cordone, J. Phys. Chem. B **107**, 13211 (2003)
78. G. Caliskan, A. Kisliuk, A.M. Tsai, C.L. Soles, A.P. Sokolov, J. Phys. Chem. **118**, 4230 (2003)
79. G. Caliskan, D. Mechtani, J.H. Roh, A. Kisliuk, A.P. Sokolov, S. Azzam, M.T. Cicerone, S. Lin-Gibson, I. Peral, J. Phys. Chem. **121**, 1978 (2004)
80. A. Longo, S. Giuffrida, G. Cottone, L. Cordone, Phys. Chem. Chem. Phys. **12**, 6852 (2010)
81. G. Bellavia, S. Giuffrida, G. Cottone, A. Cupane, L. Cordone, J. Phys. Chem. B. **115**, 6340 (2011)
82. E.F. Semeraro, S. Giuffrida, G. Cottone, A. Cupane, J. Phys. Chem. B **121**, 8731 (2017)
83. G. Cottone, L. Cordone, G. Ciccotti, Biophys. J. **80**, 931 (2001)
84. G. Cottone, S. Giuffrida, G. Ciccotti, L. Cordone, Proteins: Struct., Funct., Bioinf. **59**, 291 (2005)
85. A. Lerbret, F. Affouard, A. Hedoux, S. Krenzlin, J. Siepmann, M.-C. Bellissent-Funel, M. Descamps, J. Phys. Chem. B **116**, 11103 (2012)
86. H. Frauenfelder, B.H. McMahon, Ann. Phys. (Leipzig) **9**, 655 (2000)
87. J.G. Sampedro, S. Uribe, Mol. Cell. Biochem. **256**, 319 (2004)
88. J.L. Green, C.A. Angell, J. Phys. Chem. **93**, 2880 (1989)
89. C. Schebor, M.P. Buera, J. Chirife, J. Food. Eng. **30**, 269 (1996)
90. B.S. Chang, R.M. Beauvais, A. Dong, J.F. Carpenter, Arch. Biochem. Biophys. **331**, 249 (1996)
91. W.Q. Sun, P. Davidson, Biochim. Biophys. Acta **1425**, 235 (1998)
92. M.T. Cicerone, J.F. Douglas, Soft Matter **8**, 2983 (2012)
93. J. Buitink, C. Walters-Vertucci, F.A. Hoekstra, O. Leprince, Plant Physiol. **111**, 235 (1996)
94. J.F. Carpenter, J.H. Crowe, Biochemistry **28**, 3916 (1989)
95. S.N. Timasheff, Biochemistry **41**, 13473 (2002)

96. T. Arakawa, S.N. Timasheff, Biochemistry **21**, 6536 (1982)
97. P.S. Belton, A.M. Gill, Biopolymers **34**, 957 (1994)
98. G. Cottone, G. Ciccotti, L. Cordone, J. Chem. Phys. **117**, 9862 (2002)
99. C. Olsson, S. Genheden, V. García Sakai, J. Swenson, J. Phys. Chem. B **123**, 3679 (2019)
100. S.N. Timasheff, Biochemistry **31**, 9857 (1992)
101. T. Arakawa, S.N. Timasheff, Biophys. J. **47**, 411 (1985)
102. F. Francia, M. Dezi, A. Mallardi, G. Palazzo, L. Cordone, G. Venturoli, J. Am. Chem. Soc. **130**, 10240 (2008)
103. G. Cottone, S. Giuffrida, S. Bettati, S. Bruno, B. Campanini, M. Marchetti, S. Abbruzzetti, C. Viappiani, A. Cupane, A. Mozzarelli, L. Ronda, Catalists **9**, 1024 (2019)
104. K.D. Rector, J. Jiang, M.A. Berg, M.D. Fayer, J. Phys. Chem. B. **105**, 1081 (2001)
105. M. Tarek, D.J. Tobias, Phys. Rev. Lett. **88**, 138101 (2002)
106. K. Wood, F.-X. Gallat, R. Otten, A.J. van Heel, M. Lethier, L. van Eijck, M. Moulin, M. Haertlein, M. Weik, F.A.A. Mulder, Angew. Chem. Int. Ed. **52**, 665 (2013)
107. H. Frauenfelder, B.H. McMahon, Proc. Natl. Acad. Sci. USA **95**, 4795 (1998)
108. F. Librizzi, C. Viappiani, S. Abbruzzetti, L. Cordone, J. Chem. Phys. **116**, 1193 (2002)
109. A.M. Massari, I.J. Finkelstein, B.L. McClain, A. Goj, X. Wen, K.L. Bren, R.F. Loring, M.D. Faye, J. Am. Chem. Soc. **127**, 14279 (2005)
110. M. Malferrari, A. Savitsky, W. Lubitz, K. Möbius, G. Venturoli, J. Phys. Chem. Lett. **7**, 4871 (2016)
111. G. Palazzo, A. Mallardi, A. Hochkoeppler, L. Cordone, G. Venturoli, Biophys. J. **82**, 558 (2002)
112. F. Francia, G. Palazzo, A. Mallardi, L. Cordone, G. Venturoli, Biophys. J. **85**, 2760 (2003)
113. F. Francia, G. Palazzo, A. Mallardi, L. Cordone, G. Venturoli, Biochim. Biophys. Acta Bioenerg. **1658**, 50 (2004)
114. P. Lunkenheimer, A. Loidl, Chem. Phys. **284**, 205 (2002)
115. M. Orrit, Angew. Chem. Inter. Ed. **52**, 163 (2013)
116. G.P. Johari, M. Goldstein, J. Chem. Phys. **55**, 4245 (1971)
117. P. Allegrini, J.F. Douglas, S.C. Glotzer, Phys. Rev. E. **60**, 5714 (1999)
118. K. Kaminski, E. Kaminska, K.L. Ngai, M. Paluch, P. Wlodarczyk, A. Kasprzycka, W. Szeja, J. Phys. Chem. B **113**, 10088 (2009)
119. H. Frauenfelder, G. Chen, J. Berendzen, P.W. Fenimore, H. Jansson, B.H. McMahon, I.R. Stroe, J. Swenson, R.D. Young, Proc. Natl. Acad. Sci. USA **106**, 5129 (2009)
120. M.D. Ediger, Ann. Rev. Phys. Chem. **51**, 99 (2000)
121. R.A. Riggleman, J.F. Douglas, J.J. de Pablo, Soft Matter **6**, 292 (2010)
122. L. Sloten, Biochim. Biophys. Acta **275**, 208 (1972)
123. J.H. Freed, in *Very High Frequency (VHF) ESR/EPR*, ed. by O. Grinberg, L.J. Berliner (Springer, New York, 2004), p. 19
124. K. Möbius, W. Lubitz, N. Cox, A. Savitsky, Magnetochemistry **4**, 50 (2018)
125. T.F. Prisner, M. Rohrer, K. Möbius, Appl. Magn. Reson. **7**, 167 (1994)
126. K. Möbius, A. Savitsky, A. Schnegg, M. Plato, M. Fuchs, Phys. Chem. Chem. Phys. **7**, 19 (2005)
127. A. Savitsky, J. Niklas, J.H. Golbeck, K. Möbius, W. Lubitz, Phys. Chem B. **117**, 11184 (2013)
128. A. Nalepa, K. Möbius, W. Lubitz, A. Savitsky, J. Magn. Reson. **242**, 203 (2014)
129. K. Möbius, W. Lubitz, A. Savitsky, Prog. Nucl. Magn. Res. Spec. **75**, 1 (2013)
130. A. Schweiger, G. Jeschke, *Principles of Pulse Electron Paramagnetic Resonance* (Oxford University Press, Oxford, 2001)
131. D. Goldfarb, S. Stoll (eds.), *EPR Spectroscopy: Fundamentals and Methods* (Wiley, New York, 2018)
132. C. Kirmaier, D. Holten, Photosynth. Res. **13**, 225 (1987)
133. G. Feher, J.P. Allen, M.Y. Okamura, D.C. Rees, Nature **339**, 111 (1989)
134. J.C. Williams, R.G. Alden, H.A. Murchison, J.M. Peloquin, N.W. Woodbury, J.P. Allen, Biochemistry **31**, 11029 (1992)
135. C.-K. Tang, J.A. Williams, A.K.W. Taguchi, P. James, J.P. Allen, N.W. Woodbury, Biochemistry **38**, 8794 (1999)
136. M.Y. Okamura, M.L. Paddock, M.S. Graige, G. Feher, Biochim. Biophys. Acta **1458**, 148 (2000)
137. H. Frauenfelder, B.H. McMahon, P.W. Fenimore, Proc. Natl. Acad. Sci. USA **100**, 8615 (2003)
138. H. Wang, S. Lin, J.P. Allen, J.C. Williams, S. Blankert, C. Laser, N.W. Woodbury, Science **316**, 747 (2007)

139. G. Katona, A. Snijder, P. Gourdon, U. Andréasson, Ö. Hansson, L.-E. Andréasson, R. Neutze, Nat. Struct. Mol. Biol. **12**, 630 (2005)
140. M.H.B. Stowell, T.M. McPhillips, D.C. Rees, S.M. Soltis, E. Abresch, G. Feher, Science **276**, 812 (1997)
141. Q. Xu, M.R. Gunner, Biochemistry **40**, 3232 (2001)
142. Q. Xu, M.R. Gunner, Biochemistry **41**, 2694 (2002)
143. Q. Xu, L. Baciou, P. Sebban, M.R. Gunner, Biochemistry **41**, 10021 (2002)
144. J. Breton, C. Boullais, C. Mioskowski, P. Sebban, L. Baciou, E. Nabedryk, Biochemistry **41**, 12921 (2002)
145. J. Breton, Biochemistry **43**, 3318 (2004)
146. C.R.D. Lancaster, Biochim. Biophys. Acta **1365**, 143 (1998)
147. A. Kuglstatter, U. Ermler, H. Michel, L. Baciou, G. Fritzsch, Biochemistry **40**, 4253 (2001)
148. U. Zachariae, C.R.D. Lancaster, Biochim. Biophys. Acta **1505**, 280 (2001)
149. S.E. Walden, R.A. Wheeler, J. Phys. Chem. B **106**, 3001 (2002)
150. J.M. Kriegl, G.U. Nienhaus, Proc. Natl. Acad. Sci. USA **101**, 123 (2004)
151. J.M. Kriegl, F.K. Forster, G.U. Nienhaus, Biophys. J. **85**, 1851 (2003)
152. M. Malferrari, A. Savitsky, F. Francia, K. Möbius, G. Venturoli, in preparation (2020)
153. R.A. Marcus, N. Sutin, Biochim. Biophys. Acta Rev. Bioenerget. **811**, 265 (1985)
154. C.C. Moser, J.M. Keske, K. Warncke, R.S. Farid, P.L. Dutton, Nature **355**, 796 (1992)
155. S.S. Deshmukh, J.C. Williams, J.P. Allen, L. Kalman, Biochemistry **50**, 340 (2011)
156. S.S. Deshmukh, J.C. Williams, J.P. Allen, L. Kalman, Biochemistry **50**, 3321 (2011)
157. E. Nabedryk, K.A. Bagley, D.L. Thibodeau, M. Bauscher, W. Mäntele, J. Breton, FEBS Lett. **266**, 59 (1990)
158. T. Iwata, M.L. Paddock, M.Y. Okamura, H. Kandori, Biochemistry **48**, 1220 (2009)
159. M. Malferrari, A. Mezzetti, F. Francia, G. Venturoli, Biochim. Biophys. Acta Bioenerg. **1827**, 328 (2013)
160. E.C. López-Díez, S. Bone, Biochim. Biophys. Acta **1673**, 139 (2004)
161. B. Roser, Biopharm. **4**, 47 (1991)
162. C. Colaco, S. Sen, M. Thangavelu, S. Pinder, B. Roser, Biotechnology **10**, 1007 (1992)
163. M. Uritani, M. Takai, K. Yoshinaga, J. Biochem. **117**, 774 (1995)
164. S. Giuffrida, G. Cottone, L. Cordone, J. Phys. Chem. B **108**, 15415 (2004)
165. S. Giuffrida, G. Cottone, L. Cordone, Biophys. J. **91**, 968 (2006)
166. M. Malferrari, A. Nalepa, G. Venturoli, F. Francia, W. Lubitz, K. Möbius, A. Savitsky, Phys. Chem. Chem. Phys. **16**, 9831 (2014)
167. P. Gast, R.T.L. Herbonnet, J. Klare, A. Nalepa, C. Rickert, D. Stellinga, L. Urban, K. Möbius, A. Savitsky, H.J. Steinhoff, E.J.J. Groenen, Phys. Chem. Chem. Phys.**16**, 15910 (2014)
168. C.J. Roberts, P.G. Debenedetti, J. Phys. Chem. B **103**, 7308 (1999)
169. P.B. Conrad, J.J. de Pablo, J. Phys. Chem. A **103**, 4049 (1999)
170. A. Lerbret, P. Bordat, F. Affouard, M. Descamps, F. Migliardo, J. Phys. Chem. B **109**, 11046 (2005)
171. G.A. Jeffrey, S. Takagi, Acc. Chem. Res. **11**, 264 (1978)
172. D.B. Davies, J.C. Christofides, Carbohydr. Res. **163**, 269 (1987)
173. N.C. Ekdawi-Sever, P.B. Conrad, J.J. de Pablo, J. Phys. Chem. A **105**, 734 (2001)
174. S. Magazu, V. Villari, P. Migliardo, G. Maisano, M.T.F. Telling, J. Phys. Chem. B **105**, 1851 (2001)
175. U. Heugen, G. Schwaab, E. Bruendermann, M. Heyden, X. Yu, D.M. Leitner, M. Havenith, Proc. Natl. Acad. Sci. USA **103**, 12301 (2006)
176. F. Affouard, P. Bordat, M. Descamps, A. Lerbret, S. Magazu, F. Migliardo, A.J. Ramirez-Cuesta, M.F.T. Telling, Chem. Phys. **317**, 258 (2005)
177. M.V. Fedorov, J.M. Goodman, D. Nerukh, S. Schumm, Phys. Chem. Chem. Phys. **13**, 2294 (2011)
178. J.H. Golbeck (ed.), *Photosystem I. The light-Driven Plastocyanin: Ferredoxin Oxidoreductase* (Springer, Dordrecht, 2006)
179. P. Jordan, P. Fromme, H.T. Witt, O. Klukas, W. Saenger, N. Krauß, Nature **411**, 909 (2001)
180. K. Brettel, W. Leibl, Biochim. Biophys. Acta **1507**, 100 (2001)
181. M. Mamedov, Govindjee, V. Nadtochenko, A. Semenov, Photosynth. Res. **125**, 51 (2015)
182. M. Guergova-Kuras, B. Boudreaux, A. Joliot, P. Joliot, K. Redding, Proc. Natl. Acad. Sci. USA **98**, 4437 (2001)
183. N. Srinivasan, J.H. Golbeck, Biochim. Biophys. Acta **1787**, 1057 (2009)

184. J. Deisenhofer, O. Epp, K. Miki, R. Huber, H. Michel, Nature **318**, 618 (1985)
185. H. Komiya, T.O. Yeates, D.C. Rees, J.P. Allen, G. Feher, Proc. Natl. Acad. Sci. USA **85**, 9012 (1988)
186. I.V. Shelaev, F.E. Gostev, M.D. Mamedov, O.M. Sarkisov, V.A. Nadtochenko, V.A. Shuvalov, A.Y. Semenov, Biochim. Biophys. Acta **1797**, 1410 (2010)
187. K. Brettel, Biochim. Biophys. Acta **1318**, 322 (1997)
188. P. Setif, H. Bottin, Biochemistry **28**, 2689 (1989)
189. I.R. Vassiliev, Y.S. Jung, M.D. Mamedov, AYu Semenov, J.H. Golbeck, Biophys. J. **72**, 301 (1997)
190. K. Brettel, J.H. Golbeck, Photosynth. Res. **45**, 183 (1995)
191. D.A. Cherepanov, G.E. Milanovsky, O.A. Gopta, R. Balasubramanian, D.A. Bryant, A.Y. Semenov, J.H. Golbeck, J. Phys. Chem. B **122**, 7943 (2018)
192. P. Sétif, P. Mathis, T. Vänngård, Biochim. Biophys. Acta **767**, 404 (1984)
193. E. Schlodder, K. Falkenberg, M. Gergeleit, K. Brettel, Biochemistry **37**, 9466 (1998)
194. G. Milanovsky, O. Gopta, A. Petrova, M. Mamedov, M. Gorka, D. Cherepanov, J. Golbeck, A. Semenov, Biochim. Biophys. Acta Bioenerget. **1860**, 601 (2019)
195. I. Shelaev, M. Gorka, A. Savitsky, V. Kurashov, M. Mamedov, F. Gostev, K. Möbius, V. Nadtochenko, J. Golbeck, A. Semenov, Zeitschrift für Physikalische Chemie (J. Phys. Chem.) **231**, 325 (2017)
196. V. Kurashov, M. Gorka, G.E. Milanovsky, T.W. Johnson, D.A. Cherepanov, AYu Semenov, J.H. Golbeck, Biochim. Biophys. Acta Bioenerget. **1859**, 1288 (2018)
197. P. Fromme, I. Grotjohann, in *Photosystem I. The Light-Driven Plastocyanin:Ferredoxin Oxidoreductase*, ed. by J. Golbeck (Springer, Dordrecht, 2006), p. 47
198. V.P. Shinkarev, in *Photosystem I. The Light-Driven Plastocyanin: Ferredoxin Oxidoreductase*, ed. by J. Golbeck (Springer, Dordrecht, 2006), p. 612
199. S. Santabarbara, R. Jennings, G. Zucchelli, in *The Biophysics of Photosynthesis*, ed. by J. Golbeck, A. van der Est (Springer, New York, 2014) p. 241
200. D.H. Rasmussen, A.P. MacKenzie, J. Phys. Chem. **75**, 967 (1971)
201. J.G. Constantin, M. Schneider, H.R. Corti, J. Phys. Chem. B **120**, 5047 (2016)
202. P.J. Hore, in *Advanced EPR. Applications in Biology and Biochemistry*, ed. by A.J. Hoff (Elsevier, Amsterdam, 1989), p.405
203. M. Kanduč, A. Schlaich, E. Schneck, R.R. Netz, Langmuir **32**, 8767 (2016)
204. C. Olsson, H. Jansson, J. Swenson, J. Phys. Chem. B **120**, 4723 (2016)
205. A. Nalepa, M. Malferrari, W. Lubitz, G. Venturoli, K. Möbius, A. Savitsky, Phys. Chem. Chem. Phys. **19**, 28388 (2017)
206. J. Koepke, E.M. Krammer, A.R. Klingen, P. Sebban, G.M. Ullmann, G. Fritzsch, J. Mol. Biol. **371**, 396 (2007)
207. D.E. Giangiacomo, M.R. Gunner, L.P. Dutton, in *Progress in Photosynthesis Research*, ed. by J. Biggins (Springer, Dordrecht, 1987), p. 409
208. J.A. Rard, J. Solution Chem. **48**, 271 (2019)
209. M. Malferrari, G. Venturoli, F. Francia, A. Mezzetti, Spectrosc. Int. J. **27**, 337 (2012)
210. L.B. Rockland, Anal. Chem. **32**, 1375 (1960)
211. S. Khodadadi, A.P. Sokolov, Biochim. Biophys. Acta **1861**, 3546 (2017)
212. K. Henzler-Wildman, D. Kern, Nature **450**, 964 (2007)
213. S. Khodadadi, A.P. Sokolov, Soft Matter **11**, 4984 (2015)
214. R.G. Bryant, C. R. Phys. **11**, 128 (2010)
215. B. Halle, Philos. Trans. R. Soc. Lond., B, Biol. Sci. **359**, 1207 (2004)
216. N.V. Nucci, M.S. Pometun, A.J. Wand, J. Am. Chem. Soc. **133**, 12326 (2011)
217. N.V. Nucci, M.S. Pometun, A.J. Wand, Nat. Struct. Mol. Biol. **18**, 245 (2011)
218. K. Yokoyama, T. Kamei, H. Minami, M. Suzuki, J. Phys. Chem. B **105**, 12622 (2001)
219. V.C. Nibali, M. Havenith, J. Am. Chem. Soc. **136**, 12800 (2014)
220. A.I. McIntosh, B. Yang, S.M. Goldup, M. Watkinson, R.S. Donnan, Chem. Soc. Rev. **41**, 2072 (2012)
221. A.C. Fogarty, D. Laage, J. Phys. Chem. B **118**, 7715 (2014)
222. J.T. King, K.J. Kubarych, J. Am. Chem. Soc. **134**, 18705 (2012)
223. D. Laage, G. Stirnemann, F. Sterpone, R. Rey, J.T. Hynes, Ann. Rev. Phys. Chem. **62**, 395 (2011)
224. D.M. Leitner, M. Gruebele, M. Havenith, Hfsp J. **2**, 314 (2008)
225. H.J. Bakker, J.L. Skinner, Chem. Rev. **110**, 1498 (2010)
226. H. Frauenfelder, S.G. Sligar, P.G. Wolynes, Science **254**, 1598 (1991)

227. H. Frauenfelder, P.W. Fenimore, G. Chen, B.H. McMahon, Proc. Nat. Acad. Sci. USA **103**, 15469 (2006)
228. F. Sussich, C. Skopec, J. Brady, A. Cesaro, Carbohydr. Res. **334**, 165 (2001)
229. W.L. Hubbell, in *Membrane Protein Structure: Experimental Approaches*, ed. by S.H. White (Oxford University Press, London, 1994), p. 224
230. P. Gajula, I.V. Borovykh, C. Beier, T. Shkuropatova, P. Gast, H.J. Steinhoff, Appl. Magn. Reson. **31**, 167 (2007)
231. P. Ball, Chem. Rev. **108**, 74 (2008)
232. P. Ball, Proc. Natl. Acad. Sci. USA **114**, 13327 (2017)
233. A. Losi, W. Gärtner, Annu. Rev. Plant Biol. **63**, 49–72 (2012)
234. V.P. Shinkarev, C.A. Wraight, Proc. Natl. Acad. Sci. USA **90**, 1834 (1993)
235. F. Müh, C. Glöckner, J. Hellmich, A. Zouni, Biochim. Biophys. Acta **1817**, 44 (2012)
236. J-R. Shen, Annu. Rev. Plant Biol. **66**, 23 (2015)
237. F. Rappaport, B.A. Diner, Coord. Chem. Rev. **252**, 259 (2008)
238. D.J. Vinyard, G.W. Brudvig, Annu. Rev. Phys. Chem. **68**, 101 (2017)
239. N. Cox, D.A. Pantazis, W. Lubitz, Annu. Rev. Biochem. **89**, 795 (2020)
240. Y. Umena, K. Kawakami, J.-R. Shen, N. Kamiya, Nature **473**, 55 (2011)
241. W. Lubitz, M. Chrysina, N. Cox, Photosyn. Res. **142**, 105 (2019)
242. L. Rapatskiy, N. Cox, A. Savitsky, W.M. Ames, J. Sander, M.M. Nowaczyk, M. Roegner, A. Boussac, F. Neese, J. Messinger, W. Lubitz, J. Am. Chem. Soc. **134**, 16619 (2012)
243. K. Brettel, E. Schlodder, H.T. Witt, Biochim. Biophys. Acta **766**, 403 (1984)
244. M. Karge, K.D. Irrgang, S. Sellin, R. Feinäugle, B. Liu, H.J. Eckert, H.J. Eichler, G. Renger, FEBS Lett. **378**, 140 (1996)
245. C. Tommos, G.T. Babcock, Biochim. Biophys. Acta **1458**, 199 (2000)
246. H. Conjeaud, P. Mathis, Biochim. Biophys. Acta **590**, 353 (1980)
247. E. Schlodder, B. Meyer, Biochim. Biophys. Acta **890**, 23 (1987)
248. E. Schlodder, M. Çetin, F. Lendzian, Biochim. Biophys. Acta **1847**, 1283 (2015)
249. M.J. Schilstra, F. Rappaport, J.H.A. Nugent, C.J. Barnett, D.R. Klug, Biochemistry **37**, 3974 (1998)
250. F. Rappaport, J. Lavergne, Biochim. Biophys. Acta **1503**, 246 (2001)
251. M. Mamedov, F. Francia, L. Vitukhnovskaya, A. Semenov, G. Venturoli, in *Proceedings of the 10th International Conference "Photosynthesis and Hydrogen Energy Research for Sustainability"* (St. Petersburg, Russia, 23-28 June 2019) p. 75
252. B.A. Diner, D.A. Force, D.W. Randall, R.D. Britt, Biochemistry **37**, 17931 (1998)
253. R. Ahlbrink, M. Haumann, D. Cherepanov, O. Bögershausen, A. Mulkidjanian, W. Junge, Biochemistry **37**, 1131 (1998)
254. P.J. Steinbach, R. Ionescu, C.R. Matthews, Biophys. J. **82**, 2244 (2002)
255. M. Mamedov, A. Semenov, F. Francia, G. Venturoli, in preparation (2020)
256. S. Reinmann, P. Mathis, Biochim. Biophys. Acta **635**, 249 (1981)
257. S. Gerken, J.P. Dekker, E. Schlodder, H.T. Witt, Biochim. Biophys. Acta **977**, 52 (1989)
258. B. Hillmann, E. Schlodder, Biochim. Biophys. Acta **1231**, 76 (1995)
259. G. Lentzen, T. Schwarz, Appl. Microbiol. Biotechnol. **72**, 623 (2006)
260. C.G. Hounsa, V.E. Brandt, J. Thevelein, S. Hohmann, B.A. Prior, Microbiology **144**, 671 (1998)
261. P. Lamosa, L.O. Martins, M.S. da Costa, H. Santos, Appl. Environ. Microbiol. **6**, 3591 (1998)
262. Z. Silva, S. Alarico, A. Nobre, R. Horlacher, J. Marugg, W. Boos, A.I. Mingote, M.S. da Costa, J. Bacteriol. **185**, 5943 (2003)
263. C. De Virgilio, T. Hottinger, J. Domínguez, T. Boller, A. Wiemken, Eur. J. Biochem. **219**, 179 (1994)
264. M.R. Michaud, D.L. Denlinger, J. Comp. Physiol. B **177**, 753 (2007)
265. A. Kraegeloh, H.J. Kunte, Extremophiles **6**, 453 (2002)
266. K. Lippert, E.A. Galinski, Appl. Microbiol. Biotechnol. **37**, 61 (1992)
267. C. Tanne, E.A. Golovina, F.A. Hoekstra, A. Meffert, E.A. Galinski, Front. Microbiol. **5**, 150 (2014)
268. I. Yu, M. Nagaoka, Chem. Phys. Lett. **388**, 316 (2004)
269. G. Zaccai, I. Bgyan, J. Combet, G.J. Cuello, B. Demé, Y. Fichou, F.-X. Gallat, V.M. Galvan Josa, S. von Gronau, M. Haertlein, A. Martel, M. Moulin, M. Neumann, M. Weik, D. Oesterhelt, Sci. Rep. **6**, 31434 (2016)
270. N. Borges, A. Ramos, N.D.H. Raven, R.J. Sharp, H. Santos, Extremophiles **6**, 209 (2002)
271. A. Nalepa, K. Möbius, M. Plato, W. Lubitz, A. Savitsky, Appl. Magn. Reson. **50**, 1 (2019)

Affiliations

Klaus Möbius[1] · Anton Savitsky[2] · Marco Malferrari[3] · Francesco Francia[4] · Mahir D. Mamedov[5] · Alexey Yu. Semenov[5,6] · Wolfgang Lubitz[7] · Giovanni Venturoli[4]

✉ Klaus Möbius
moebius@physik.fu-berlin.de

Anton Savitsky
anton.savitsky@tu-dortmund.de

Alexey Yu. Semenov
semenov@genebee.msu.ru

Giovanni Venturoli
giovanni.venturoli@unibo.it

1 Department of Physics, Free University Berlin, Berlin, Germany

2 Faculty of Physics, Technical University Dortmund, Dortmund, Germany

3 Department of Chemistry "Giacomo Ciamician", University of Bologna, Bologna, Italy

4 Laboratory of Biochemistry and Molecular Biophysics, Department of Pharmacy and Biotechnology, FaBiT, University of Bologna, Bologna, Italy

5 A.N. Belozersky Institute of Physical-Chemical Biology, Lomonosov Moscow State University, Moscow, Russia

6 N.N. Semenov Federal Research Center for Chemical Physics, Russian Academy of Sciences, Moscow, Russia

7 Max-Planck-Institute for Chemical Energy Conversion, Mülheim (Ruhr), Germany